IAEA
International Atomic Energy Agency

INDC(BLR)-0021
Distr. J+MN

INDC International Nuclear Data Committee

Neutron Data Evaluation of ^{237}Np

V.M. Maslov[1], V.G. Pronyaev[2], N.A. Tetereva[1], A.M. Kolesov[1],
K.I. Zolotarev[2], T. Granier[3], F.-J. Hambsch[4]

[1)] Joint Institute of Nuclear and Energy Research
SOSNY 220109 Minsk, Belarus
[2)] Institute of Physics and Power Engineering,
249020 Obninsk, Russia
[3)] CEA/DAM, Ile de France
Arpajon, France
[4)] JRC Institute for Reference Materials and Measurements
B-2440 Geel, Belgium

November 2010

IAEA Nuclear Data Section, Vienna International Centre, A-1400 Vienna, Austria

Selected INDC documents may be downloaded in electronic form from
http://www-nds.iaea.org/reports-new/indc-reports/
or sent as an e-mail attachment.
Requests for hardcopy or e-mail transmittal should be directed to *services@iaeand.iaea.org*
or to:
Nuclear Data Section
International Atomic Energy Agency
Vienna International Centre
PO Box 100
A-1400 Vienna
Austria

Printed by the IAEA in Austria

November 2010

INDC(BLR)-0021
Distr. J+MN

Neutron Data Evaluation of ^{237}Np

V.M. Maslov[1], V.G. Pronyaev[2], N.A. Tetereva[1], A.M. Kolesov[1],
K.I. Zolotarev[2], T. Granier[3], F.-J. Hambsch[4]

[1)] Joint Institute of Nuclear and Energy Research
SOSNY 220109 Minsk, Belarus
[2)] Institute of Physics and Power Engineering,
249020 Obninsk, Russia
[3)] CEA/DAM, Ile de France
Arpajon, France
[4)] JRC Institute for Reference Materials and Measurements
B-2440 Geel, Belgium

Abstract

The diverse measured data base of n+^{237}Np was evaluated using a statistical theory and generalized least squares codes. Consistent description of the total, fission and partial inelastic scattering data in 1-3 MeV energy range provides an important constraint for the absorption cross section, which is quite important for the robust estimate of the capture cross section in the 0.5-500 keV energy range. Important constraints for the measured capture cross section come from the average radiative S_0 and S_1 strength functions. The evaluated inelastic cross sections of available evaluations are in severe disagreement with measured data on the inelastic scattering of neutrons with excitation of specific groups of levels. A change of the inelastic data shape at E_n ~1.5 MeV might be explained by the sharp increase of the level density of the residual odd-even nuclide ^{237}Np due to the onset of three-quasi-particle excitations.

The influence of exclusive (n, xnf) pre-fission neutrons on prompt fission neutron spectra (PFNS) and (n, xn) spectra is modeled. Contributions of emissive/non-emissive fission and exclusive spectra of (n, xnf) reactions are defined by a consistent description of the ^{237}Np (n, F), ^{237}Np (n, 2n) ^{236s}Np reactions and the ratio of the yields of short-lived (1^-) and long-lived (6^-) ^{236}Np states measured at 14 MeV. Excited levels of ^{236}Np are modeled using predicted Gallher-Moshkowski doublets.

This work is performed under the project Agreement B-1604 with the International Science and Technology Center (Moscow). The financing party is EU. Partial support of International Atomic Energy Agency under Research Contract 14809 is acknowledged by JINER[1].

November 2010

Contents

1. Introduction

Neptunium-237 is a major constituent of the spent nuclear fuel. Main chains for its production are neutron captures in ^{235}U and (n, 2n) reactions in ^{238}U, these are: $^{235}U(n, \gamma)$ $^{236}U(n, \gamma)$ $^{237}U(\beta^-)$ ^{237}Np and $^{238}U(n, 2n)$ $^{237}U(\beta^-)^{237}Np$. The transmutation of the ^{237}Np in thermal power reactors is affected by the neutron capture cross sections of the reaction chain $^{237}Np(n, \gamma)$ $^{238}Np(\beta^-)^{238}Pu(n, \gamma)$ ^{239}Pu. The yield of the $^{236(s)}Np$ short-lived isomer, in the reaction chain $^{237}Np(n, 2n)$ $^{236s}Np(\beta^-)$ $^{236}Pu(\alpha)^{232}U$, is another important item which defines the radiation environment of the spent fuel.

Repository or transmutation of ^{237}Np as a major constituent of the spent fuel needs rather precise knowledge of the ^{237}Np neutron-induced fission, capture, inelastic scattering, (n, 2n) cross sections, branching ratio for the yields of short-lived ^{236s}Np and long-lived ^{236l}Np states of $^{237}Np(n, 2n)$ reaction. Prompt fission neutron spectrum (PFNS) and prompt fission neutron multiplicity are another important items, measurements of which for the $^{237}Np(n, F)$ reaction are scarce. These characteristics of n+^{237}Np interaction much affect the criticality (critical mass) of the ^{237}Np sphere, investigated by Sanchez, *et al.* [1], which is important for the long-term storage of metallic/oxidized ^{237}Np. In [1] the calculated criticality of bare neptunium/HEU and GODIVA experiments is much affected by uncertainties of $^{235}U(n, F)$ prompt fission spectrum [2]. That potentially is a very strong factor for the fission rate in a ^{237}Np. In view of large systematic uncertainties of ENDF/B-VII.0 [3] evaluated PFNS of $^{235}U(n, F)$ prompt fission spectrum the sensitivity of the ^{237}Np critical mass to the fission and inelastic cross sections might be even stronger, than envisaged in [1]. The prompt fission neutron spectra of $^{237}Np(n, F)$ potentially also might be rather influential factor, moreover so that its realistic uncertainties might be much higher than those imposed by the observed differences of various evaluations [1, 3]. In fact, the replacements of different evaluated cross sections exercised in [1] could at most provide guidance about the “sign” of the sensitivity but not the actual sensitivity. The reason for that conclusion is the controversial description of available differential data on the neutron cross sections and prompt fission neutron spectra [4-6] in available data libraries [3, 7].

The improvements of the nuclear reaction modeling and nuclear parameter systematic, developed based on neutron data description of neutron data for major actinides ^{232}Th, ^{233}U, ^{235}U, ^{238}U and ^{239}Pu provide a sound basis for critical assessment of the (n, F), (n, γ), (n, n), (n, n’) cross sections and secondary neutron spectra for the n+^{237}Np interaction. The main reasons of improvement might be consistent description of total, fission, inelastic scattering and capture data in 0.1 keV-5 MeV energy range. For neutron capture reaction on ^{237}Np target nuclide in the unresolved resonance and fast neutron energy ranges the methods, proven in case of $^{232}Th(n, \gamma)$ and $^{238}U(n, \gamma)$ data analysis would be used. Disentangling of the model deficiencies and model parameter uncertainties, when measured cross section data base fits are rather poor, especially when the data are scattering and there are systematic shifts between different data sets, turns out to be a major problem in case of ^{237}Np+n data analysis and prediction. Important constraints for the calculated capture cross section come from the average radiation width and neutron strength functions S_0 and S_1. Consistent description of the total, fission and partial inelastic scattering data in 1~3 MeV incident neutron energy range provide an important constraint for the absorption cross section, which is quite important for the robust estimate of the capture cross section in keV- energy range.

At higher incident neutron energies consistent description of $^{237}Np(n, 2n)^{236S}Np$ and $^{237}Np(n, F)$ cross sections and the latter as a superposition of the (n, f) and (n, xnf) reactions, with simultaneous calculation of exclusive neutron spectra of (n, xn) and (n, xnf) reactions, may provide robust estimates of prompt fission neutron spectra and their average energies [4, 5, 6]. The comparison of average energies of prompt fission neutron spectra for $^{237}Np(n, F)$ reaction of different evaluated data libraries with present calculated and measured data gave a strong impetus for a new evaluation of PFNS. For that a phenomenological approach, proven in case of ^{232}Th, ^{235}U and ^{238}U PFNS data analysis is used (see [5, 6] references therein).

Realistic assessment of the uncertainties of ^{237}Np evaluated data should take into account the results of the consistent description of total, fission, capture and inelastic scattering cross sections with nuclear reaction theory. Purpose of the present evaluation is to clear out whether the available data on total and partial cross sections and average resonance parameters could be described (reproduced) consistently. Preliminary ^{237}Np+n data analysis is described in [4].

2. Resonance Parameters

Here we will briefly review the status of resolved neutron resonance parameters of ^{237}Np. Resolved and unresolved resonance parameters are adopted from JENDL-3.3 [7] were defined as follows:

1) resolved resonance parameters for multilevel Breit-Wigner formalism (up to 500 eV) are adopted;
2) neutron and capture widths are adopted from the analyses by Gressier, *et al.* [8] and Auchampaugh, *et al.* [9];
3) fission widths are adopted from the analyses by Borzakov, *et al.* [10], Dermendjiev, *et al.* [11] and Auchampaugh, *et al.* [9].

Two bound level were placed at E_r= -0.56 eV and -0.49 eV to reproduce adopted thermal total, fission, elastic and capture cross sections. Parameters of the 0.56-eV and 0.49-eV negative resonances were adjusted to reproduce thermal fission and capture cross sections by Kozharin, *et al.* [12] and Wagemans, *et al.* [13, 14]. Scattering radius of 10.5 fm was adopted, thermal total cross section, calculated with Gressier, *et al.* [8] parameters equals 175.79 barn.

The resonance parameters of JENDL-3.3 [7], basically accepted in the present data file of ^{237}Np, might provide a test of neutron width and resonance spacing distributions. We performed a resonance parameter analysis based on maximum likelihood estimates [15, 16] both of mean level spacing $<D_{obs}>$ and neutron strength function S_o. Fig 2.1 shows that strong missing of neutron resonances is pronounced starting from ~150 eV, where the number of observed resonances is slightly more than 250. Here we deal with 553 neutron resonances up to 400 eV. Correction for the missing of levels based on simultaneous analysis of level spacing distribution and neutron width distribution gives estimates of the average s-wave neutron resonance spacing $<D_{obs}>=0.553\pm0.022$ eV (see Figs. 2.1, 2.2) and strength function estimate $S_o= 0.954\pm0.075\text{x}10^{-4}$ (see Figs. 2.3, 2.4). These estimates are compatible with those of Reference Input Parameter Library File [17] recommendations $<D_{obs}>=$ 0.57 ± 0.032 eV and $S_o= 0.97\pm0.07\ 10^{-4}$. Cumulative sum of reduced neutron widths of s-resonances Γ_n^o is compared with present strength function estimate of $S_o=0.954\pm0.075\text{x}10^{-4}$ on Fig. 2.3.

The resolution function parameters as well as Γ_n^o and $<D_{obs}>$ are obtained by maximum likelihood method when comparing experimental distributions of reduced neutron width and resonance spacing with Porter-Thomas and Wigner distributions, modified for the resonance missing [15, 16]. The latter distributions will be called expected distributions. Figs 2.2 and 2.4 demonstrate the comparison of predicted level spacing $<D_{obs}>$ and reduced neutron width Γ_n^o distributions with present resonance parameter set.

Quantiles on Fig. 2.2 show ten equal probability intervals ($P(x\le x_{0.1})= \int p(x)dx = 0.1$) for expected level spacing distribution of s-wave resonances $<D_{obs}>$. Expected level spacing distribution, which takes into account missing of weak resonances and unresolved doublets, is compatible with experimental distribution. Expected distribution is qualitatively similar to Wigner distribution (see Fig. 2.2). However, actual sample of neutron resonances has somewhat different spacing distribution than that of Wigner, since the number of spacings close to $<D_{obs}>$ is obviously excessive. Estimates of the s-wave strength function much depend on the size of the resonance sample. For the ~150 eV neutron energy range the linear trend of the cumulative sum of reduced neutron widths gives $S_o=0.954\pm0.075\text{x}10^{-4}$. At higher energies the excess of large neutron width is pronounced (see Fig. 2.4). Quantiles on Fig. 2.4 show ten equal probability ($P(x\le x_{0.1})= \int p(x)dx = 0.1$) intervals for Γ_n^o expected distribution. It demonstrates that reduced neutron Γ_n^o width distribution with account of missing is compatible with observed distribution

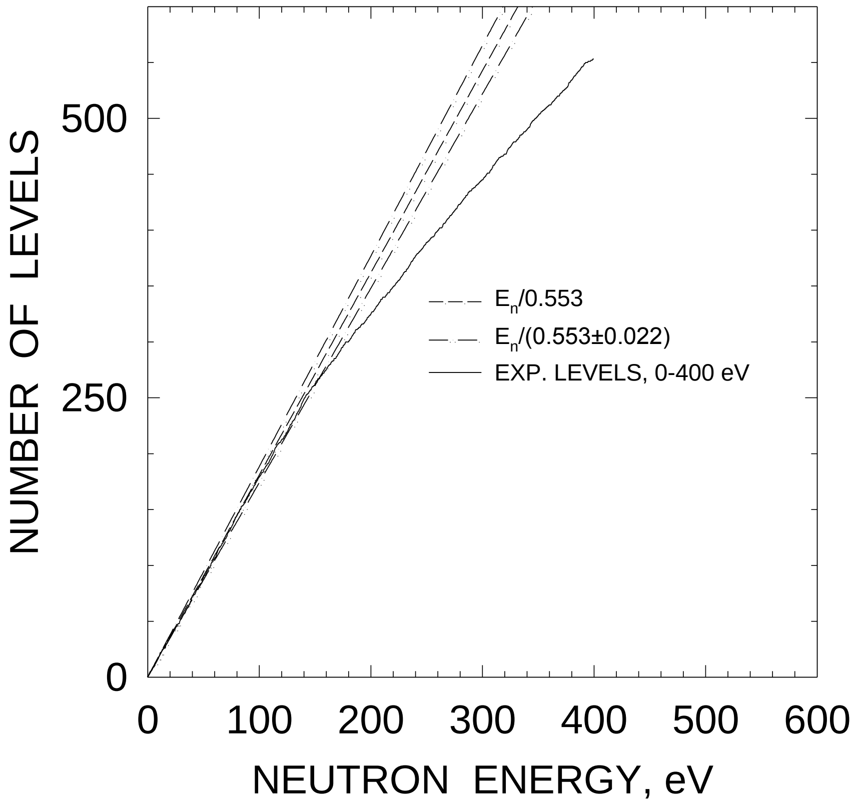

FIG. 2.1. Cumulative sum of neutron resonances of ^{237}Np.

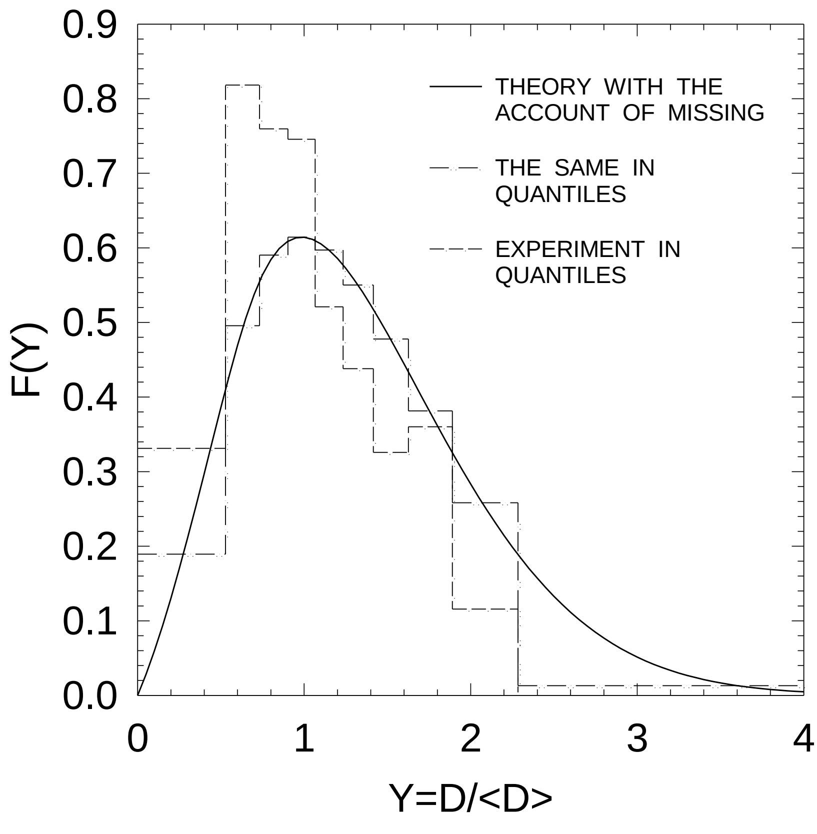

FIG. 2.2. Level spacing distribution of ^{237}Np.

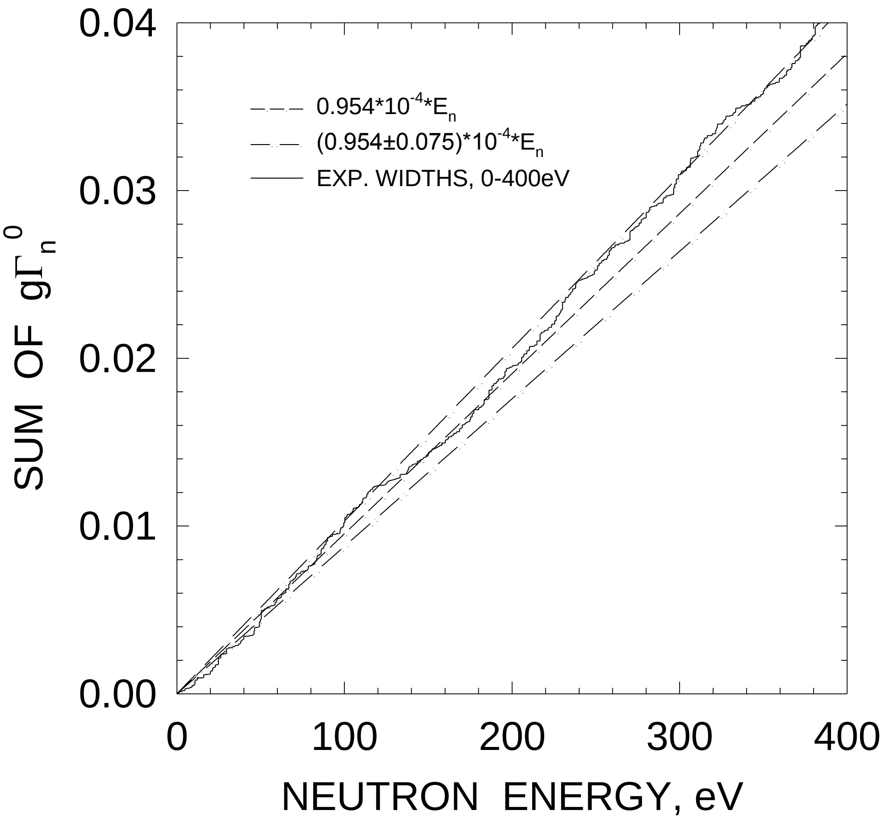

FIG. 2.3. Cumulative sum of reduced neutron widths of ^{237}Np.

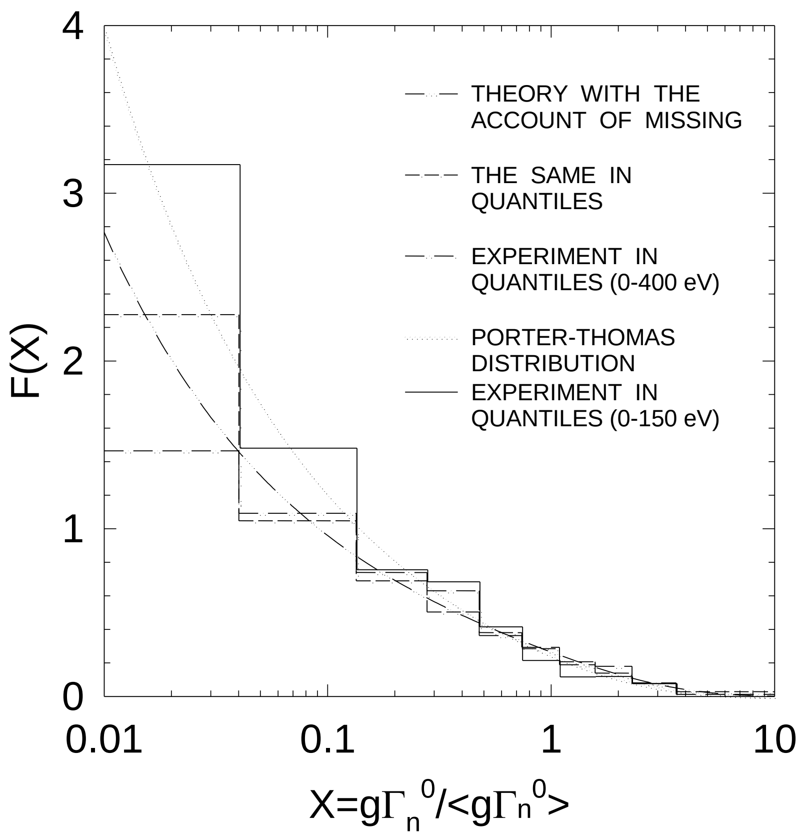

FIG. 2.4. Reduced neutron width distribution of ^{237}Np.

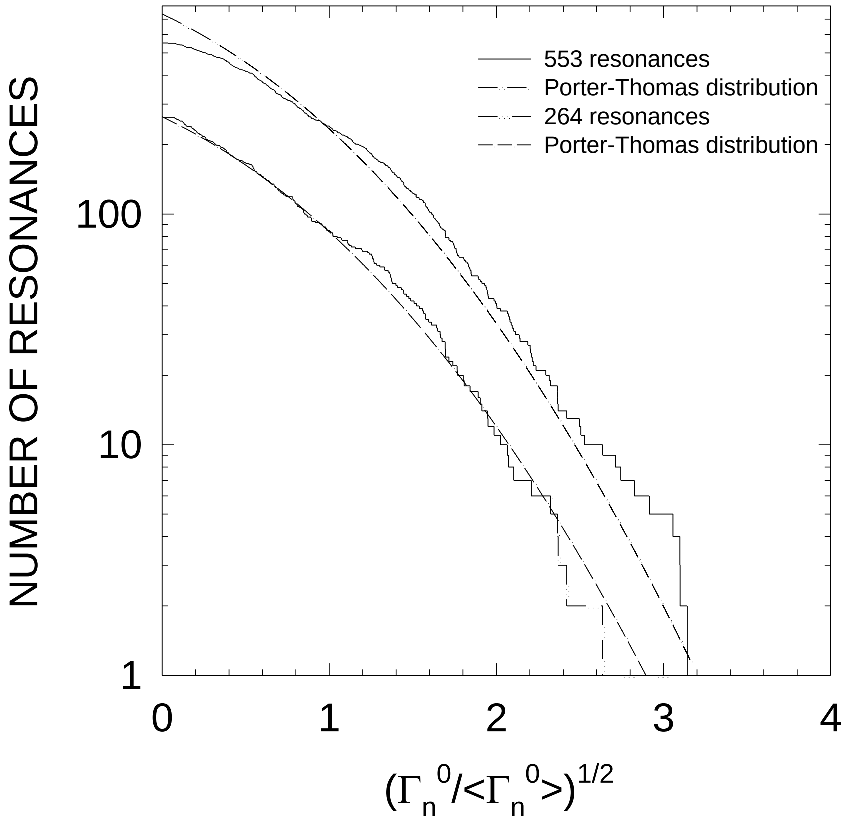

FIG. 2.5. Cumulative distribution of reduced neutron widths of ^{237}Np.

also in the range of small reduced neutron width values. For the neutron energy range up to ~150 eV the neutron width distribution is quite compatible with the Porter-Thomas distribution.

Fig. 2.5 shows a comparison of experimental distribution of reduced neutron widths with cumulative Porter-Thomas distribution of reduced neutron widths with (expected distribution) for neutron resonance samples of 263 (up to ~150 eV) and 553 (up to ~400 eV). Cumulative distribution of reduced neutron widths of smaller sample is quite compatible with Porter-Thomas distribution, while for the larger sample missing of quarter resonances is assumed (N=737). The excess of the neutron resonance widths, which are twice larger than average width, may be due to unresolved doublets (see histograms on Fig. 2.5).

Thermal total, capture and fission cross sections and resonance integrals are shown in Table 2.1.

TABLE 2.1. THERMAL TOTAL, ELASTIC, CAPTURE AND FISSION CROSS SECTIONS AND RESONANCE INTEGRALS

Reaction	σ^{th},barn	RI	σ^{th},barn	RI	σ^{th},barn	RI	σ^{th},barn	RI
	Present		JENDL-3.3 [7]		ENDF/B-VII.0 [3]		BNL-325 [18]	
Total	175.79		175.79		175.792			
Elastic	14.057		14.06		14.0569			
Fission	0.0204	6.94	0.0204	6.90	0.0204	6.95		
Capture	161.71	654.32	161.71	657	161.71	655.84	175.9±2.9	

3. Evaluation of neutron capture and fission cross sections for ^{237}Np in the generalized least-squares method

There are a number of systematic discrepancies between ^{237}Np different neutron data sets and different evaluations as well as between different evaluated data. However, the measured data base on fission and capture cross sections is quite diverse to initiate a combined evaluation effort with a statistical theory and generalized least squares code GMA [19].

Data of many experiments for the ^{237}Np(n, γ) capture cross section cover the energy range from thermal up to ≈2.2 MeV, while for fission reaction ^{237}Np(n, F) from thermal up to 200 MeV. Absolute fission cross section measurements are the measurements done relative to the ^{1}H(n, p) scattering cross section or with a time-correlated associated particle method. Ratio cross section measurements were done relative to the cross sections which are used as the standards [20, 21]. Some measurements were done relative to the reaction cross sections which are not recommended as standards, but they were still used in the present evaluation as a reference. Taking this into account, it was decided to accomplish an evaluation of ^{237}Np(n, γ) capture and ^{237}Np(n, F) fission cross sections in the combined fit with all the other reactions used in the evaluation of the standards [20].

EXFOR database [20] was used for retrieval of the experimental neutron data for ^{237}Np. The data were analyzed and covariance matrices of the uncertainties for the selected data sets were prepared using the information about the partial components of the uncertainties. The total number of data sets for ^{237}Np(n, γ) and ^{237}Np(n, F) cross sections and ratios used in the combined fit is shown in Table 3.1. The data are shown in the form of matrix with the values at the major diagonal giving the total number of the data sets for given cross section, while the off-diagonal values give the number of ratios of the cross sections assigned to specific column and row. Values in the brackets show the number of absolute cross sections data sets or absolute ratios of the cross sections. The ^{238}U(n, γ) capture reaction was excluded from the combined fit by the following reasons. When the ^{238}U(n, γ) reaction is excluded, the number of fitting parameters is less than 1200 and the dimensions of the evaluated covariance matrix are smaller than 1200×1200. The inversion of the matrices of larger dimensions in the evaluation procedure can be quite problematic. The second reason for the exclusion is that the data for ^{238}U(n, γ) capture reaction in the database for standards are rather discrepant. Since there is no ^{237}Np(n, γ)/^{238}U(n, γ) capture cross section ratio measurements, that exclusion will have almost no influence on the GMA [21] evaluation of ^{237}Np(n, γ) cross section.

TABLE 3.1. TOTAL NUMBER OF DATA SETS FOR REACTIONS (SHOWN AT THE MAJOR DIAGONAL) AND NUMBER OF THEIR RATIOS (OFF-DIAGONAL VALUES) IN THE GMA DATABASE FOR ^{237}Np(n, γ) AND ^{237}Np(n, F) EVALUATION. VALUES IN BRACKETS ARE THE NUMBER OF DATA SETS WITH ABSOLUTE CROSS-SECTIONS.

	^{6}Li(n,α)	^{10}B(n,α□0)	^{10}B(n,α□)	^{10}B(n,α)	Au(n,γ)	^{237}Np(n,γ)	^{235}U(n,f)	^{239}Pu(n,f)	^{238}U(n,f)	^{237}Np(n,f)
^{6}Li(n,α)	18 (7)									
^{10}B(n,α□0)	0	5 (4)								
^{10}B(n,α□)	1 (0)	12 (10)	11 (2)							
^{10}B(n,α)	4 (0)	0	0	5 (2)						
Au(n,γ)	3 (3)	0	6 (3)	4 (4)	27 (21)					
^{237}Np(n,γ)	0	0	0	0	2(2)	8(3)				
^{235}U(n,f)	14 (0)	0	2 (1)	25 (0)	12 (10)	2(2)	68 (52)			
^{239}Pu(n,f)	2 (0)	0	0	19(0)	0	0	19 (14)	22 (19)		
^{238}U(n,f)	2 (1)	0	0	0	0	0	34 (29)	3 (1)	18 (11)	
^{237}Np(n,f)	0	0	0	0	0	0	20(18)	2(1)	3(2)	11(10)

3.1. ^{237}Np(n,f) cross section evaluation

Total score of the data sets used in the evaluation of the fission cross section is 35 [22 - 48]. There is a very good agreement between most of experimental data sets for incident neutron energies above 100 keV. The chi-square per degree of freedom in the fit is about 1. The fit was done separately for the cross sections in the energy range between 0.0253 eV and 20 MeV and for the higher energy range of 20 and 200 MeV. The experimental data sets used in the evaluation are listed in Table 3.1.

The evaluated data for the energy below 20 MeV in the comparison with other evaluations and experimental data are shown in Figs. 3.1 - 3.7. The ENDF/B-VII.0 evaluation below 0.5 keV is represented as a group-averaged cross section, calculated using the resolved resonance parameters. Data for the incident neutron energies higher than 35 keV were normalized using the new ^{235}U(n, F) standard [20], which is almost identical with the ^{235}U(n, F) cross section obtained in the present combined fit. The comparison for the energies above 0.1 MeV in the linear and logarithmic scales is shown in figures 3.2 and 3.3, ratio of the present fit to the ENDF/B-VII.0 [3] evaluation is shown in the figure 3.4. The differences between present and ENDF/B-VII.0 evaluation [3] for the energies above 0.1 MeV are rather small. Independent evaluation, done for the dosimetry applications in the Pade model least-squares fit with detailed analysis of the experimental data [49] is also in a good agreement with the GMA evaluation except energy ranges around 8 MeV and above 14 MeV. The origin of the structure observed in the evaluated cross section near 0.2 MeV will be discussed later. The data by Tovesson and Hill [23], shown in the Fig. 3.3, are obtained by the group averaging of the measured cross section ratios ^{237}Np(n, F)/^{235}U(n, F), multiplied by the absolute cross section of ^{235}U(n, F), obtained in the present combined fit.

The data below E_n=0.1 MeV are very discrepant. All available experimental data, reduced to the energy groups used in the evaluation, are shown in the Fig. 3.5. Data by Yamanaka, *et al.* [46], obtained at the lead slowing-down spectrometer with very poor energy resolution, were not used in the present evaluation. They agree generally with the data by Tovesson and Hill [23] when large mesh is used. Data by Carlson, *et al.* [44] are in fact a preliminary measurement done at LANSCE (LANL) more than 10 years ago, after that the measurements were repeated by Tovesson and Hill [23]. Because the data by Carlson, *et al.* [44] are systematically low, they also were not used in the present evaluation. Data by Hoffman, *et al.* [45], obtained in the nuclear bomb-shot experiment, were treated below 0.01 MeV as the shape data because of the large uncertainty of the normalization. The data by Carlson, *et al.* [44] above 0.01 MeV were not used in the evaluation. The evaluated data at neutron energies below 0.1 MeV are defined by the data of Tovesson and Hill [23] between 0.1 keV and 200 keV. In the energy region between 0.1 and 0.2 MeV the data sets below and above 0.1 MeV overlap. The agreement between experimental data of different authors and evaluated cross section in this energy range is between 1.5–15 %. Tovesson and Hill [23] data deviate from the evaluated cross section by 1.5–4.3 %.

The evaluated value of thermal fission cross section at 0.0253 eV is 0.0204 barn with an uncertainty of 4.8 %. Tovesson and Hill [23] data were not used in the evaluation of thermal cross section because of their large uncertainty. If assumed that shape of neutron fission cross section in the energy range from 0.01 to 0.1 eV is similar for ^{235}U(n, f) and ^{237}Np(n, f) and close to *1/v*, then the measured ratio of ^{237}Np(n, f) and ^{235}U(n, f) cross sections should be energy-independent. Because of the large statistical uncertainty (≈25%), the measured ratio strongly fluctuates. Averaging the cross section measured in a large number of energy points strongly reduces the statistical component of the uncertainty. The ratio averaged in the energy range between 0.01 and 0.1 eV is equal to 4.664×10^{-5}. Using ^{235}U(n, f) cross section at 0.0253 eV, evaluated in the combined fit, in case of Tovesson and Hill [19] measurements we will get an estimate of ^{237}Np(n, f) thermal cross section of 0.0272 barn. Taking into account, that non-statistical components of the uncertainties for Tovesson and Hill [23] measurements in the energy range from 0.01 to 0.1 eV are ≈70 %, the agreement between measured and evaluated value is acceptable. It might be concluded that the shape of cross section obtained by Tovesson and Hill [23] probably is not distorted in the energy range between 0.01 eV and 0.2 MeV.

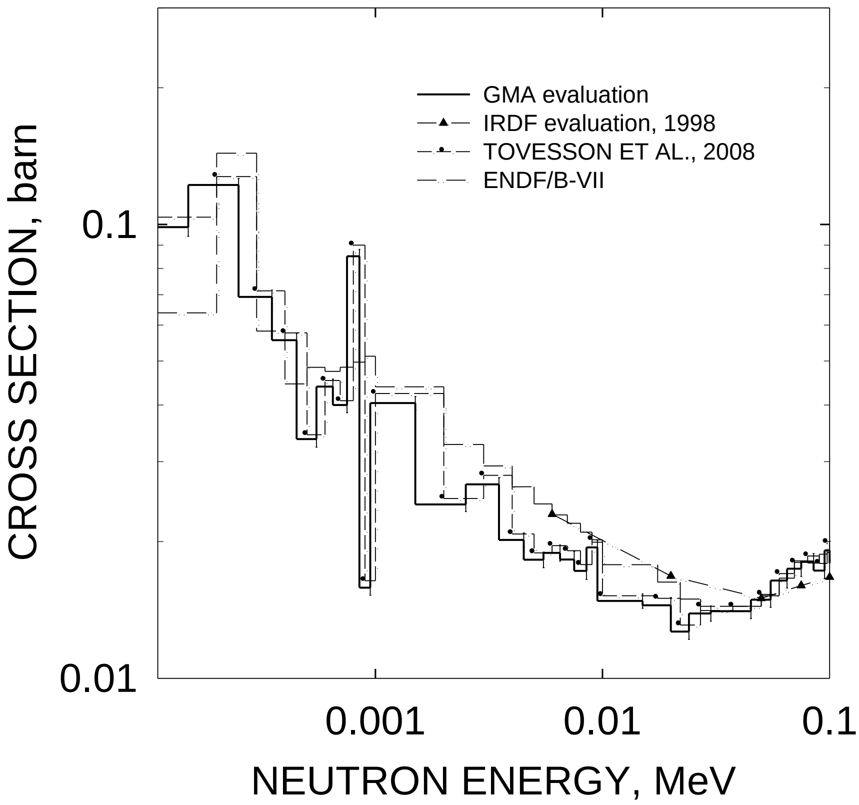

FIG. 3.1. Comparison of GMA' evaluated fission cross section of ^{237}Np with previous evaluations

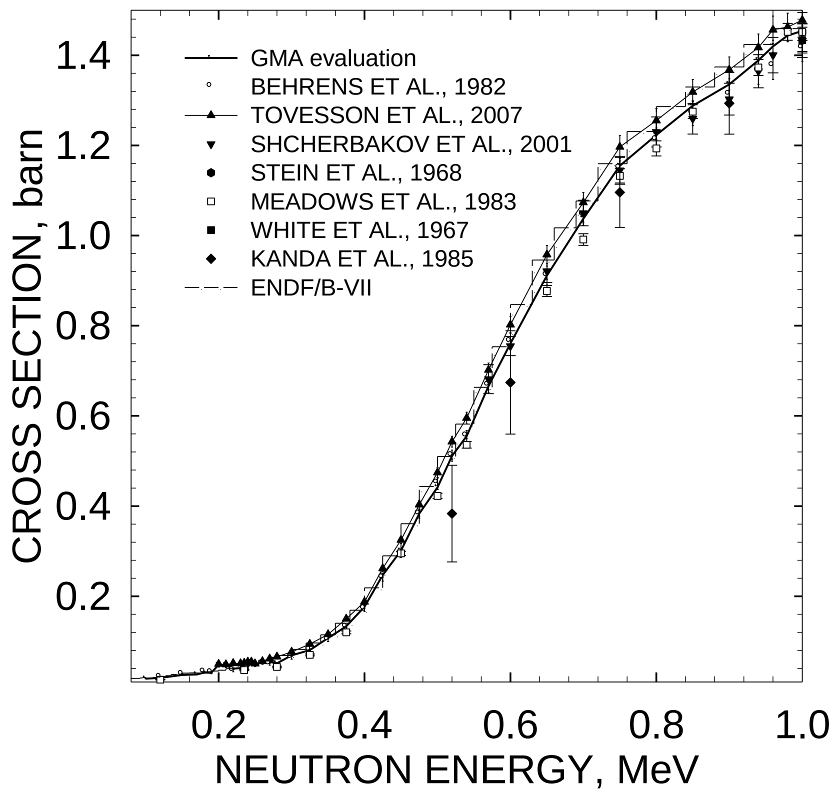

FIG. 3.2. Comparison of GMA' evaluated fission cross section of ^{237}Np with previous evaluations and measured data.

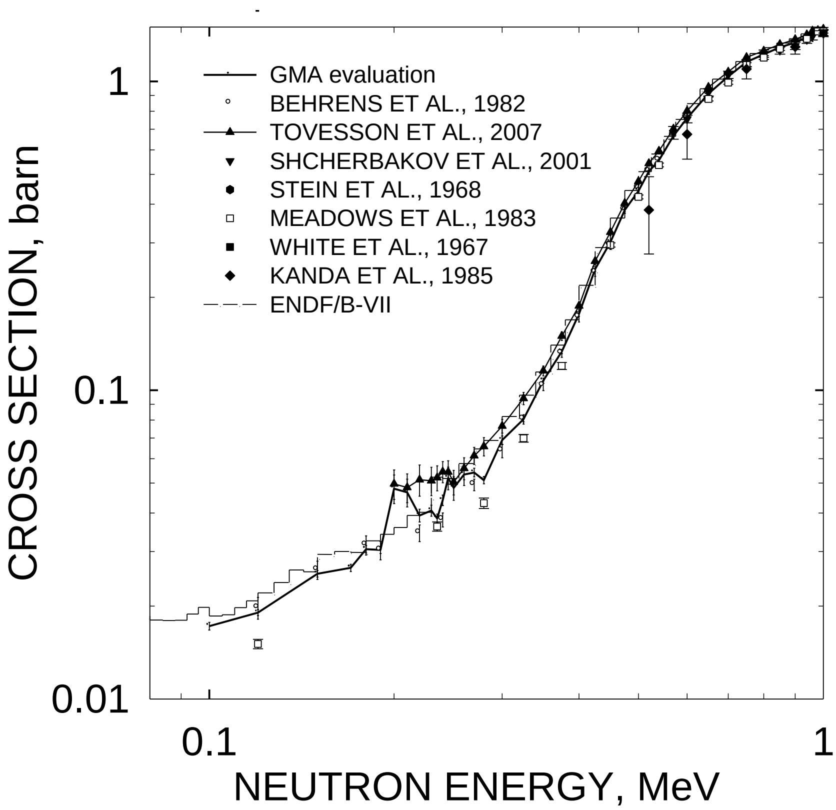

FIG. 3.3. Comparison of GMA' evaluated fission cross section of ^{237}Np with previous evaluations and measured data.

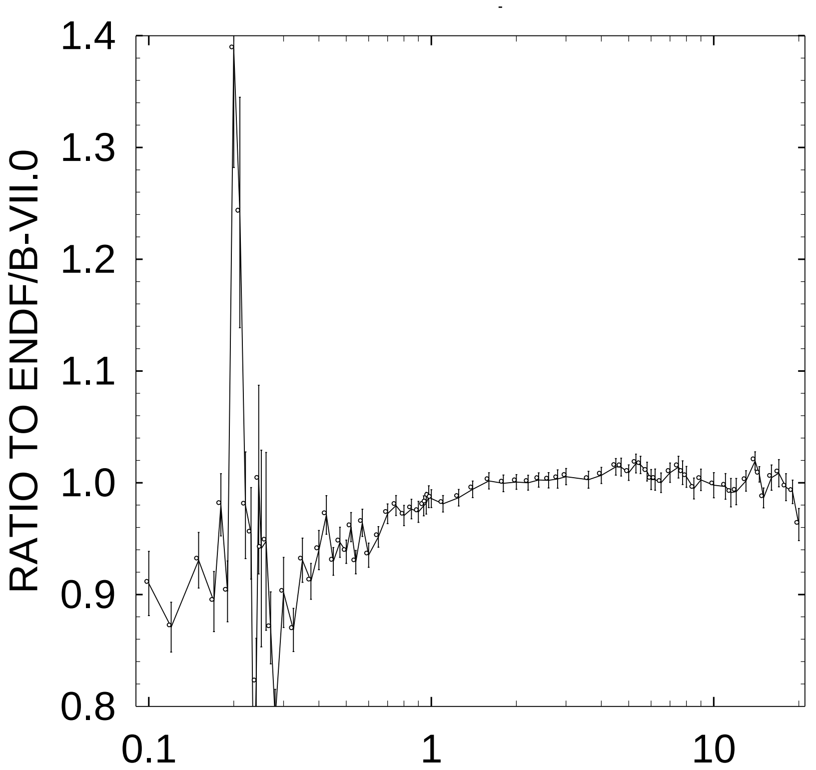

FIG. 3.4. Comparison of GMA' evaluated fission cross section of ^{237}Np with previous evaluations.

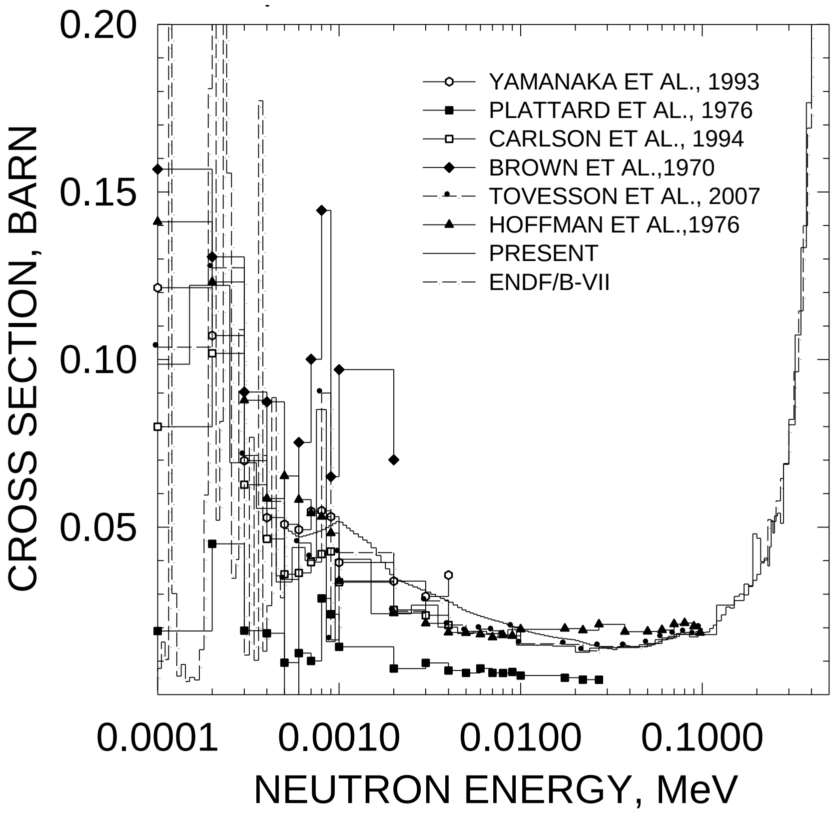

FIG. 3.5. Comparison of GMA' evaluated fission cross section of ^{237}Np with previous evaluations and measured data.

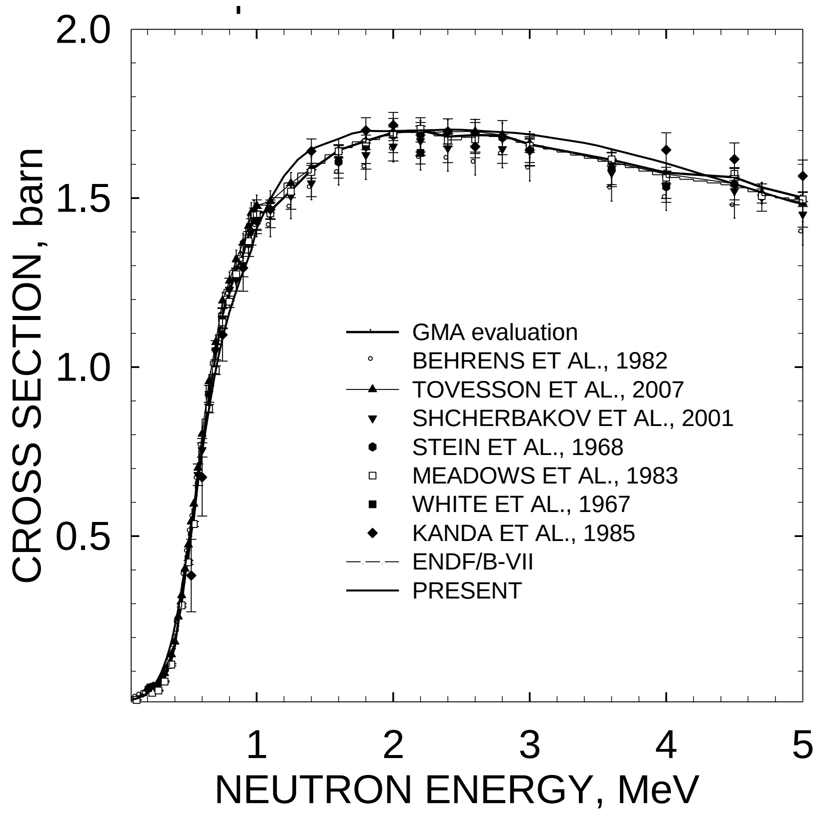

FIG. 3.6. Comparison of GMA' evaluated fission cross section of ^{237}Np with previous evaluations and measured data.

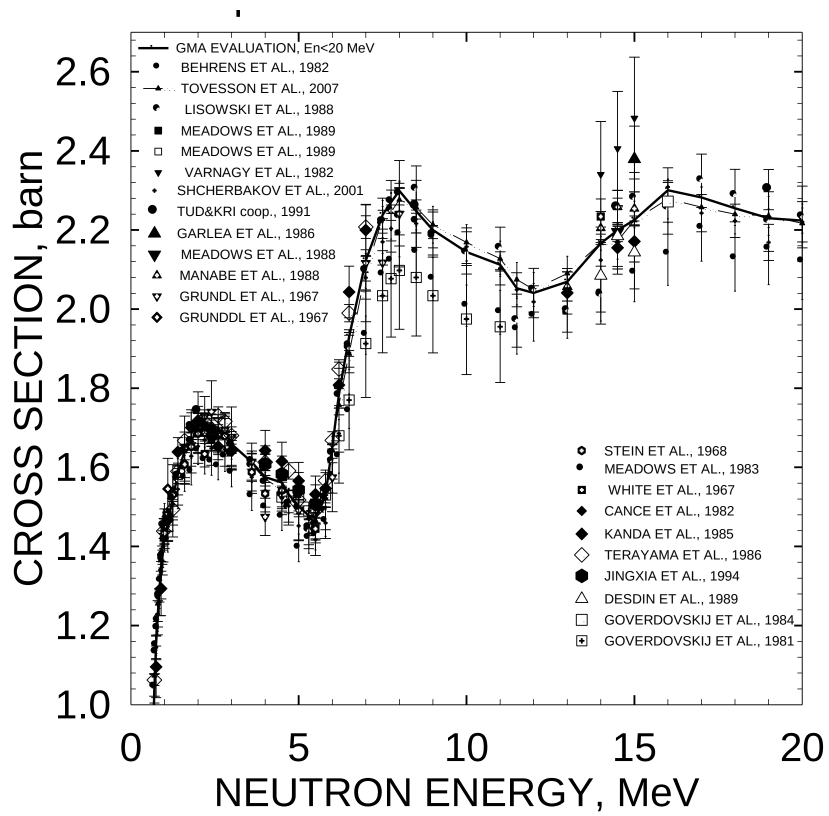

FIG. 3.7. Comparison of GMA' evaluated fission cross section of ^{237}Np with previous evaluations and measured data.

3.2. ^{237}Np(n, f) evaluated cross section in the energy range from 20 to 200 MeV

There are no absolute ^{237}Np(n, F) cross section measurements in the energy range between 20 and 200 MeV (see Table 3.2). Tovesson and Hill [23] measured the shape of the ^{237}Np(n, F) and ^{235}U(n, F) cross sections ratio, other data sets are the measurements of the absolute cross section ratios. Eventually the measured cross sections ratio of [23] was normalized to the ENDF/B-VII.0 data [3]. Present evaluated ^{237}Np(n, F) cross section obtained in the combined fit with the other cross sections is shown in figure 3.8. The evaluated cross section was smoothed using simple mathematical model of the "three-point smoothing". The error bars show the evaluated uncertainties. Comparison of the evaluated and experimental data is shown in Figs. 3.8 and 3.9. Data by Tovesson and Hill [23] are shown non-multiplied by the normalization coefficient (0.9838) obtained in the fit. All other sets were obtained in absolute ratio type measurements. Although the evaluations of ^{237}Np(n, F) cross section below and above 20 MeV were done separately, the agreement between both cross section values at the 20 MeV point is better than ≈0.5%.

TABLE 3.2. THE DATASETS FOR ^{237}Np(n, f) REACTION CROSS SECTION INCLUDED INTO THE GMA COMBINED FIT.

EXFOR data set number	First author	EXFOR entry, (date)	Data	Type of measurem.	Energy range covered, MeV	Comments
3101	J.W. Behrens	10647 (1982)	^{237}Np(n,f)/^{235}U(n,f)	absolute	0.12–20 20-34	
3102	F. Tovesson	14130 (2007)	^{237}Np(n,f)/^{235}U(n,f)	shape	0.2–20 20-200	data below 0.2 MeV are too discrepant and excluded; corre-lated with data set 3130
3130	F. Tovesson	14166	^{237}Np(n,f)/^{235}U(n,f)	absolute	0.0002–0.19	correlated with

EXFOR data set number	First author	EXFOR entry, (date)	Data	Type of measurem.	Energy range covered, MeV	Comments
		(2008)				data set 3102
3103	P.W. Lisowski	14176 (1988)	^{237}Np(n,f)/^{235}U(n,f)	absolute	1.1– 20.0 20–200	preliminary data, digitized from figure
3106	J.W. Meadows	13169 (1989)	^{238}U(n,f) /^{237}Np(n,f)	absolute	2.2–2.4	correlated with data set 3107
3107	J.W. Meadows	13169 (1989)	^{238}U(n,f) /^{237}Np(n,f)	shape	2.0–2.6	correlated with data set 3106
3108	M. Varnagy	30588 (1982)	^{238}U(n,f) /^{237}Np(n,f)	absolute	14–15	correlated with ratios for ^{238}U(n,f) and ^{239}Pu(n,f)
3109	O.A. Shcherbakov	41455 (2001)	^{237}Np(n,f)/^{235}U(n,f)	absolute	0.57–20 20–200	
3110	KRI+TUD collaboration	22304 (1991) 40927 (1986)	^{237}Np(n,f)	absolute	2, 5, 8.5, 14.5, 19.0	combined in one correlated data set
3111	I. Garlea	30813 (1986)	^{237}Np(n,f)/^{235}U(n,f)	absolute	15	
3112	J.W. Meadows	13134 (1988)	^{237}Np(n,f)/^{235}U(n,f)	absolute	14.5	correlated with ratios for ^{238}U(n,f) and ^{239}Pu(n,f)
3113	F. Manabe	22282 (1988)	^{237}Np(n,f)/^{235}U(n,f)	absolute	13-15	
3114	J.A. Grundl	10417 (1967)	^{237}Np(n,f)/^{238}U(n,f)	absolute	2.2-8	correlated with data set 3115
3115	J.A. Grundl	10417 (1967)	^{237}Np(n,f)/^{235}U(n,f)	absolute	1.1–1.6	correlated with data set 3114
3117	W.E. Stein	12452 (1968)	^{237}Np(n,f)/^{235}U(n,f)	absolute	1.0–4.5	
3118	J.W. Meadows	12852 (1983)	^{237}Np(n,f)/^{235}U(n,f)	absolute	0.12–9.0	normalized at 2.12–2.53 MeV region
3119	P.H. White	21195 (1967)	^{237}Np(n,f)/^{238}U(n,f)	absolute	1, 2.2, 5.5, 14.	
3120	M. Cance	21821 (1982)	^{237}Np(n,f)	absolute	2.4	
3121	K. Kanda	21963 (1985)	^{237}Np(n,f)/^{238}U(n,f)	absolute	0.52-15	
3122	H. Terayama	22024 (1986)	^{237}Np(n,f)/^{238}U(n,f)	absolute	0.7–7	
3123	F. Manabe	22282 (1986)	^{237}Np(n,f)/^{238}U(n,f)	absolute	13–15	correlated with ratios for ^{238}U(n,f)
3124	Wu Jingxia	30717 (1984)	^{237}Np(n,f)	absolute	4–5.5	
3125	L. Desdin	31425 (1989)	^{237}Np(n,f)/^{238}U(n,f)	absolute	14-15	
3126	V.M. Kuprijanov	40507 (1978)	^{237}Np(n,f)/^{239}Pu(n,f)	absolute	2-3	correlated with data set 3127
3127	V.M. Kuprijanov	40507 (1978)	^{237}Np(n,f)/^{239}Pu(n,f)	shape	0.12–7	correlated with data set 3126

EXFOR data set number	First author	EXFOR entry, (date)	Data	Type of measurem.	Energy range covered, MeV	Comments
3128	A. Goverdovskij	40835 (1984)	^{237}Np(n,f)/^{235}U(n,f)	absolute	16	correlated with data set 3129
3129	A. Goverdovskij	40861 (1985)	^{237}Np(n,f)/^{235}U(n,f)	shape	4.5-11	correlated with data set 3128
3131	A.D. Carlson	14035 (1994)	^{237}Np(n,f)/^{235}U(n,f)	absolute	4.5-11	
3132	M.M. Hoffman	10366 (1976)	^{237}Np(n,f)	shape	1.0E-4–0.1	data above 0.1 MeV were excluded
3133	V.V. Kozharin	(1986)	^{237}Np(n,f)	absolute	2.53E-8	
3134	C. Wagemans	(1981)	^{237}Np(n,f)	absolute	2.53E-8	
3135	C. Wagemans	(1977)	^{237}Np(n,f)	absolute	2.53E-8	

3.3. ^{237}Np(n, γ) cross section evaluation

In total, 12 data sets [45, 50-56] were selected for the ^{237}Np(n, *γ*) capture cross section evaluation. Their main characteristics are shown in the Table 3.3. The data sets are rather discrepant. If the uncertainties, assigned by the authors, are used, then value of chi-square per degree of freedom is about 4. The fitted curve is shown at the Figs 3.10-3.12 in comparison with the ENDF/B-VII.0 evaluation (same as JENDL-3.3) and latest experimental data by Esch, *et al.* [51]. The uncertainties shown for the GMA evaluation were doubled to account poor chi- square value of the fit. The analysis of the outliers (data outlaying relative to the true values) was done. GMA evaluated data were considered as a true values. Additional component of the uncertainty was added for outliers with more than 2σ deviation from the evaluated cross section. New fit gave the chi-square value of ≈1. The results of this evaluation are shown at the Fig. 3.10. The difference between both evaluations is shown at Fig. 3.11. The increase of the uncertainty for outliers leads to some changes in the evaluated data, although these changes stay within the limits of the evaluated uncertainties.

Data were smoothed using the shape of cross section obtained in the statistical model calculations, which would be described below. The covariance matrix constructed for the data “smoothing” had strong medium energy range correlations. The smoothing was used only for the energies above 8 keV. Agreement with ENDF/B-VII.0 [3] or JENDL-3.3 [7] evaluations is observed in the energy range from 0.5 keV to 200 keV. At incident neutron energies lower than 0.5 keV, the average capture cross sections in ENDF/B-VII.0 [3] were calculated using the evaluated resonance parameters. The observed difference with GMA evaluation can be explained by the non-accounted contribution from the missed resonances. Experimental data for incident neutron energies above 200 keV are very discrepant. The ENDF/B-VII.0 [3] evaluation in this energy range is based on Weston and Todd [50] data. Present evaluation is based on seven data sets [50-56], available in this energy range, although the systematic discrepancies between them are rather large. To resolve these discrepancies new measurements are needed for the neutron energy range of 1 keV-3 MeV. The model “smoothing” reduces the variances and increases the covariances near diagonal of the uncertainty matrix. Without model smoothing the percent uncertainties in the MeV-energy range are at the level of 10–30 %, increasing at some points up to 60%, which equals the level of a prior non-informative uncertainty. The model smoothing allows also fill up the gaps in the experimental data for some energy groups (interpolating cross sections using the local model dependence). Extended comments for some capture cross section data sets are given below.

Data by Weston and Todd [50] were used in a GMA fitting as a shape-type (floating) data. The capture data were normalized in [50] to 180 barn at thermal point E_n= 0.0253 eV.

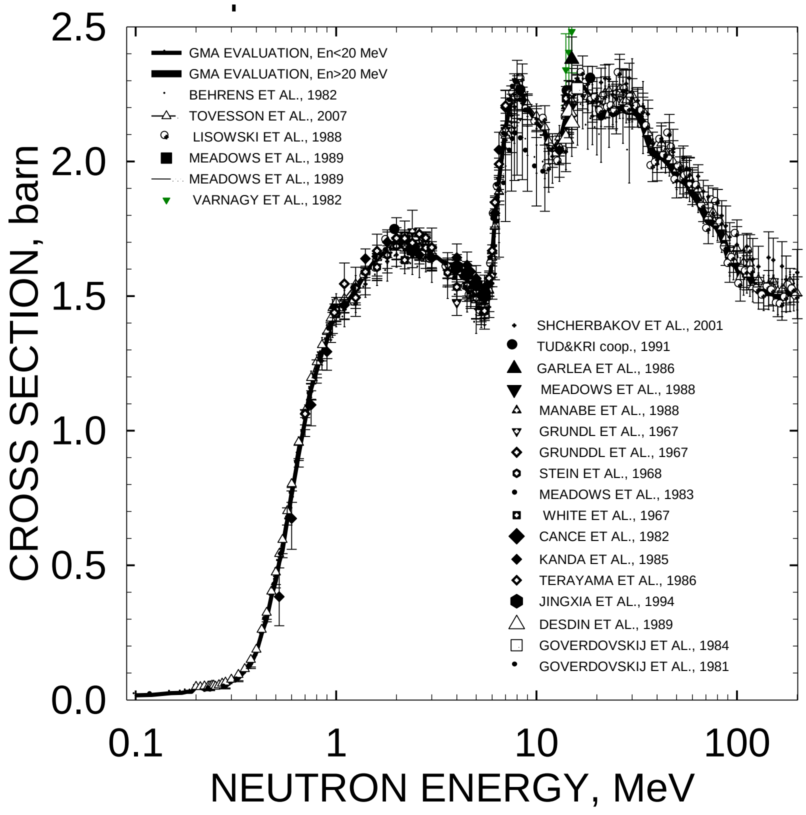

FIG. 3.8. Comparison of GMA' evaluated fission cross section of ^{237}Np with measured data.

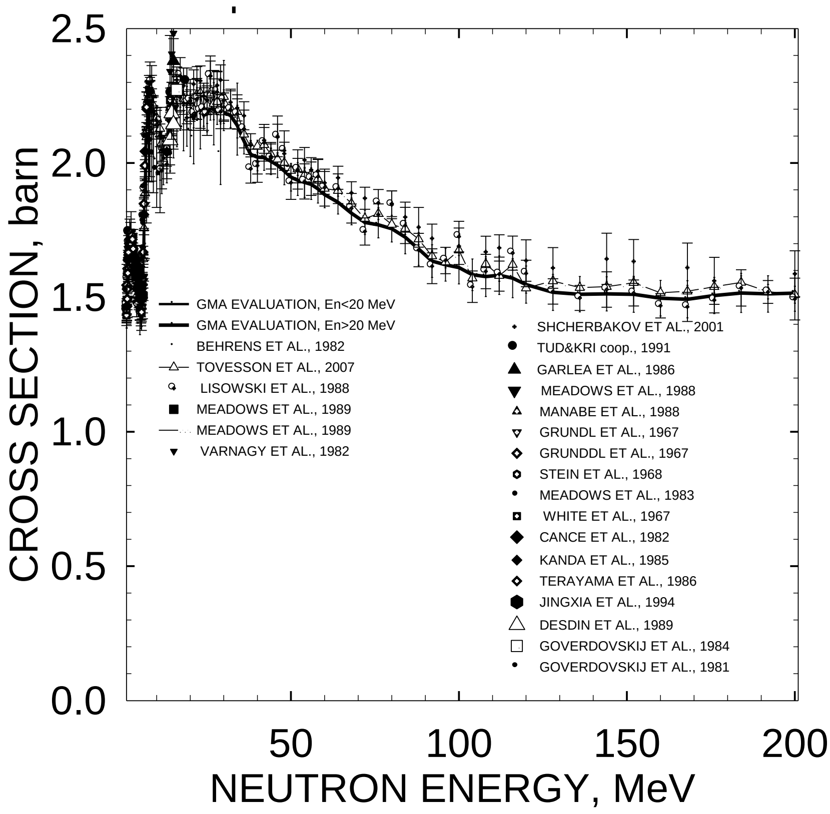

FIG. 3.9. Comparison of GMA' evaluated fission cross section of ^{237}Np with measured data.

TABLE 3.3. THE DATASETS FOR ^{237}Np(n, γ) CAPTURE CROSS SECTION FOR THE GMA COMBINED FIT.

EXFOR data set number	First author	EXFOR entry, (date)	Data	Type of measure-ment	Energy range, MeV	Comments
3000	S.F. Mughabghab	- (2006)	^{237}Np(n,γ)	absolute	2.53E-8	pre-evaluated data
3001	M.M. Hoffman	10366 (1976)	^{237}Np(n,γ)	shape	0.0001–0.1	low uncertainty
3002	W. Lindner	10221 (1976)	^{237}Np(n,γ)/^{235}U(n,f)	absolute	0.12–2.2	
3003	L.W. Weston	10887 (1981)	^{237}Np(n,γ)	shape	Therm.–0.21	
3004	E.I. Esch	14032 (2008)	^{237}Np(n,γ)	absolute	Therm.–0.3	normalized at thermal point
3005	N.N. Buleeva	40969 (1988)	^{237}Np(n,γ)	absolute	0.17–1.1	relative ^{1}H(n,p)
3006	N.N. Buleeva	40969 (1988)	^{237}Np(n,γ)/^{235}U(n,f)	absolute	0.65, 0.75	large disagreement with set 3008
3007	N.N. Buleeva	40969 (1988)	^{237}Np(n,γ)/^{197}Au(n,γ)	absolute	0.17–1.1	large disagreement with set 3008
3008	Yu.N. Trofimov	40975 (1987)	^{237}Np(n,γ)/^{197}Au(n,γ)	absolute	0.325–2.0	large disagreement with sets 3005, 3006, 3007
3011	K.Kobayashi	22858 (2002)	^{237}Np(n,γ)	shape	Therm.–0.01	poor resolution
3012	K.Kobayashi	22858 (2002)	^{237}Np(n,γ)	shape	1.E-4–0.001	poor resolution
3013	statistical model calculations	(2007)	^{237}Np(n,γ)	shape	0.08–2.2	used for smoothing

Generally, they should be used as a shape of the ratio of cross sections of ^{237}Np(n, γ)/^{10}B(n, α_0), because BF_3 counter was used for the neutron flux monitoring. It should be noted that the *1/v*- shape of the ^{10}B(n, α_0) reaction cross section in the energy range of the measurements is well established and was not changed in later evaluations. Spline fits of data by Weston and Todd [50] in the energy range from 0.02 to 0.03 eV have shown that the normalization is to the value 180.66 barn.

Data by Esch, *et al.* [51] are obtained in an absolute time-of-flight cross section measurements using 4π-BF_3 calorimetric gamma-ray detector. The data were normalized using "black" resonance at E_r = 0.49 eV. The capture cross section obtained at E_n = 0.0253 eV (176.7±5.0 b) is very close to the value evaluated earlier by Mughabghab [18] (175.9±2.9 barn), which is used in the least squares fit as pre-evaluated value. The result of present evaluation is 175.9±2.2 barn. The Maxwellian spectrum averaged at kT = 0.0253 eV calculated using point-wise data obtained by Esch, *et al.* [51] is 167.1±4.1 barn. It is very close to the value of 169±4.0 barn, evaluated by Harada [57]. This clearly shows that data by Esch, *et al.* [51] give reliable absolute cross sections, although, as pointed out by Esch, *et al.* [51] the uncertainty in the shape of the cross section at higher energy range with "black" resonance normalization cannot be better than ≈5%. Data measured by Esch, *et al.* [51] are given in the EXFOR data base [20] as group-averaged cross sections. To reduce these data to the energy grid used in the GMA least-squares fit they were further averaged for neutron energies below 20 keV. In that energy range they were originally presented in the narrower energy groups, than it is used in the GMA fits.

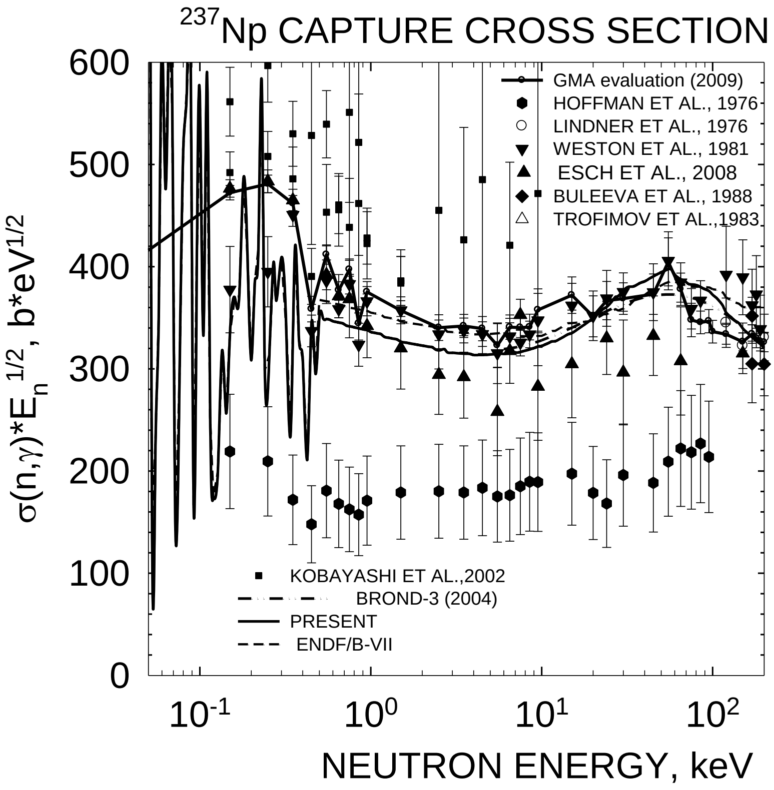

FIG. 3.10. Comparison of GMA' evaluated capture cross section of ^{237}Np with previous evaluations and measured data.

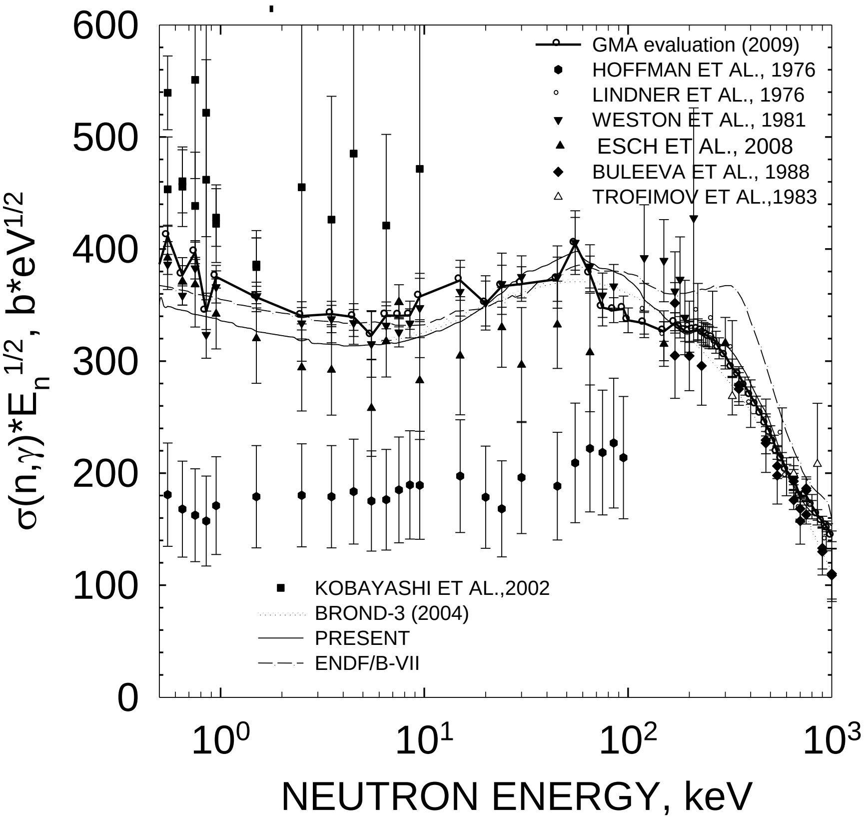

FIG. 3.11. Comparison of GMA' evaluated capture cross section of ^{237}Np with previous evaluations and measured data.

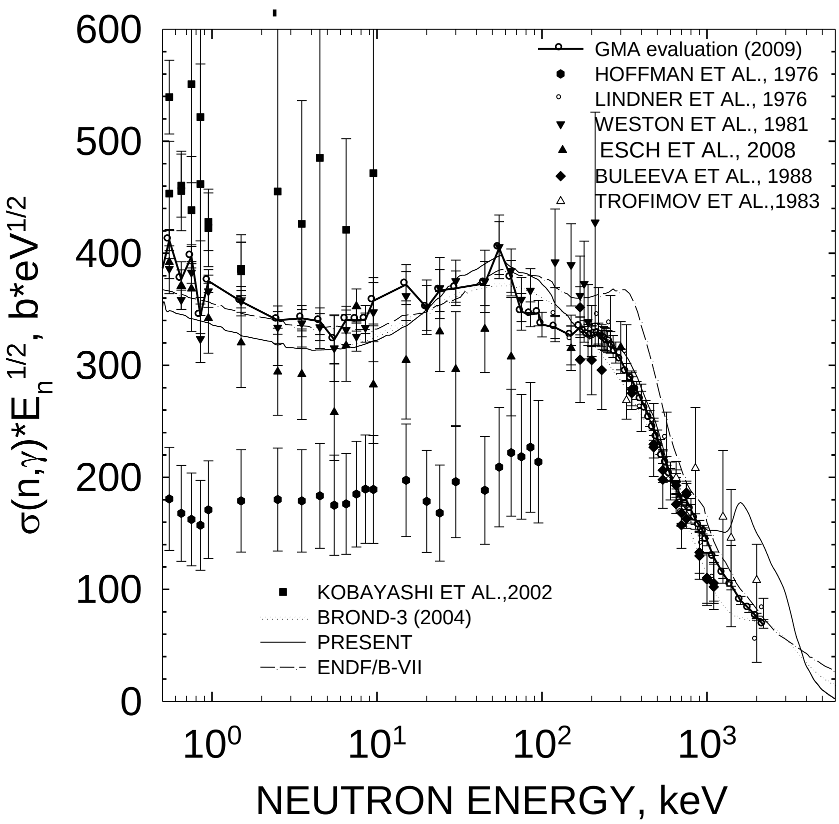

FIG. 3.12 Comparison of GMA' evaluated capture cross section of ^{237}Np with previous evaluations and measured data.

For the capture data above E_n ≈20 keV the original energy groups are wider than the energy bins used in the GMA fit. The data were transformed to the GMA bins using standard procedure of the GMA database preparation.

Three sets of data by Buleeva, *et al.* [53] were obtained in activation measurements using thee different monitors for neutron flux determination: ^{1}H(n, p), ^{197}Au(n, γ) and ^{235}U(n, f). Data obtained with the hydrogen monitor were renormalized to the latest value of the ^{1}H(n, p) reaction cross section standard and is treated finally as the absolute cross sections. Data obtained with ^{197}Au(n, γ) and ^{235}U(n, f) neutron flux monitors were converted into the absolute ratios of the ^{237}Np (n, γ), ^{197}Au(n, γ) and ^{235}U(n, f) cross sections.

Data by Trofimov, *et al.* [55], obtained by the activation method relative to the ^{197}Au(n, γ) capture cross section, were used as absolute ratios of ^{237}Np(n, γ) and ^{197}Au(n, γ) reaction. The data were renormalized to the new values of the decay radiation characteristics.

3.4. The unresolved problems of GMA evaluation

There are a few problems left unresolved in a combined evaluation of ^{237}Np(n, γ) and ^{237}Np(n, F) cross sections in a GMA approach [21]. The discrepancies of the capture cross sections of ENDF/B-VII.0 [3] and present GMA evaluation at incident neutron energies lower than 500 eV is explained by the missed resonances in the ENDF/B-VII.0 resolved resonance range. This is probably true, because with average distance between s-resonances of ≈0.552 eV, there are about 140 resonances up to 100 eV. With that large number of resonances it is difficult to expect the jump in the average cross section observed at the boundary between resolved and unresolved resonance regions in the ENDF/B-VII evaluation (see Fig. 3.10). From this point of view, the present evaluation of average cross sections in this energy range looks more reliable. However, that statement needs further testing, possibly using some benchmarks sensitive to this energy range.

Structure in the ^{237}Np(n, F) cross section around ≈200 keV can be an artifact of the present evaluation. It can be explained by lack of the sufficient number of data points in the energy range of

200–230 keV. This structure would be removed when the physical model is used for the smoothing of the data.

4. Unresolved resonance parameters (500 eV-76.243 keV)

Here we will briefly review the status of unresolved neutron resonance parameters of ^{237}Np and provide a cross section parameterization of total, capture, elastic and inelastic scattering cross sections. The average resonance parameters were determined as described in [4] to reproduce average cross sections in the energy range of 0.5 keV-76.243 keV. The unresolved resonance energy region of ENDF/B-VII.0 [3] is adopted from JENDL-3.3 [7] and extends from 500 eV up to 35 keV. Provided are energy independent average s- and p-wave resonance parameters.

We assume that the lower energy of unresolved resonance energy region in present evaluation is the end-point of resolved resonance region, i.e. 500 eV, the upper energy is 76.243 keV, twice higher than in previous evaluations [3, 7]. We suppose s-, p- and d-wave neutron-nucleus interactions to be effective (see Tables 4.1 and 4.2).

TABLE 4.1. AVERAGE NEUTRON RESONANCE PARAMETERS FOR ^{237}Np

	D_{obs}, eV	Γ_γ, meV	S_o x 10^{-4}	S_1 x 10^{-4}	R, fm
JENDL-3.3	0.45	40	1.0218		9.8491
ENDF/B-VII.0	0.45	40	1.0218		9.8491
RIPL	0.57±0.03	40.8±1.2	0.97±0.07		
BNL	0.52±0.04	40.7±0.5	1.02±0.06	2.0±0.2	
Present	0.553	37.5	1.006	2.203	9.516

TABLE 4.2. NUMBER OF DEGREES OF FREEDOM

l,J	$\nu_{n'}^{lJ}$	ν_{n}^{lJ}	ν_{f}^{lJ}
0,2	2	1	4
0,3	1	1	4
1,1	2	1	4
1,2	1	2	4
1,3	2	2	4
1,4	2	1	4
2,0	2	1	4
2,1	1	2	4
2,2	2	2	4
2,3	1	2	4
2,4	1	2	4
2,5	2	1	4

4.1. Neutron resonance spacing

Neutron resonance spacing D_{obs} was calculated with the phenomenological model [58], which takes into account the shell, pairing and collective effects. The main parameter of the model, asymptotic value of level density parameter a, was normalized to the observed neutron resonance spacing D_{obs} = 0.553 eV. Other parameters are provided in [15]. As the level density is assumed to be parity-independent, on Figs. 4.1 - 4.4 are compared the (l, J) - states level spacings, relevant for some spin values relevant for the unresolved resonance energy range. It is evident that the energy dependence of $\langle D \rangle_J$ decreases the level spacing at 70 keV by 20%. In ENDF/B-VII.0 evaluation the energy dependence of $\langle D \rangle_J$ is ignored arbitrarily.

4.2. Neutron width

Average neutron width is calculated as follows

$$\langle \Gamma_n^{lJ} \rangle = S_l \langle D \rangle_J E_n^{1/2} P_l \nu_n^{lJ}, \tag{4.1}$$

where E_n is the incident neutron energy, P_l is the transmission factor for the l-th partial wave, which was calculated within black nucleus model, ν_n^{lJ} is the number of degrees of freedom of the Porter-Thomas distribution (see Table 4.2). The p-wave neutron strength function $S_1 = 2.203 \times 10^{-4}$ at 500 eV was calculated with the optical model, using the deformed optical potential, described below. Figs 4.5 - 4.10 compare the average reduced neutron widths for the (*l, J)*- states, which are excited in the unresolved resonance energy range. The $\langle \Gamma_n^{0lJ} \rangle$ values for s-wave neutrons in ENDF/B-VII.0 data file are much more energy-dependent than those of present evaluation. That is a consequence of the assumed energy-independent $\langle D \rangle_J$ in ENDF/B-VII.0 [3]. The $\langle \Gamma_n^{0lJ} \rangle$ values for p-wave neutrons in ENDF/B-VII.0 data file are assumed energy-independent.

4.3. Radiative capture width

Energy and angular momentum dependence of radiative capture widths are calculated within a two-cascade γ-emission model with allowance for the (n, γn') [59] and (n, γf) [60] reactions competition to the (n, γγ) reaction. The (n, γγ) reaction is supposed to be a radiation capture reaction. The radiation capture width was normalized to the value of Γ_γ = 37.5 meV, adopted here to describe the neutron capture cross section data. Detailed treatment is described below.

4.4. Neutron inelastic width

Average neutron inelastic width is calculated as follows

$$\langle \Gamma_{n'}^{lJ} \rangle_s = S_l \langle D \rangle_J (E_n - E')^{1/2} P_l (E_n - E') \nu_{n'}^{lJ}, \tag{4.2}$$

where $\nu_{n'}^{lJ}$ is number of degrees of freedom of Porter-Thomas distribution (see Table 4.2). Excited levels of ^{237}Np are taken from Nuclear Data Sheets [61].

4.5. Fission width

Fission widths are calculated within a double-humped fission barrier model by Strutinsky [62]. Energy and angular momentum dependence of fission width is defined by the transition state spectra at inner and outer barrier humps [63, 64]. We constructed transition spectra by supposing the tri-axiality of inner saddle and mass asymmetry at outer saddle. Numbers of degrees of freedom ν_f^{lJ} of Porter-Thomas distribution are defined in Table 4.2. The details will be given below.

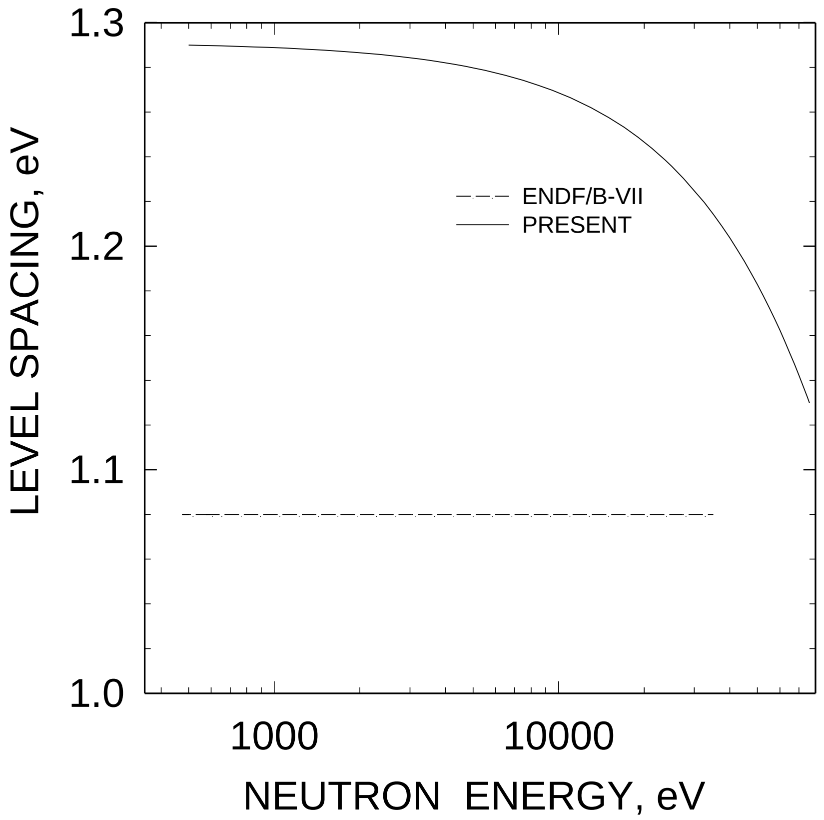

FIG. 4.1. Average level spacing of ^{237}Np, l=0, J=2.

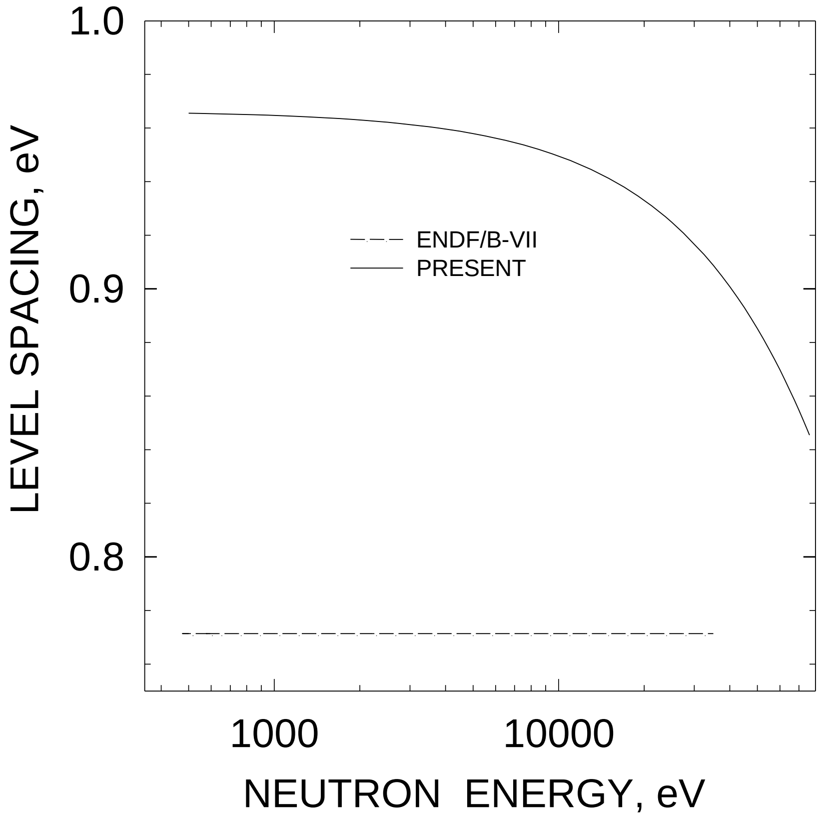

FIG. 4.2. Average level spacing of ^{237}Np, l=0, J=3.

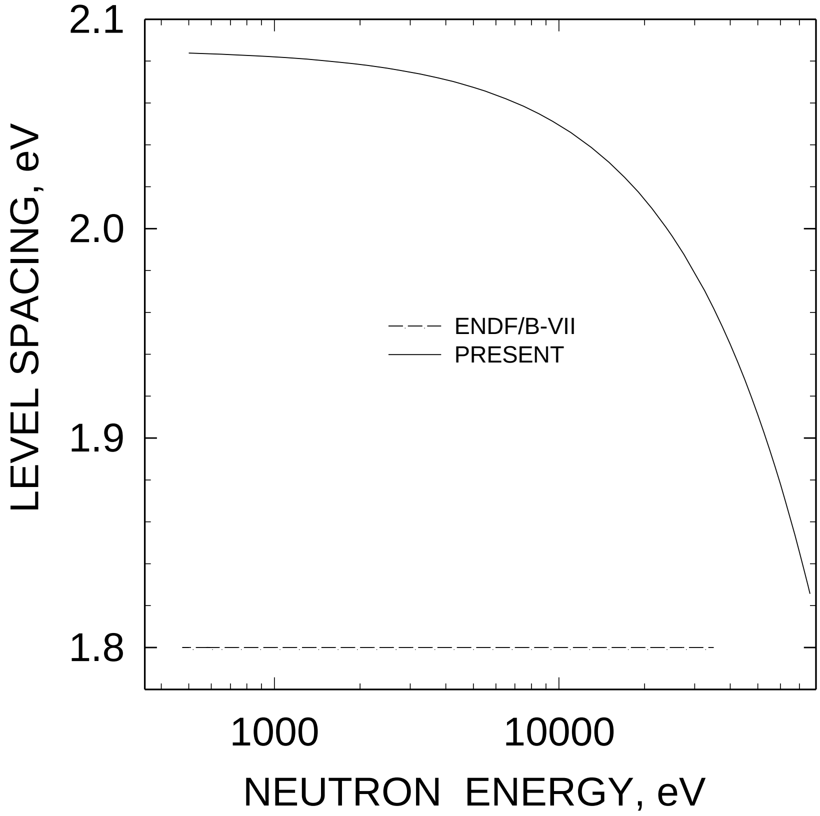

FIG. 4.3. Average level spacing of ^{237}Np, l=1, J=1.

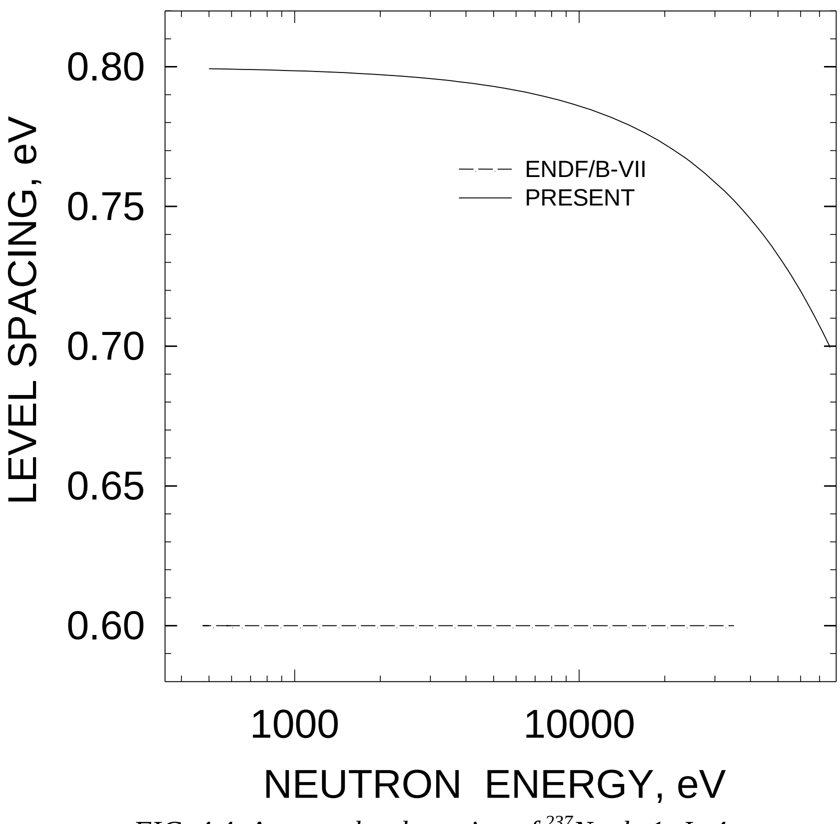

FIG. 4.4. Average level spacing of ^{237}Np, l=1, J=4.

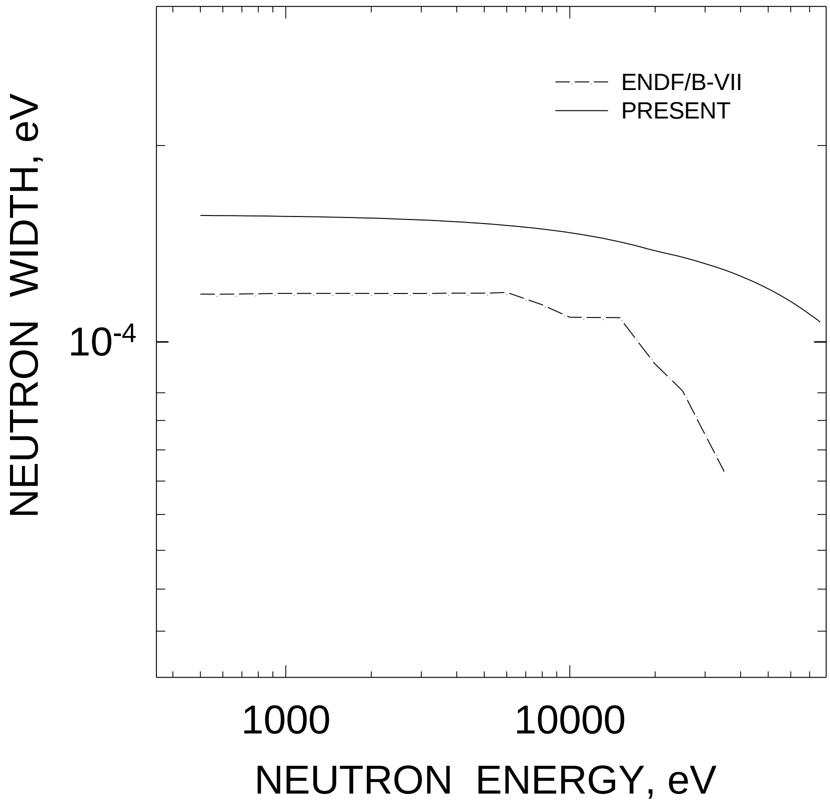

FIG. 4.5. Average reduced neutron width of ^{237}Np, l=0, J=2.

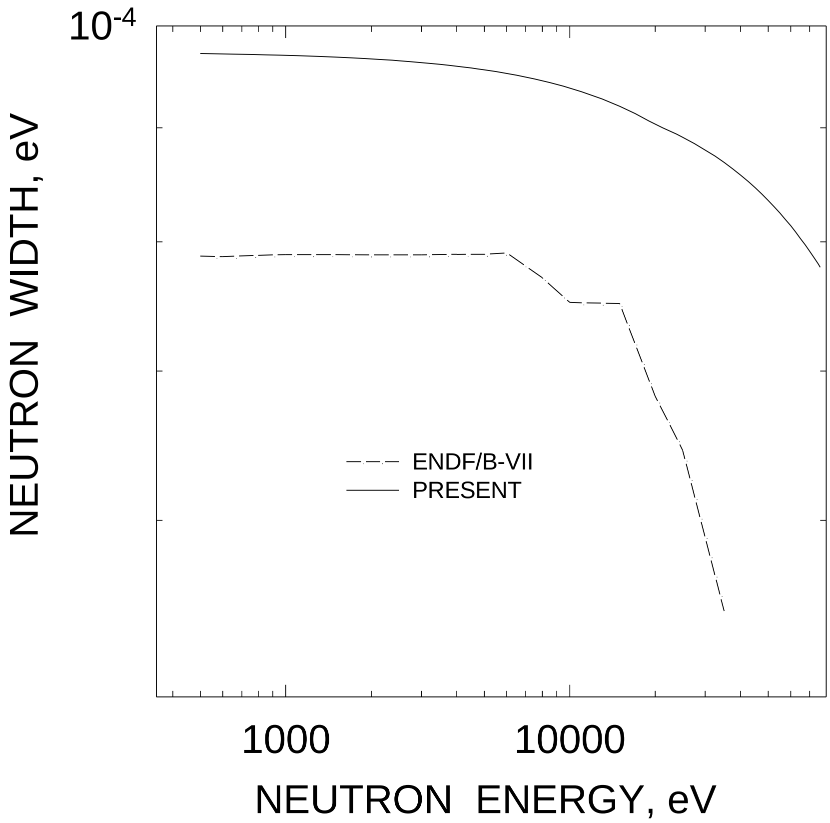

FIG. 4.6. Average reduced neutron width of ^{237}Np, l=0, J=3.

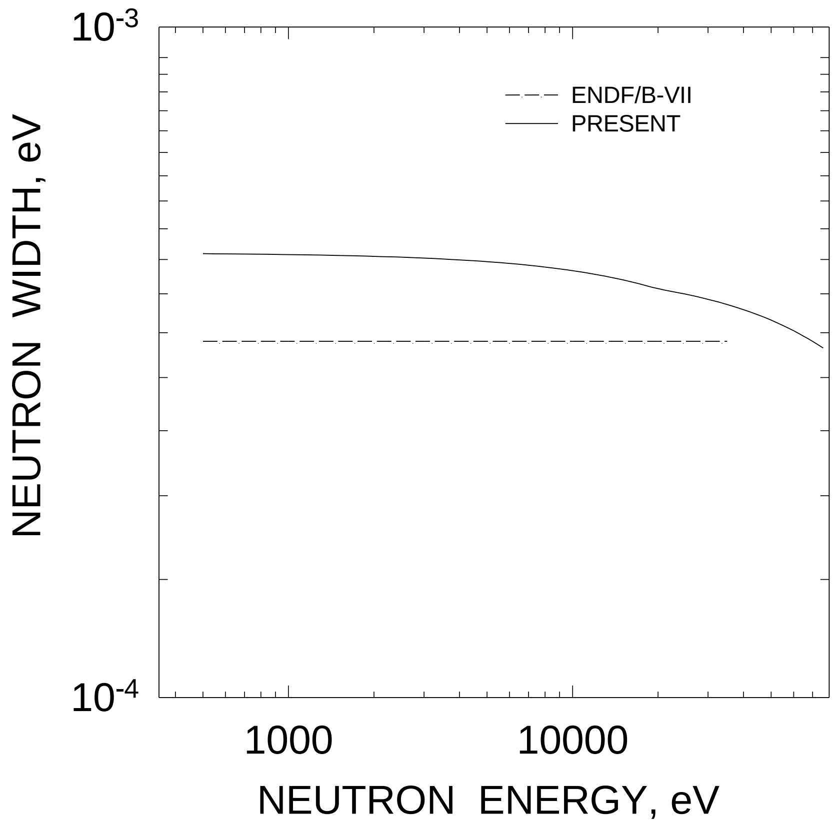

FIG. 4.7. Average reduced neutron width of ^{237}Np, l=1, J=1.

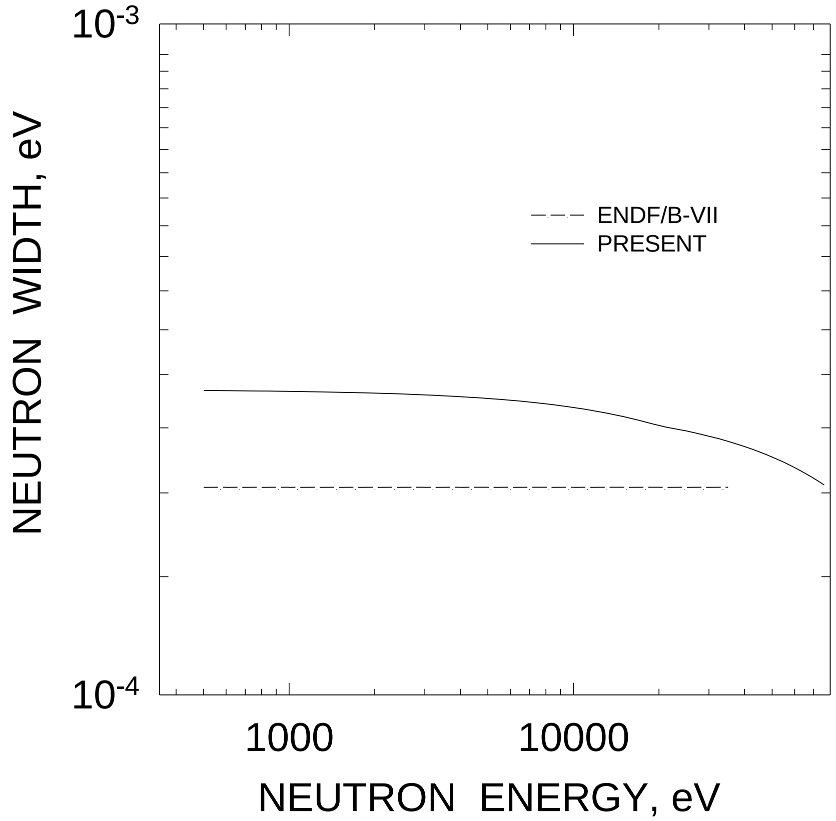

FIG. 4.8. Average reduced neutron width of ^{237}Np, l=1, J=2.

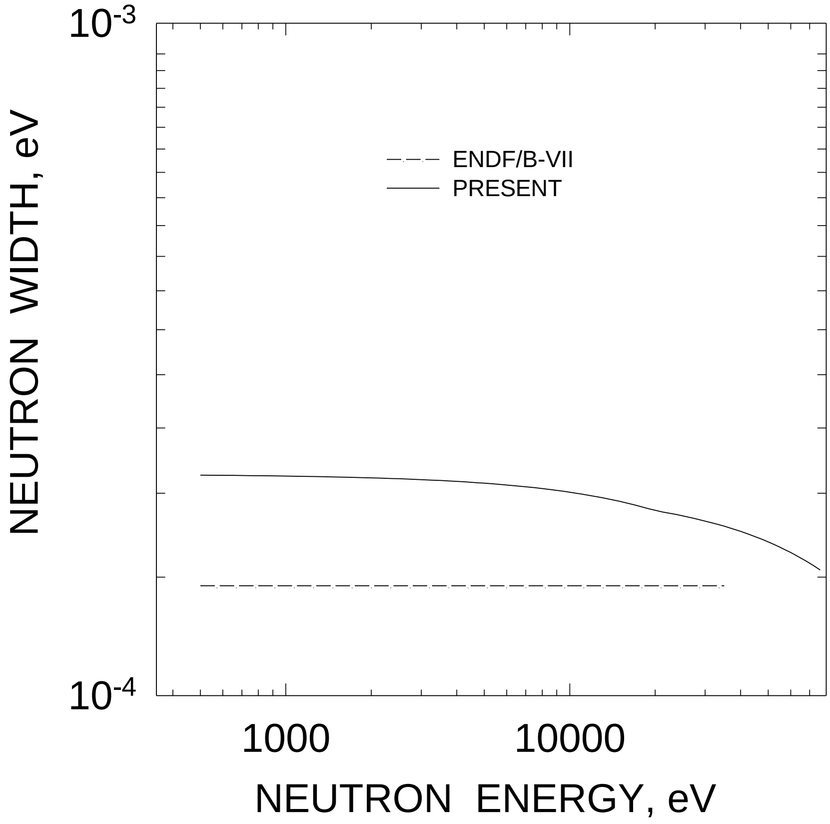

FIG. 4.9. Average reduced neutron width of ^{237}Np, l=1, J=3.

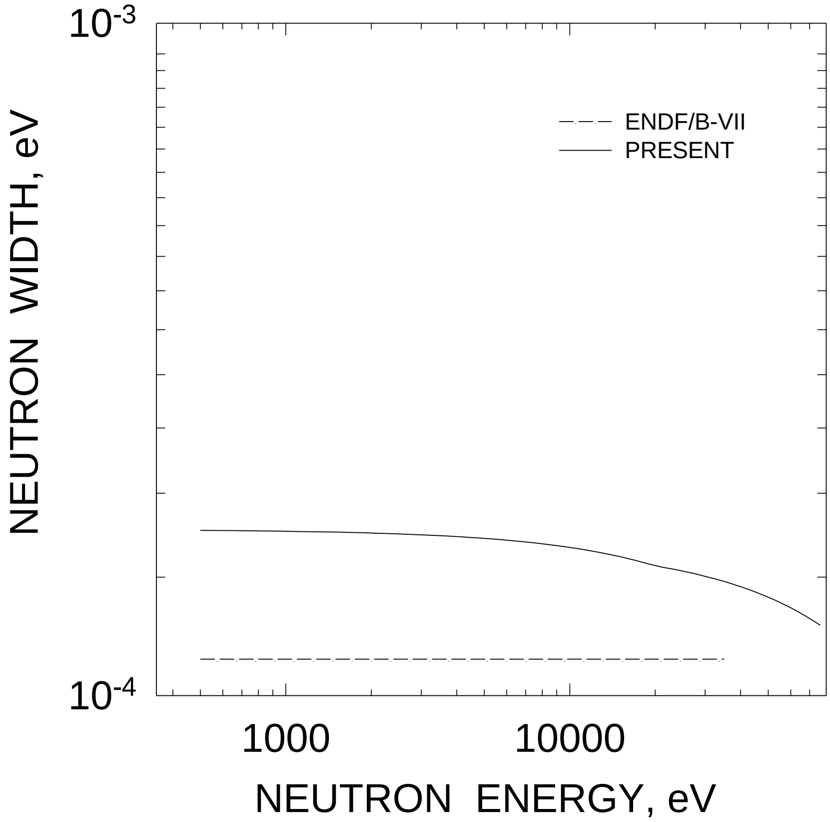

FIG. 4.10. Average reduced neutron width of ^{237}Np, l=1, J=4.

4.6. Total cross section in the region 0.5 keV-76.243 keV

Total cross section data by Auchampaugh, *et al.* [9] in the energy range 20-200 keV were roughly reproduced with the rigid rotator optical model calculations. Coupled channel parameters, fitting data by Kornilov, *et al.* [65] - in the energy range of 0.5-9 MeV and Grigoriev, *et al.* [66] at energies below 50 keV, are defined in [4]. Fig. 4.11 shows that data sets of [9] and [65], which are mutually consistent in wide incident neutron energy range, are systematically discrepant with data [66]. In the energy ranges 0.5-20 keV and 20-76 keV the optical model calculations of the total cross section were reproduced assuming a decreasing trends of S_o, S_1 and S_2 strength function values as the latter and potential radius, which was adopted from the optical model calculations, define total cross section up to E_n=76.243 keV.

The total cross section is calculated with equation:

$$\langle\sigma_t\rangle = \frac{4\pi}{k^2}\sum_l (2l+1)\sin^2\varphi_l + \frac{2\pi^2}{k^2}\sum_l (2l+1)E^{1/2}P_l S_l + \sigma_{\text{int}}. \qquad (4.3)$$

The first term in the equation (4.1) defines the potential scattering cross section, the second one is the neutron absorption cross section and the last one is the interference of resonance and potential scattering:

$$\sigma_{\text{int}} = -\frac{4\pi}{k^2}\sum_l (2l+1)E^{1/2}P_l S_l \sin^2\varphi_l. \qquad (4.4)$$

Neutron wave number of relative motion is defined as:

$$k = \frac{AW}{AW+1}\cdot 2{,}196771\cdot 10^{-3} E_n^{\;1/2}, \qquad (4.5)$$

here E_n is the incident neutron energy, AW is the isotopic mass of the target nuclide. Barrier transmission coefficients P_l and phase shifts φ_l are defined as

$$\begin{aligned} P_0 &= 1; \\ P_1 &= \frac{\rho^2}{1+\rho^2}; \\ P_2 &= \frac{\rho^4}{9+3\rho^2+\rho^4}; \\ P_3 &= \frac{\rho^6}{225+45\rho^2+6\rho^4+\rho^6}; \end{aligned} \qquad (4.6)$$

$$\begin{aligned} \varphi_0 &= z; \\ \varphi_1 &= z - arctg(z); \\ \varphi_2 &= z - arctg(\frac{3z}{3-z^2}); \\ \varphi_3 &= z - arctg(\frac{15z-z^3}{15-6-z^2}), \end{aligned} \qquad (4.7)$$

here $\rho = ka$; $z = kR$; a – channel radius, $a = 0{,}123(AW\cdot 1{,}008665)^{1/3} + 0{,}08{,}10^{-12}$ cm, R – scattering radius, defined as $б_p = 4\pi R^2$ at low incident neutron energies.

To reproduce the ^{237}Np total cross section, calculated with optical model, we assume S_o value linearly decreasing starting from 0.5 keV to 0.9212 × 10^{-4}, while S_1 decreases linearly to 1.8158 × 10^{-4}

at 77 keV (see Fig. 4.11). The d-wave neutron strength function was assumed to be equal to S_2= 1.275 × 10^{-4}. In JENDL-3.3 [7] evaluation the potential scattering radius is R= 0.98491 fm, we assumed R= 0.9516 fm, it is consistent with the coupled channel optical model calculations.

4.7. Elastic scattering cross section

The elastic scattering cross section is composed of shape elastic (see Fig. 4.12) and compound elastic contributions. The latter is calculated as (x=n, s=J^π)

$$\langle \sigma_{nx} \rangle = \frac{2\pi^2}{k^2} \sum_s \frac{g_s}{\langle D \rangle_s} \cdot \frac{\langle \Gamma_n \rangle_s \langle \Gamma_x \rangle_s}{\langle \Gamma \rangle_s} \langle S_x \rangle_s , \tag{4.8}$$

The total decay width equals

$$\langle \Gamma \rangle_s = \langle \Gamma_n \rangle_s + \langle \Gamma_{n'} \rangle_s + \langle \Gamma_f \rangle_s + \langle \Gamma_\gamma \rangle_s , \tag{4.9}$$

the statistical factor g_s equals

$$g_s = \frac{2J+1}{2(2I+1)} . \tag{4.10}$$

Compound elastic scattering cross section estimate is rather insensitive to the ^{237}Np fission cross section estimate. The discrepancy of present and JENDL-3.3 [7] estimates from 0.5 keV and up to 77 keV, shown on Fig. 4.12, appears to be correlated with the different estimates of potential scattering radius R. The curve on Fig. 4.12, labeled as “GMA fit of ^{237}Np(n, γ)” reflects the variations of the fitted capture cross section, shown of Fig. 3.12. To avoid these imposed fluctuations smooth capture cross section as reproduced with average energy dependent resonance parameters is adopted for the evaluated data file.

4.8. Capture cross section

The description of capture cross section data by Esch, *et al.* [51] in the energy range of 1 keV–200 keV is very sensitive to the shape of the neutron absorption cross section. It was shown in [4] that around E_n~1 MeV the total cross section is virtually insensitive to the lowering of the neutron absorption cross section. Lowering of the absorption cross section, simulated by the decrease of the imaginary surface potential term W_D, could be cross-checked by the consistency of fission and inelastic scattering cross sections. In case of ENDF/B-VII.0 [3] the elastic scattering was simply adjusted to balance total and partial cross sections.

Measured data for the ^{237}Np(n, γ) reaction cross section [50, 51, 52] shown on Fig. 4.13, are scattering a lot, albeit there are a systematic shifts between different data sets. The important feedback from the consistent description of total, fission and inelastic scattering data might be the prediction of the capture cross section shape based on the reliable estimate of radiation strength function and neutron absorption cross section.

Fig. 4.14 shows the calculated curve, corresponding to the consistent description of the total, fission and inelastic scattering cross section with $\langle \Gamma\gamma \rangle$ =40.7 meV and $\langle Dobs \rangle$ =0.52 eV. Recent measured data Esch, *et al.* [51] predict distinctly different cross section shape than the other data [50, 52-56]. Relatively low cross section level in 20-200 keV energy range could be reproduced with rather low value of $\langle \Gamma\gamma \rangle$ = 30 meV or decreased by ~1 MeV value of W_D=2.69 MeV, the surface absorption imaginary term of the optical potential. Combined influence of both factors brings the calculated cross section in consistency with the data by Esch, *et al.* [51]

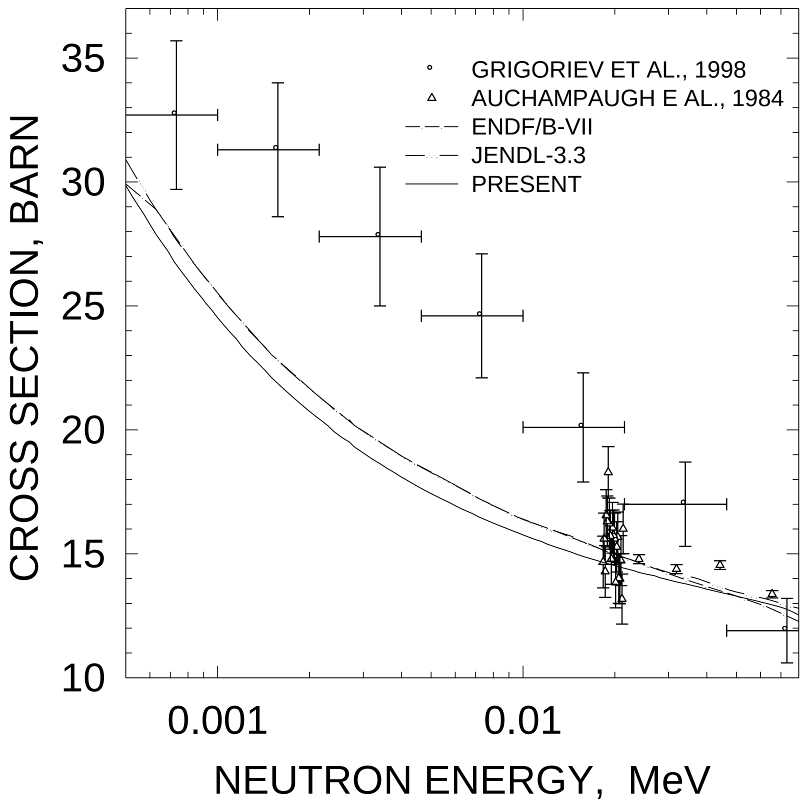

FIG. 4.11. Total cross section of ^{237}Np.

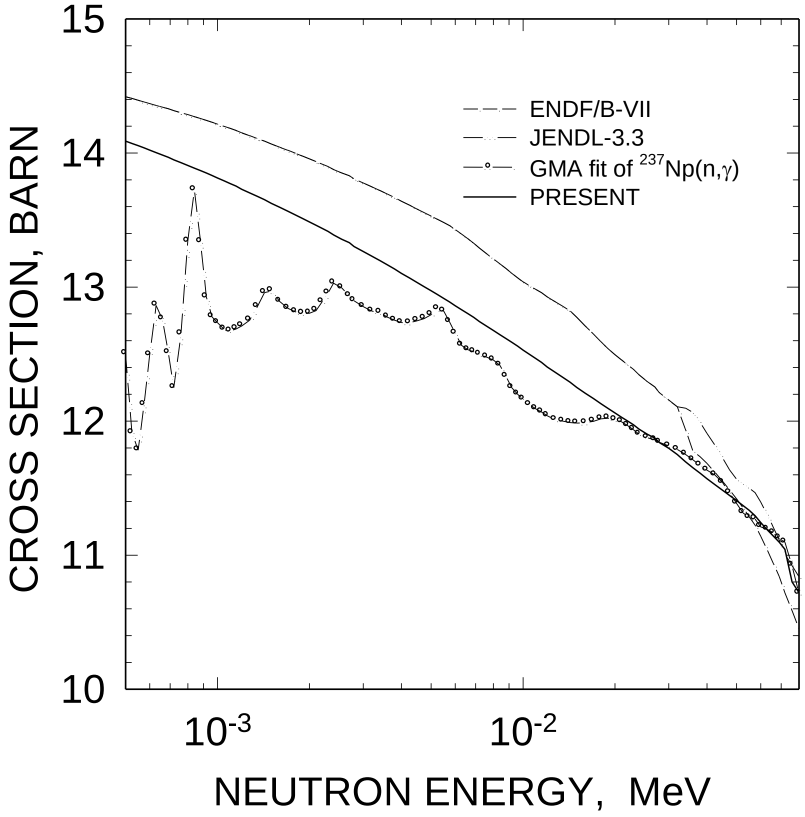

FIG. 4.12. Elastic cross section of ^{237}Np.

in the 4 keV–300 keV energy range. However, the resulting value of *s*-wave neutron strength function S_0 = 0.78×10-4 is much lower than the established value (see Table 4.1). Obviously, the S_0 value could be increased by increasing the β_2, quadrupole deformation parameter value, but after that the calculated capture cross section will again misfit the newest data [51], shown on Fig. 4.14. The high cross section level at incident neutron energies below 1 keV could be reproduced only by drastic increase of the absorption cross section, in that case the value of S_0 would increase up to S_0=1.3×10-4, that possibility should be rejected.

The important peculiarity of the calculated ^{238}U(n, γ) and ^{232}Th(n, γ) capture cross sections, Wigner cusp above first excited level threshold, is pronounced in case of calculated ^{237}Np(n, γ) reaction cross section differently because of larger number of levels in odd ^{237}Np nuclide. The pattern of *s*-, *p*- and *d*-wave entrance channel contributions to the capture cross section in the energy range of 0.5-76 keV is different from that of ^{232}Th [67, 68] or ^{238}U [69] target nuclides (see Fig. 4.15). That might be traced back to higher fissility of ^{238}Np compound nuclide. In case of ^{238}U(n, γ) reaction main contribution comes from p-wave neutrons above ~10 keV. The p-wave contribution to the ^{237}Np(n, γ) reaction cross section is higher than that of *s*-wave above ~30 keV, while that of *d*-wave neutrons is the lowest.

Evaluated capture cross section describes the following data trend: Weston and Todd [50], Kobayashi, *et al.* [52] and Eshch, *et al.* [51] using average radiation width Γ_γ=0.0375 eV and observed neutron resonance spacing D_{obs}=0.553 eV. It should be stressed that the latter data [51] are systematically lower that the calculated capture cross section (see Figs. 4.13, 4.14, 4.15).

4.9. Inelastic scattering cross section

Calculated inelastic scattering cross section is very much different from previous evaluation of JENDL-3.3 [7], but rather close to that of ENDF/B-VII.0 [3] (see Fig. 4.16). Conventional ENDF/B processing codes (i.e. RECENT [70], NJOY [71]) exemplify Hauser-Feshbach-Moldauer formalism. Fig. 4.6 shows partial contributions to the inelastic scattering coming from different *(l, J)*-channels. Major contribution, unlike in case of ^{238}U+n interaction [69], comes from *s*-wave channels (decay of 2^+ and 3^+ states), the intermediate comes from *p*-wave channel (decay of 0^-, 1^-, 2^-, 3^-, 4^- compound nucleus states) and the lowest comes from *d*-wave neutrons (decay of 0^+, 1^+, 2^+, 3^+, 4^+, 5^+ compound nucleus states). At E_n> 60 keV, the contribution from *p*-wave channel (decay of 0^-, 1^-, 2^-, 3^-, 4^- compound nucleus states) becomes the largest, as shown on Fig. 4.16. However, that might be considered as imposed by the fitting procedures employed. Because Hauser-Feshbach-Moldauer formalism is adopted in conventional
ENDF/B processing codes (i.e. RECENT [70], NJOY [71]), the direct excitation of the 0.0332 MeV, $J^\pi=7/2^+$ level is not accounted for explicitly. To compensate for that relevant strength function S_2 for the inelastic scattering exit channel was increased at 77 keV up to 2.9×10^{-4}. That helped to attain, using conventional processing codes, the fit of relevant capture cross section, calculated with the Hauser-Feshbach-Moldauer formalism. In the latter case the direct excitation of the ground state band levels is accounted for explicitly.

4.10. Fission cross section

Evaluated fission cross section describes the trend, predicted by data of Tovesson and Hill [24], Carlson, *et al.* [44], Hoffman, *et al.* [45], Yamanaka, *et al.* [46], Plattard, *et al.* [47] and Brown, *et al.* [48]. We estimated fission cross section in the unresolved resonance energy region using for transition state spectra of ^{238}Np, fission barrier parameters were obtained fitting fission cross section data in the first plateau region (see Fig. 4.17). The fission cross section, calculated with the Hauser-Feshbach-Moldauer formalism, reproduces the GMA evaluation within assigned errors in the incident neutron energy range of 2 keV~77 keV. At lower energies the smooth curve overshoots the data by Tovesson and Hill [24] and Yamanaka, *et al.* [46], which are consistent with each other. As an option possibility was included to use the average resonance

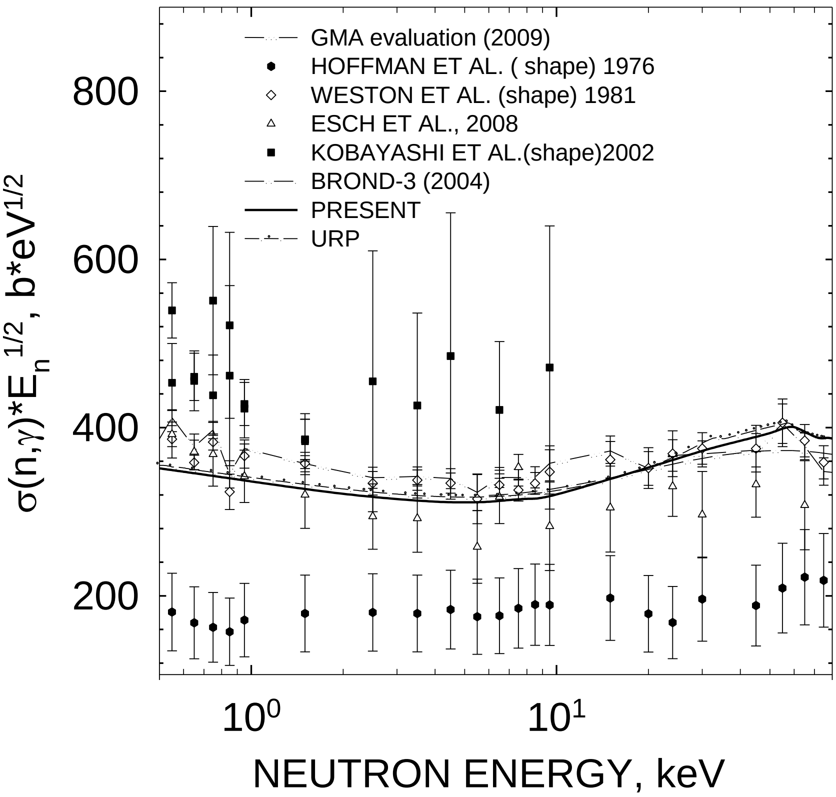

FIG. 4.13. Capture cross section of ^{237}Np.

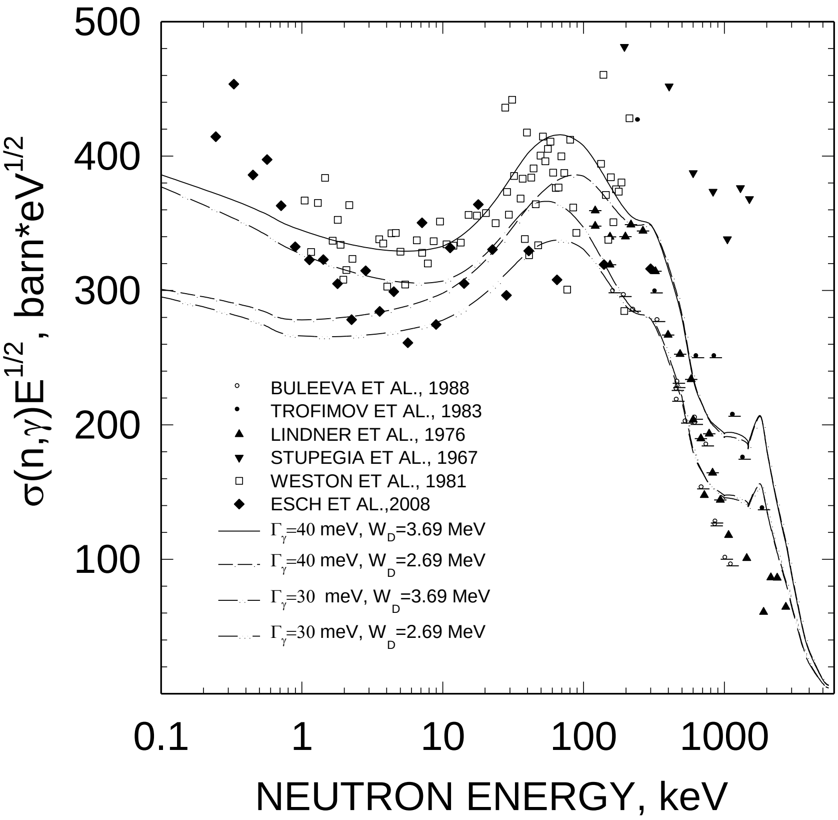

FIG. 4.14. Capture cross section of ^{237}Np.

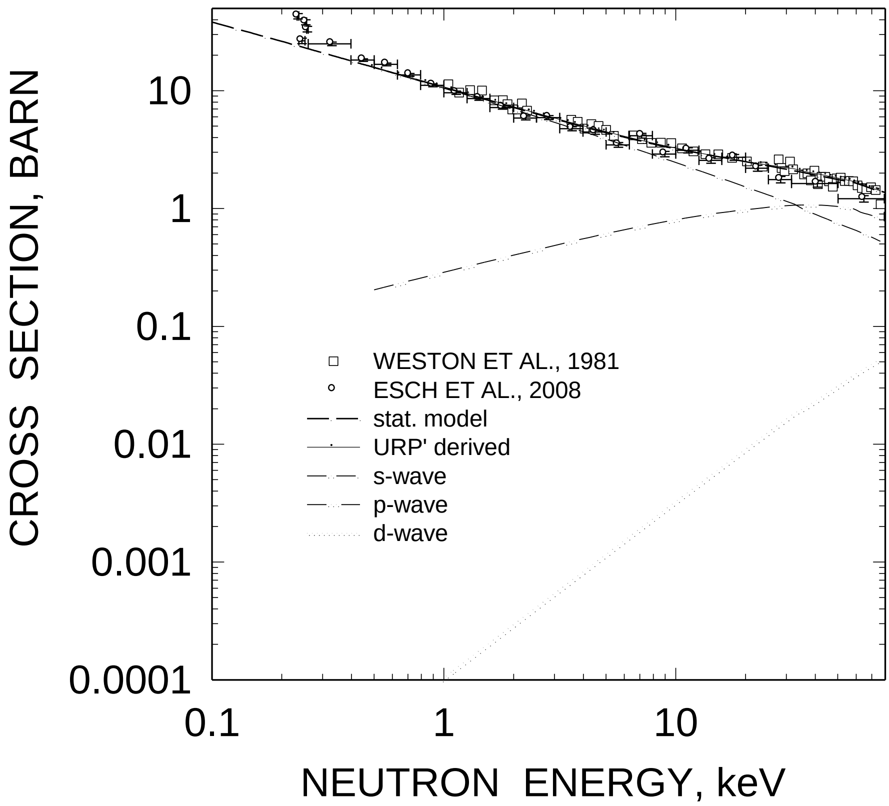

FIG. 4.15. Capture cross section of ^{237}Np.

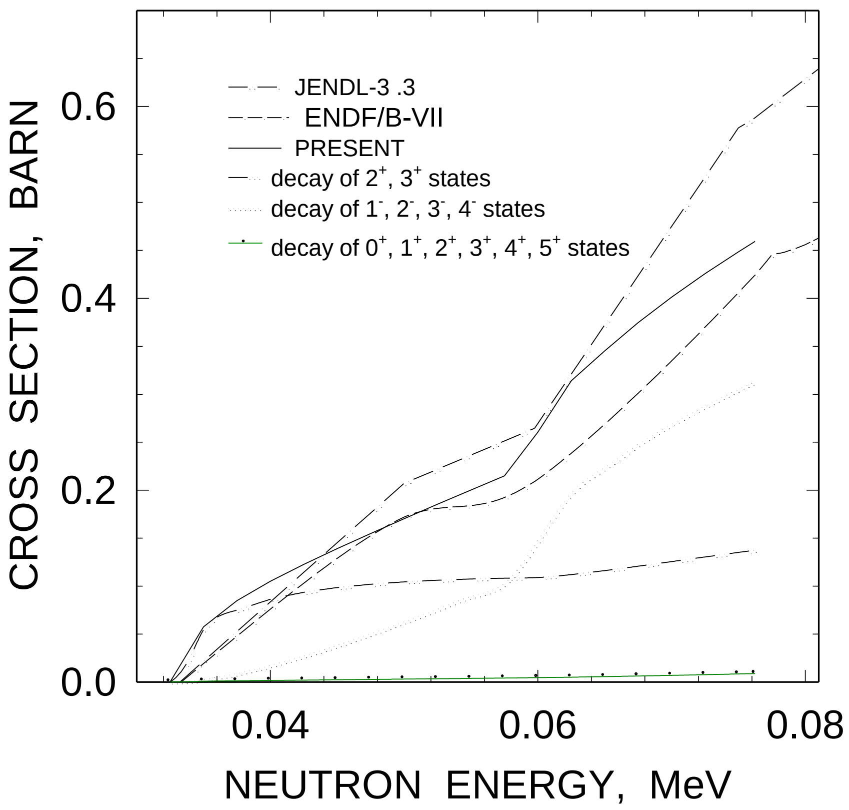

FIG. 4.16. Inelastic cross section of ^{237}Np.

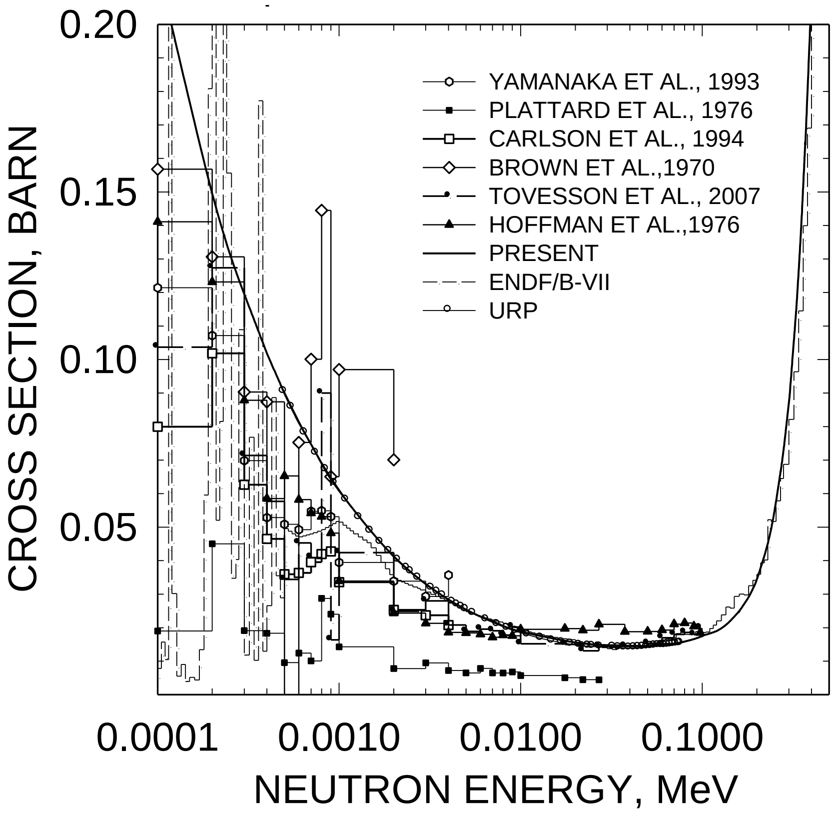

FIG. 4.17. Fission Cross section of ^{237}Np.

parameters for self-shielding calculations only, while the fission cross section is defined by GMA fits.

4. 11. Comparison of average resonance parameters

Figs 4.1-4.4 compare average neutron resonance spacing. Reduced neutron widths are compared on Figs 4.5-4.10. Differences are pronounced in Γ_n^o reduced neutron widths either for *s*- and *p*-wave entrance channels. The advantage of present evaluation is that it provides average energy dependent resonance parameters which reproduce evaluated cross sections, using conventional ENDF/B processing codes [70, 71] up to ~76 keV.

5. Optical potential

Calculated total, elastic scattering and absorption cross sections were obtained with the coupled-channel potential parameters, obtained for the ^{238}U [72], as described in [4]. The experience of describing the capture cross section of ^{232}Th [67, 68] is the motivation to decrease the real volume potential term V_R by 0.5 MeV. Rotational levels of ground state band $5/2^+$-$7/2^+$-$9/2^+$-$11/2^+$ are assumed coupled (see Table 5.1).

Deformation parameters were tuned to fit S_o and S_1 strength function values. Optical model potential parameters are defined as follows:

V_R= (45.722-0.334E) MeV;		r_R =1.2600 fm; a_R =.6300 fm;
W_D= (3.690+0.400E) MeV, E_n< 10 MeV		r_D =1.24 fm;
W_D= 7.690 MeV, $E_n \geq 10$ MeV		a_D =.5200 fm;
V_{SO}= 6.2 MeV;		r_{SO}=1.12 fm;
a_{SO}=.47 fm;	β_2= 0.190	β_4=0.06.

TABLE 5.1. ^{237}Np LEVEL SCHEMA [61].

No.	V_R	J^π
1	0.0	5/2+
2	0.0331964	7/2+
3	0.0595412	5/2-
4	0.07592	9/2+
5	0.10296	7/2-
6	0.1300	11/2+
7	0.15851	9/2-
8	0.19146	13/2+
9	0.22596	11/2-
10	0.26754	3/2-
11	0.2699	15/2+
12	0.28135	1/2-
13	0.30506	13/2-
14	0.32442	7/2-
15	0.33236	1/2+
16	0.3485	17/2+
17	0.3597	5/2-
18	0.36859	5/2+
19	0.37093	3/2+
20	0.39552	15/2-
21	0.43412	11/2-
22	0.45253	9/2+
23	0.45400	19/2+
24	0.45969	7/2+
25	0.48596	9/2-
26	0.49702	17/2-
27	0.51419	3/2-

Partitioning of the total cross section into absorption (reaction) and scattering cross sections allows to get a consistent description of fission and inelastic cross sections in a 1-3 MeV incident neutron energy range within a statistical model.

6. Total and elastic scattering cross section

Auchampaugh, *et al.* [9] measured ^{237}Np+n total cross section in the energy range of 20-200 keV, Kornilov, *et al.* [65] - in the energy range of 0.5-9 MeV and Grigoriev, *et al.* [66] at incident neutron energies below 50 keV. Fig. 6.1 shows that data sets of [65] and [9] appear to be mutually consistent, while systematic discrepancy with data [66] is obvious. The description of capture cross section data by Esch, *et al.* [51] at incident neutron energy range of 1–200 keV is very sensitive to the shape of the absorption cross section. In [4] it was shown (see Fig. 6.2), that around E_n~1 MeV the total cross section is virtually insensitive to the decrease of the imaginary surface potential term W_D, while the lowering of the absorption cross section could be cross checked by consistency of fission and inelastic scattering cross sections. In case of ENDF/B-VII.0 [3] the elastic scattering was simply adjusted to balance total and partial cross sections (see Fig. 6.3).

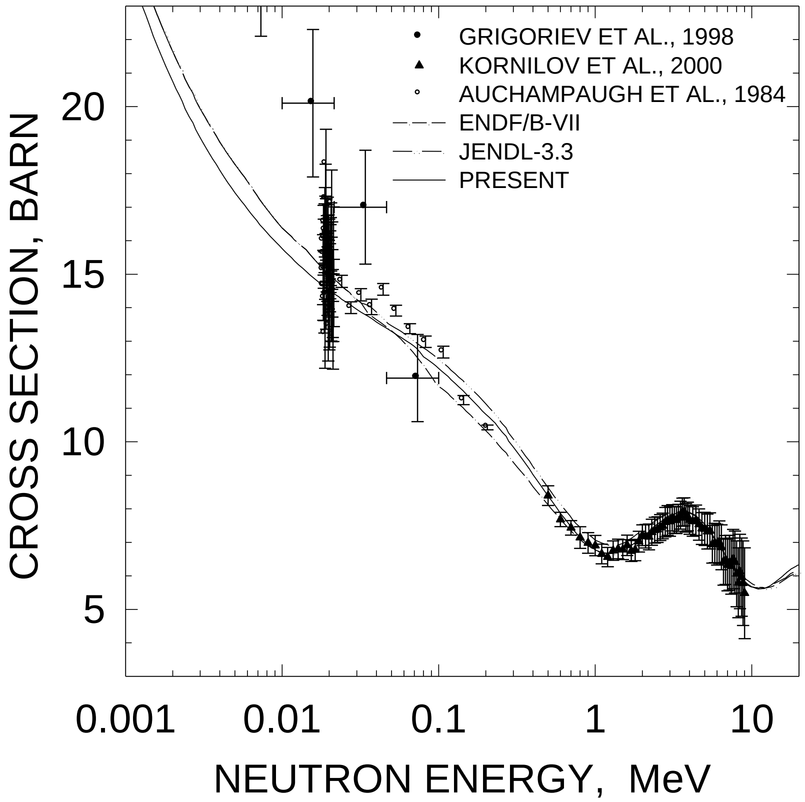

FIG. 6.1. Total cross section of ^{237}Np.

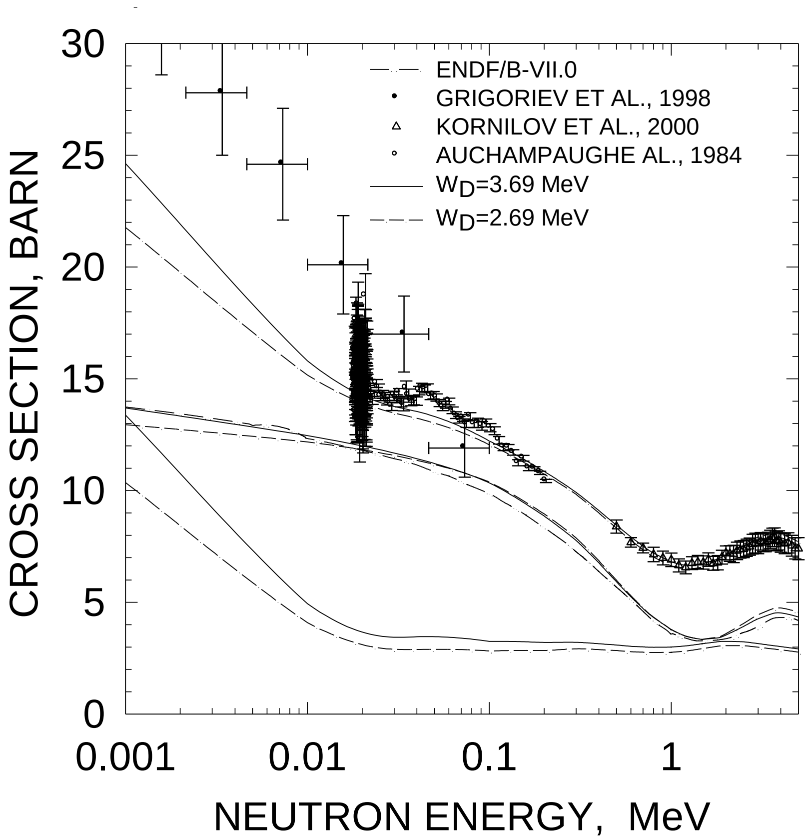

FIG. 6.2. Total, elastic and absorption cross section of ^{237}Np.

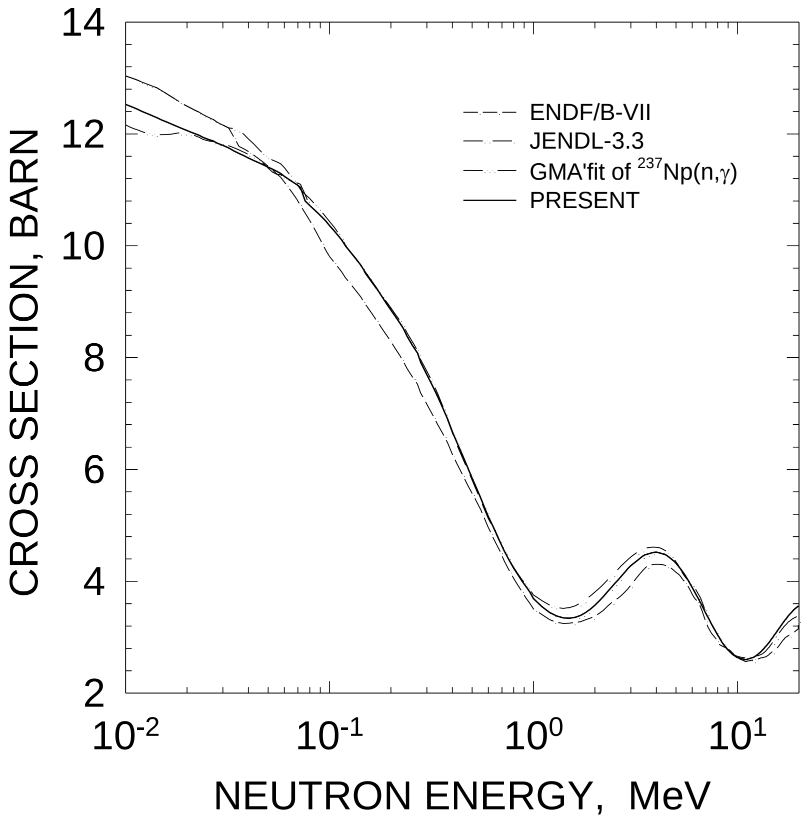

FIG. 6.3. Elastic cross section of ^{237}Np.

7. Statistical model

We calculated neutron cross sections within Hauser-Feshbach theory, coupled channel optical model and double-humped fission barrier model, as distinct from the previous evaluations of JENDL-3.3 [7] and ENDF/B-VII.0 [3].

Hauser-Feshbach-Moldauer [73] and Tepel-Hoffman-Weidenmuller [74] statistical theory is employed for partial cross section calculations below emissive fission threshold. Fissioning and residual nuclei level densities as well as fission barrier parameters are key ingredients, involved in actinide neutron-induced cross section calculations.

In case of fast neutron ($E_n \leq$ 6 MeV) interaction with ^{237}Np target nucleus, the main reaction channel is the fission reaction and fission cross section data description serves as a major constraint for the neutron inelastic scattering and radiative neutron capture cross section estimates. Below there is an outline of the statistical model employed.

Neutron-induced reaction cross section (n, x) for excitation energies up to emissive fission threshold is defined as

$$\sigma_{\mathrm{nf}}\left(\mathrm{E_n}\right)=\frac{\pi\bar{\lambda}^2}{2(2I+1)}\sum_{\mathrm{ljJ}\pi}(2\mathrm{J}+1)\mathrm{T}_{\mathrm{lJ}}^{\mathrm{J}\pi}\left(\mathrm{E_n}\right)\mathrm{P}_{\mathrm{f}}^{\mathrm{J}\pi}\left(\mathrm{E_n}\right)\mathrm{S}_{\mathrm{nf}}^{\mathrm{ljJ}\pi}\ . \tag{7.1}$$

The compound nucleus decay probability $\mathrm{P}_{\mathrm{fL}}^{\mathrm{J}\pi}\left(\mathrm{E_n}\right)$ (x=n, f, γ) is

$$\mathrm{P}_{\mathrm{f}}^{\mathrm{J}\pi}(U)=\frac{\mathrm{T}_{\mathrm{f}}^{\mathrm{J}\pi}(U)}{\mathrm{T}_{\mathrm{f}}^{\mathrm{J}\pi}(U)+\mathrm{T}_{\mathrm{nx}}^{\mathrm{J}\pi}(U)+\mathrm{T}_{\gamma x}^{\mathrm{J}\pi}(U)}, \tag{7.2}$$

where $U=B_n+E_n$ is the excitation energy of the compound nucleus, B_n is the neutron binding energy, $\mathrm{T}_{\mathrm{lJ}}^{\mathrm{J}\pi}\left(\mathrm{E_n}\right)$ are the entrance neutron transmission coefficients for the channel (ljJπ), I is the target nucleus spin, j is the entrance channel spin. Decay probability $\mathrm{P}_{\mathrm{fL}}^{\mathrm{J}\pi}\left(\mathrm{E_n}\right)$ of the compound nucleus with excitation energy U for given spin J and parity π, depends on $T_f^{J\pi}(U), T_{nx}^{J\pi}(U)$ and $T_{\gamma x}^{J\pi}(U)$ transmission coefficients of the fission, neutron scattering and radiative decay channels, respectively, $S_{nf}^{ljJ\pi}$ denotes partial widths Porter-Thomas fluctuation factor. Below incident neutron energy equal to the cut-off energy of discrete level spectra, neutron cross sections are calculated within Hauser-Feshbach approach with correction for width fluctuation by Moldauer [73]. For width fluctuation correction calculation only Porter-Thomas fluctuations are taken into account. Effective number of degrees of freedom for fission channel is defined at the higher fission barrier saddle as $\nu_f^{J\pi} = T_f^{J\pi} / T_{fmax}^{JK\pi}$ where $T_{fmax}^{JK\pi}$ is the maximum value of the fission transmission coefficient. At higher incident neutron energies the Tepel, *et al.* [74] approach is employed, it describes cross section behavior in case of large number of open channels correctly.

7.1. Level Density

Level density is the main ingredient of statistical model calculations. Level density of fissioning, residual and compound nuclei define transmission coefficients of fission, neutron scattering and radiative decay channels, respectively. We will briefly discuss here level densities of odd-even ^{237}Np and ^{238}Np nuclides.

The level densities were calculated with a phenomenological model by Ignatyuk, *et al.* [58], which takes into account shell, pairing and collective effects in a consistent way

$$\rho(U, J^{\pi}) = K_{rot}(U, J) K_{vib}(U) \rho_{qp}(U, J^{\pi}), \tag{7.3}$$

where quasi-particle level density is defined as

$$\rho_{qp}(U, J^{\pi}) = \frac{(2J+1)\omega_{qp}(U)}{4\sqrt{2\pi}\sigma_{\perp}^2 \sigma} \exp\left[-\frac{J(J+1)}{2\sigma_{\perp}^2} \right], \tag{7.4}$$

$\rho_{qp}(U, J^{\pi})$ is the state density, $K_{rot}(U, J)$ and $K_{vib}(U)$ are factors of rotational and vibrational enhancement of the level density. The collective contribution of the level density of deformed nuclei is defined by the nuclear deformation order of symmetry. The actinide nuclei at equilibrium deformation are axially symmetric. The order of symmetry of nuclear shape at inner and outer saddles were adopted from calculations within shell correction method (SCM) by Howard & Moeller [75], neptunium nuclei of interest ($234 \leq A \leq 238$) are assumed to be axially asymmetric, then

$$K_{rot}^{sym}(U) = \sum_{K=-J}^{J} \exp\left(-\frac{K^2}{K_o^2} \right) \approx \sigma_{\perp}^2 = F_{\perp} t, \tag{7.5}$$

$$K_o^2 = (\sigma_{||}^{-2} - \sigma_{\perp}^{-2})^{-1}, \tag{7.6}$$

where $\sigma_{\perp}^2$ and $\sigma_{||}^2$ are spin cutoff parameters, $F_{\perp}$ is the nuclear momentum of inertia (perpendicular to the symmetry axis), which equals the rigid-body value

$$F_{\perp}^{rig} = F_{||} t = \frac{2}{5} m_0 r_o^2 A^{5/3} \left(1 + \frac{1}{3}\varepsilon \right), \tag{7.7}$$

at high excitation energies, where the pairing correlations are destroyed, experimental value at zero temperature and is interpolated in between, using the pairing model;

$$\sigma_{||}^2 = F_{||} t = \frac{6}{\pi^2} \langle m^2 \rangle a \left(1 - \frac{2}{3}\varepsilon \right) t, \tag{7.8}$$

where $\langle m^2 \rangle$ is the average value of the squared projection of the angular momentum of the single-particle states, and ε is the quadrupole deformation parameter. At outer saddle deformations mass asymmetry, which doubles the level density, is assumed. The closed-form expressions for thermodynamic temperature and other relevant equations which one needs to calculate $\rho(U, J^{\pi})$ provided by Ignatyuk model [58].

To calculate the residual nucleus level density at the low excitation energy, i.e. just above the last discrete level excitation energy where $N^{exp}(U) \approx N^{theor}(U)$, we employ a Gilbert-Cameron-type approach. The procedure is as follows. First, level density parameters are defined, using neutron resonance spacing $\langle D_{obs} \rangle$ estimate for ^{237}Np target nuclide. Constant temperature level density parameters T_o, E_o, U_c (see below for details) are defined by fitting cumulative number of low-lying levels of ^{237}Np (see Fig. 7.1) [15, 16]. Figure 7.2 shows the estimate of cumulative number of low-lying levels of ^{238}Np, obtained using systematic of constant temperature level density parameters T_o, E_o, U_c [15, 16]. On this figure levels of the odd-odd ^{238}Np nuclide are compared with constant temperature model estimate. The constant temperature approximation of the level density

$$\rho(U) = \frac{dN(U)}{dU} = \frac{1}{T}\exp\left(\frac{U - U_o}{T}\right) \tag{7.9}$$

is extrapolated up to the matching point U_c to the $\rho(U)$ value, calculated with a phenomenological model by Ignatyuk [60] with the condition

$$U_c = U_o - T\ln(T\rho(U_c)). \tag{7.10}$$

In this approach $U_o \approx -m\Delta_o$, where Δ_o is the pairing correlation function, $\Delta_o = 12/\sqrt{A}$, A is the mass number, m = 2 for odd-odd, 1 for odd-even nuclei, i.e. U_o has the meaning of the odd-even energy shift. The value of nuclear temperature parameter T is obtained by the matching conditions of Eq. (7.10) at the excitation energy U_c.

In present approach the modeling of total level density

$$\rho(U) = K_{rot}(U, J)K_{vib}(U)\frac{\omega_{qp}(U)}{\sqrt{2\pi}\sigma} = \frac{1}{T}\exp\left(\frac{U - U_o}{T}\right) \tag{7.11}$$

in Gilbert-Cameron-type approach looks like a simple renormalization of quasi-particle state density $\omega_{qp}(U)$ at excitation energies U< U_c. The cumulative number of observed levels for odd-even ^{237}Np and odd-odd nuclide ^{238}Np [61] are compared with constant temperature approximations for ^{237}Np and ^{237}Np on Figs 7.1 and 7.2, respectively. Missing of levels above ~0.5 MeV is markedly pronounced in case ^{238}Np.

Few-quasi-particle effects which are due to pairing correlations are essential for state density calculation at low intrinsic excitation energies only for equilibrium ^{237}Np deformations. Few-quasi-particle effects in fissioning nuclide ^{238}Np are unimportant because of its odd-odd nature.

The partial n-quasi-particle state densities for odd ^{237}Np, which sum-up to intrinsic state density of quasi-particle excitations, could be modeled using the Bose-gas model prescriptions [58, 76, 77]. The intrinsic state density of quasi-particle excitations $\omega_{qp}(U)$ could be represented as a sum of n-quasi-particle state densities $\omega_{nqp}(U)$:

$$\omega_{qp}(U) = \sum_n \omega_{nqp}(U) = \sum_n \frac{g^n (U - U_n)^{n-1}}{((n/2)!)^2 (n-1)!}, \tag{7.12}$$

where $g = 6a_{cr}/\pi^2$ is a single-particle state density at the Fermi surface, n is the number of quasi-particles. The important model parameters are threshold values U_n for excitation of n-quasi-particle configurations employed, as applied for fission, inelastic scattering or capture reaction

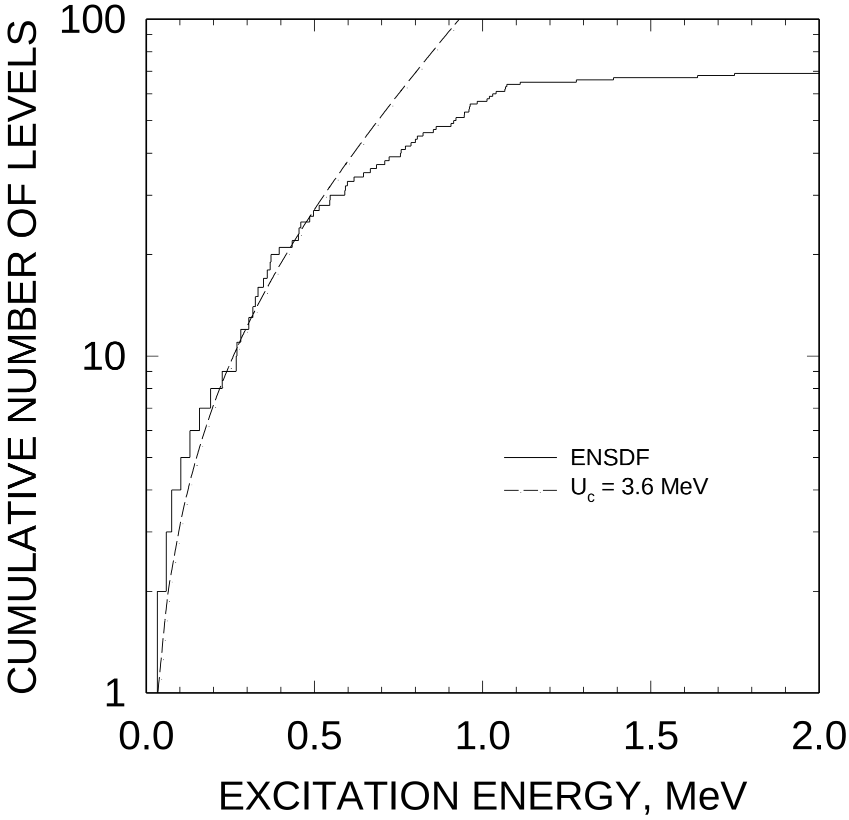

FIG. 7.1. Cumulative sum of levels of ^{237}Np.

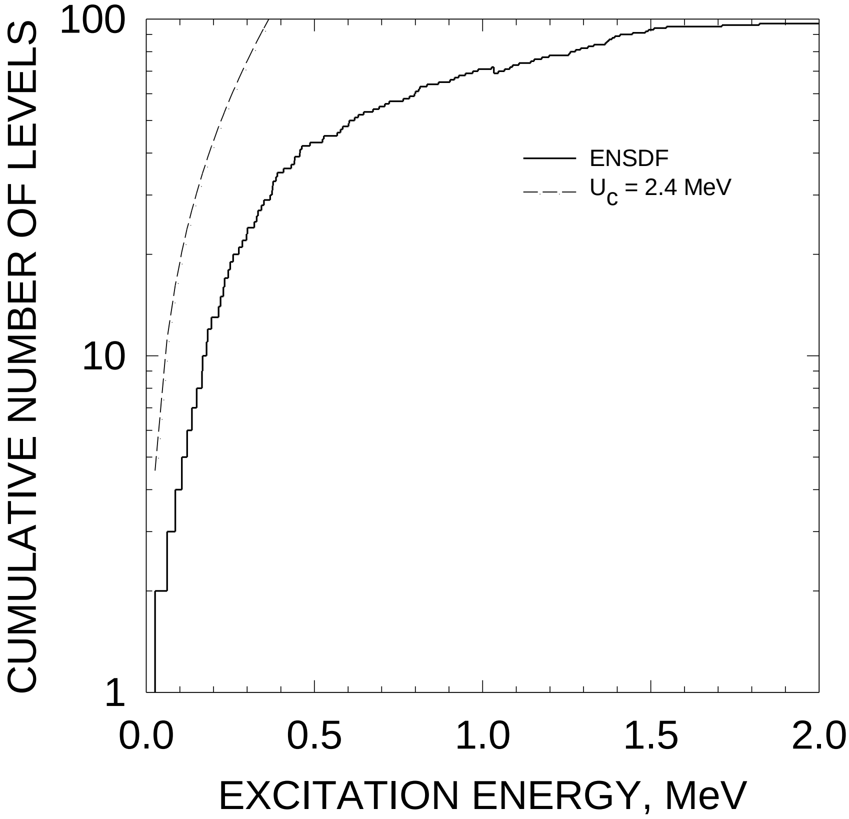

FIG. 7.2. Cumulative sum of levels of ^{238}Np.

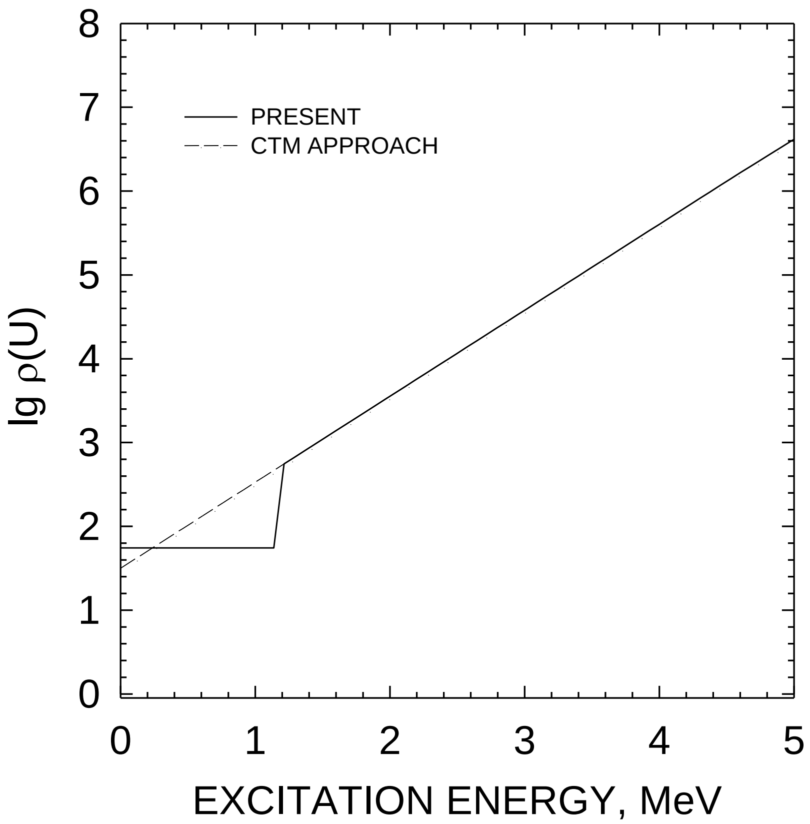

FIG. 7.3. Level density of ^{237}Np.

calculations, is provided in [77, 78].

In case of and odd-odd nucleus ^{238}Np Gilbert-Cameron-type approximation of $\rho(U)$ is employed. Nuclear level density $\rho(U)$ of odd nuclide ^{237}Np at equilibrium deformation, as compared with the Gilbert-Cameron-type approximation of $\rho(U)$ is shown on Fig. 7.3. The arrows on the horizontal axis of Fig. 7.3 indicate the excitation thresholds of odd n-quasi-particle configurations.

Main parameters of the level density model for equilibrium, inner and outer saddle deformations are as follows: shell correction δW, pairing correlation functions Δ and Δ_f, at equilibrium deformations $\Delta_o = 12/\sqrt{A}$, quadrupole deformation ε and momentum of inertia at zero temperature F_o/h^2 are given in Table 7.1. For ground state deformations the shell corrections were calculated as $\delta W = M^{exp} - M^{MS}$, where M^{MS} denotes liquid drop mass (LDM), calculated with Myers-Swiatecki parameters [79], and M^{exp} is the experimental nuclear mass. Shell correction values at inner and outer saddle deformations $\delta W_f^{A(B)}$ are adopted following the comprehensive review by Bjornholm and Lynn [80].

TABLE 7.1. LEVEL DENSITY PARAMETERS OF FISSIONING NUCLEUS AND RESIDUAL NUCLEUS

Parameter	Inner saddle	Outer saddle	Neutron channel
δW, MeV	2.5*	0.6	LDM
Δ, MeV	$\Delta_o + \delta$**	$\Delta_o + \delta$**	Δ_o
ε	0.6	0.8	0.24
F_o/h^2, MeV	100	200	73

*) for axially asymmetric deformations, 1.5 MeV for axially symmetric deformations;

**) $\delta = \Delta_f - \Delta_o$ value is defined by fitting fission cross section in the plateau region.

7.2. Fission cross section

Fission data fit is used as a major constraint for capture, elastic and inelastic scattering, (n, 2n) and (n, 3n) cross sections as well as secondary neutron spectrum estimation. Description of measured fission cross section might justify a validity of level density description and fission barrier parameterization.

7.2.1. Fission Channel

Fission barrier of Np is double-humped [80], in the first "plateau" region and at higher energies we can use double-humped barrier model and relevant barrier parameters. Even at lower energies we could describe the general shape of the fission cross section starting from 0.500 keV.

Neutron-induced fission in a double humped fission barrier model could be viewed as a two-step process, i.e. a successive crossing over the inner hump A and over the outer hump B. Hence, the transmission coefficient of the fission channel $\mathrm{T}_{\mathrm{f}}^{\mathrm{J}\pi}(U)$ can be represented as

$$\mathrm{T}_{\mathrm{f}}^{\mathrm{J}\pi}(U)=\frac{\mathrm{T}_{\mathrm{f\,A}}^{\mathrm{J}\pi}(U)\mathrm{T}_{\mathrm{f}\,B}^{\mathrm{J}\pi}(U)}{\mathrm{T}_{\mathrm{fA}}^{\mathrm{J}\pi}(U)+\mathrm{T}_{\mathrm{fB}}^{\mathrm{J}\pi}(U)}. \tag{7.13}$$

The transmission coefficient $\mathrm{T}_{\mathrm{fi}}^{\mathrm{J}\pi}(U)$ is defined by the level density $\rho_{fi}(\varepsilon, J, \pi)$ of the fissioning nucleus at the inner and outer humps (i = A, B, respectively):

$$\mathrm{T}_{\mathrm{fi}}^{\mathrm{J}\pi}(U)= \sum_{K=-J}^{J}\mathrm{T}_{\mathrm{fi}}^{\mathrm{JK}\pi}(U)+\int_0^U \frac{\rho_{fi}(\varepsilon, J, \pi)d\varepsilon}{1+\exp\left(2\pi\left(E_{fi}+\varepsilon-U\right)/\hbar\omega_i\right)}, \tag{7.14}$$

where the first term denotes the contribution of low-lying collective states and the second term that coming from the continuum levels at the saddle deformations, ε is the intrinsic excitation energy of fissioning nucleus. The first term contribution due to discrete transition states depends upon saddle symmetry. The total level density $\rho_{fi}(\varepsilon, J, \pi)$ of the fissioning nucleus is determined by the order of symmetry of nuclear saddle deformation.

Inner and outer fission barrier heights and curvatures as well as level densities at both saddles are the model parameters. They are defined by fitting fission cross section data at incident neutron energies below emissive fission threshold. Fission barrier height values and saddle order of symmetry are strongly interdependent. The order of symmetry of nuclear shape at saddles was defined by Howard and Moller [75] within shell correction method (SCM) calculation. We adopt the saddle point asymmetries from SCM calculations. According to shell correction method (SCM) calculations of Howard and Moller [75] the inner barriers were assumed axially asymmetric. Outer barriers for the neptunium nuclei are assumed mass-asymmetric.

7.2.2. Fission transmission coefficient, level density and transition state spectrum

Adopted level density description allows describe shape of measured fission cross section data of ^{237}Np (see Figs 7.4 - 7.7). One- and two-quasi-particle states in odd residual nuclide ^{237}Np could be excited. The transition state spectra of odd-odd ^{238}Np nuclide for the band-heads of Table 7.2 were constructed using values of F_o/h^2 at the inner and outer saddles shown in Table 7.1.

We construct the discrete transition spectra up to 75 keV, using collective states of Table 7.2. The discrete transition spectra, as well as continuous level contribution to the fission transmission coefficient are dependent upon the order of symmetry for fissioning nucleus at inner and outer saddles. With transition state spectra thus defined the fission barrier parameters are obtained.

7.3. Fission data analysis

Fission cross section is calculated within statistical model from 0.5 keV up to the emissive fission threshold. Measured fission data [22 - 48] analysis was accomplished within GMA approach, as described above. Statistical model calculations in the energy of .5 keV~6 MeV are maintained, calculated cross sections deviate from the GMA evaluation within the GMA-estimated uncertainties.

We fit the decreasing trend of the fission cross section data above E_n≈3 MeV increasing the correlation function value at outer saddle, which controls the ^{237}Np(n, f) cross section shape. For incident neutron energies up to E_n≈3 MeV the threshold shape is roughly reproduced by varying the density of one-quasi-particle states of the residual nuclide ^{237}Np, as described in [4] (see Figs 7.4 - 7.7). Smooth statistical model calculations are adopted as evaluated fission cross section in the energy range of 0.5 keV~6 MeV.

TABLE 7.2. TRANSITION SPECTRA BAND-HEADS, Z-odd, N-even NUCLEI

Inner saddle A		Outer saddle B	
K^π	$E_{K\pi}$, MeV	K^π	$E_{K\pi}$, MeV
2^+	0	2^+	0
3^+	0.05	3^+	0.05
3^-	0.05	3^-	0.05
2^-	0.05	2^-	0.05

7.4. Inelastic scattering

Fission data fit largely defines the compound inelastic neutron scattering contribution to the total inelastic scattering cross section. The relative contribution of direct discrete level excitation cross sections is much higher than in case of say ^{238}U target nuclide due to much higher fission competition to the compound neutron scattering. That explains the sensitivity of the ^{237}Np compound inelastic scattering cross section to the fission competition and modeling of the residual nuclide level density.

7.4.1. Neutron Channel

The lumped transmission coefficient of the neutron scattering channel is given by equation

$$T_n^{J\pi}(U) = \sum_{l'j'q'} T_{l'j'}^{J\pi}(E - E_{q'}) + \sum_{l'j'I'} \int_0^{U-U_c} T_{l'j'}^{J\pi}(E')\rho(U - E', I'^{\pi})dE', \tag{7.15}$$

where $\rho(U - E', I'^{\pi})$ is the level density of the residual nucleus. Levels of residual nuclide ^{237}Np are provided in Table 5.1. The entrance channel neutron transmission coefficients $T_{l'j'}^{J\pi}(E')$ are calculated within a rigid rotator coupled channel approach. For the compound nucleus formation cross section calculation, the cross sections of the direct excitation of ground state band levels were subtracted from the absorption cross section. The compound and direct inelastic scattering components are added incoherently. The exit neutron transmission coefficients $T_{l'j'}^{J\pi}(E')$ were calculated using the re-normalized deformed optical potential of entrance channel without coupling, which describes a neutron absorption cross section.

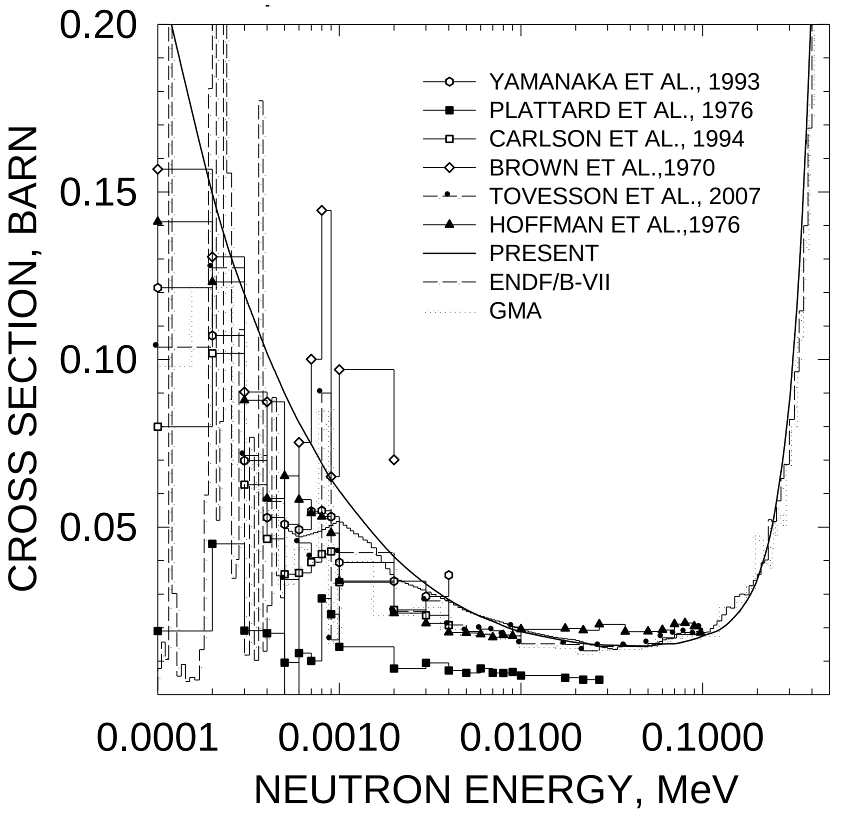

FIG. 7.4. Fission cross section of ^{237}Np.

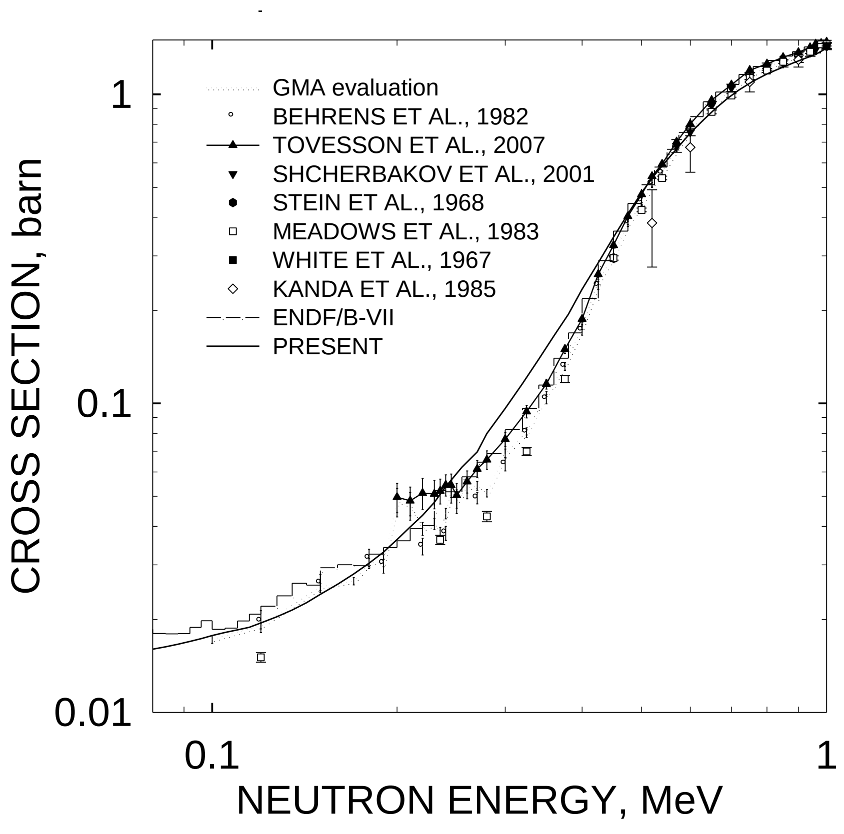

FIG. 7.5. Fission cross section of ^{237}Np.

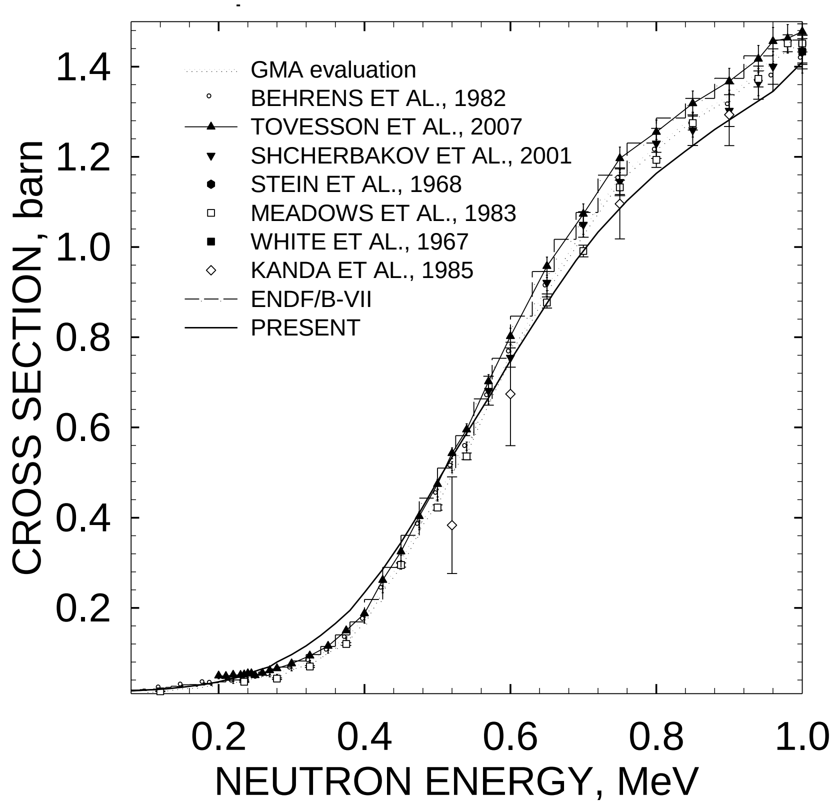

FIG. 7.6. Fission cross section of ^{237}Np.

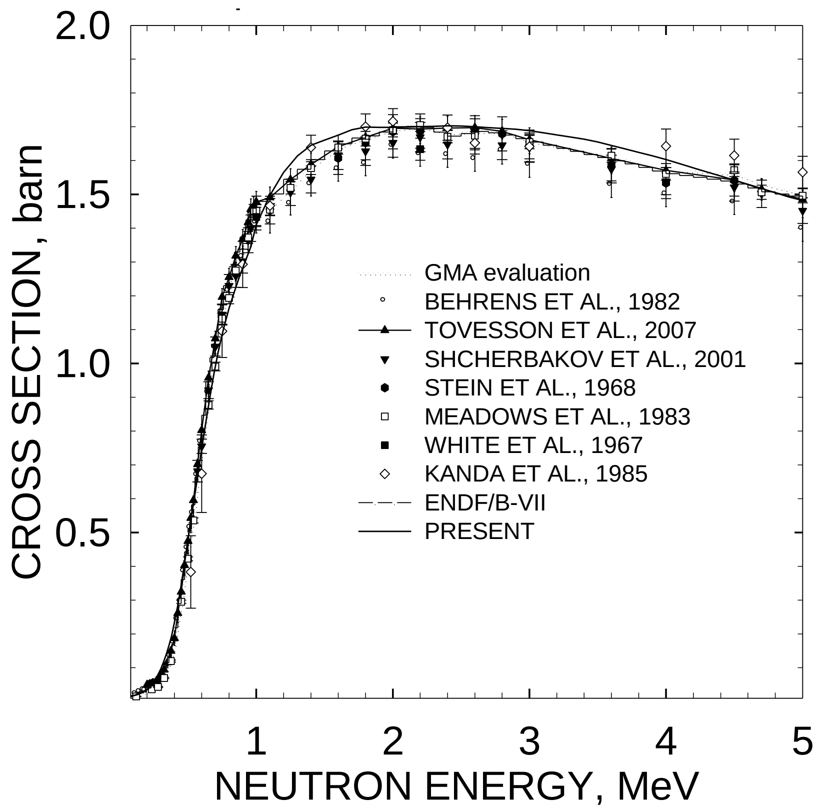

FIG. 7.7. Fission cross section of ^{237}Np.

7.4.2. Ground State Rotational Band

Predicted discrete level excitation cross section shape, calculated within a rigid rotator model, depends upon optical potential used. We assume strong missing of levels above excitations of 0.515 MeV (see Fig. 7.1), so only 27 levels up to this excitation energy were included when calculating inelastic scattering cross sections. Predicted discrete level excitation cross section shape, calculated within a rigid rotator model, strongly depends upon optical potential used. Calculated compound contribution is controlled mainly by fission competition (see Figs 7.8 - 7.10). Figs 7.8 and 7.10 show that direct scattering essentially defines the excitation cross section of $J^{\pi}=7/2^{+}$ and $J^{\pi}=9/2^{+}$ levels of the ground state band levels at $E \geq 1$ MeV. Discrepancies with previous evaluation of JENDL-3.3 [7] are due to both compound and direct contributions differences. The compound component tends to be zero above incident neutron energy of ~3 MeV.

7.4.3. Total inelastic cross section

Direct inelastic contributions were added incoherently to Hauser-Feshbach calculated values of compound nucleus inelastic scattering cross sections. Total inelastic and continuum inelastic cross sections reproduce inelastic scattering data by Kornilov, *et al.* [57] for the excitation of specific groups of continuum levels.

It seems that E_n~1 MeV is a "stabilization point" of inelastic scattering cross section (see Fig. 7.11). Present calculation is based on the fits of the total and fission cross sections. The evaluated inelastic cross sections of ENDF/B-VII.0 [3] and JENDL-3.3 [7] evaluations would be in severe disagreement with data by Kornilov, *et al.* [65] on the inelastic scattering of neutrons with excitation of specific groups of levels, with energies spanning the range 0.25 MeV–(E_n-0.25 MeV) (see Fig. 7.12 and 7.13).

Upward trend of the inelastic data at $E_n \geq 1.5$ MeV might be explained by the sharp increase of the level density of the residual nuclide ^{237}Np due to the onset of three-quasi-particle excitations [4] (see Fig. 7.3). The calculation with the decreased absorption cross section, simulated with W_D=(2.690+0.400E) MeV undershoots the measured data [65]. The total inelastic scattering cross section is much lower, than that corresponding to the higher absorption cross section That is the sound proof of the adopted estimate of the absorption cross section, which is supported both by the S_0 strength function value at low energies and consistent description of fission and inelastic scattering data. The evaluations of ENDF/B-VII.0 [3] and JENDL-3.3 [7] would overshoot the data by Kornilov, *et al.* [65] well outside the assigned experimental uncertainties. The continuum levels contribution to the total inelastic scattering cross section is shown on Fig. 7.14 and Fig. 7.15.

7.5 Capture cross sections

We have demonstrated by the analysis of measured capture cross sections of ^{238}U(n, γ) and ^{232}Th(n, γ) [67, 68, 69] that neutron capture data could be described within a Hauser-Feshbach-Moldauer [73, 74] statistical model, reproducing delicate variations of the measured cross sections with the increase of the incident neutron energies. Specifically, in a few-keV energy region calculated capture cross section is defined by the radiative strength function value $S_\gamma = \Gamma_\gamma/D$. At incident neutron energies above $E_n \approx 100$ keV calculated capture cross section shape is defined by the energy dependence of the radiative strength function S_γ. Energy dependence of S_γ is controlled mainly by the energy dependence of the level density of the compound nuclide ^{238}Np. Rather low fission threshold for the ^{238}Np nuclide defines rather strong competition of fission [60] alongside with neutron emission [59] at the second γ-cascade, i.e. after first γ-quanta emission.

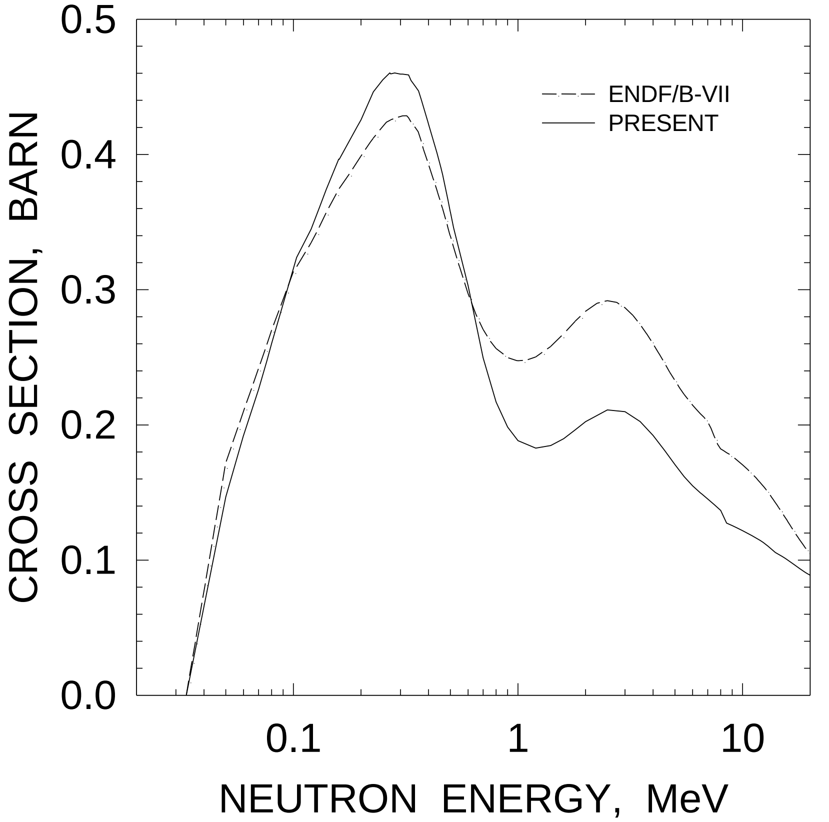

FIG. 7.8. Inelastic cross section of 1st level of ^{237}Np.

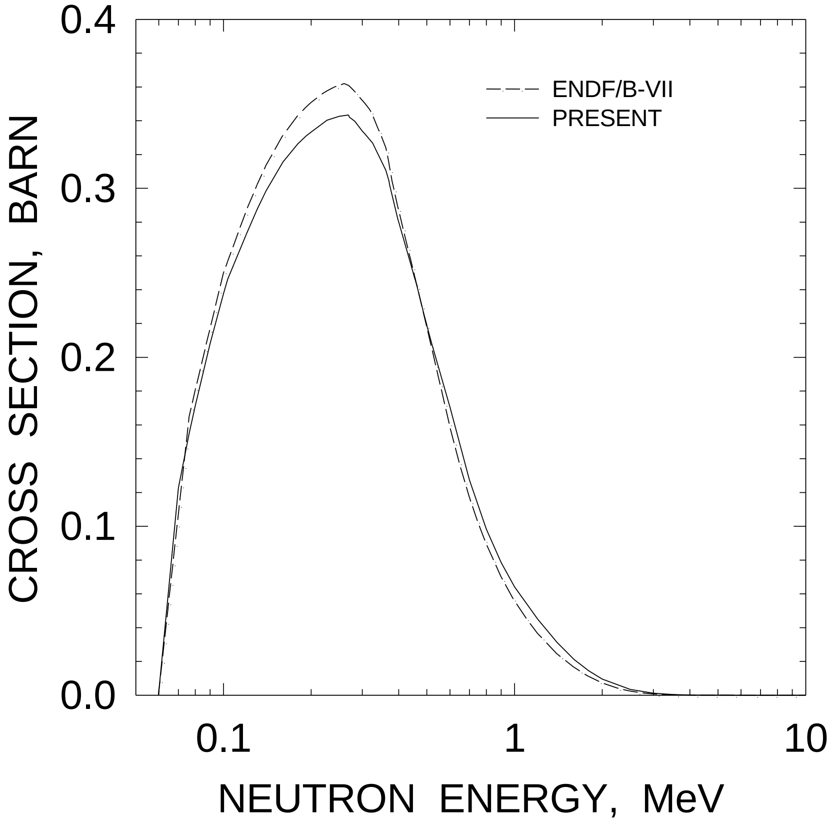

FIG. 7.9. Inelastic cross section of 2nd level of ^{237}Np.

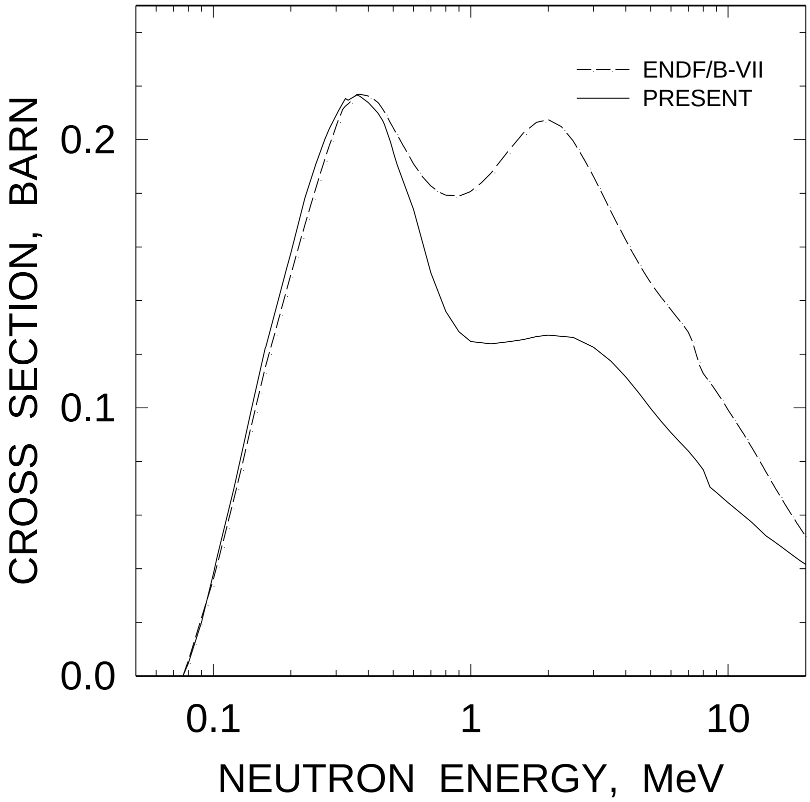

FIG. 7.10. Inelastic cross section of 3^{rd} level of ^{237}Np.

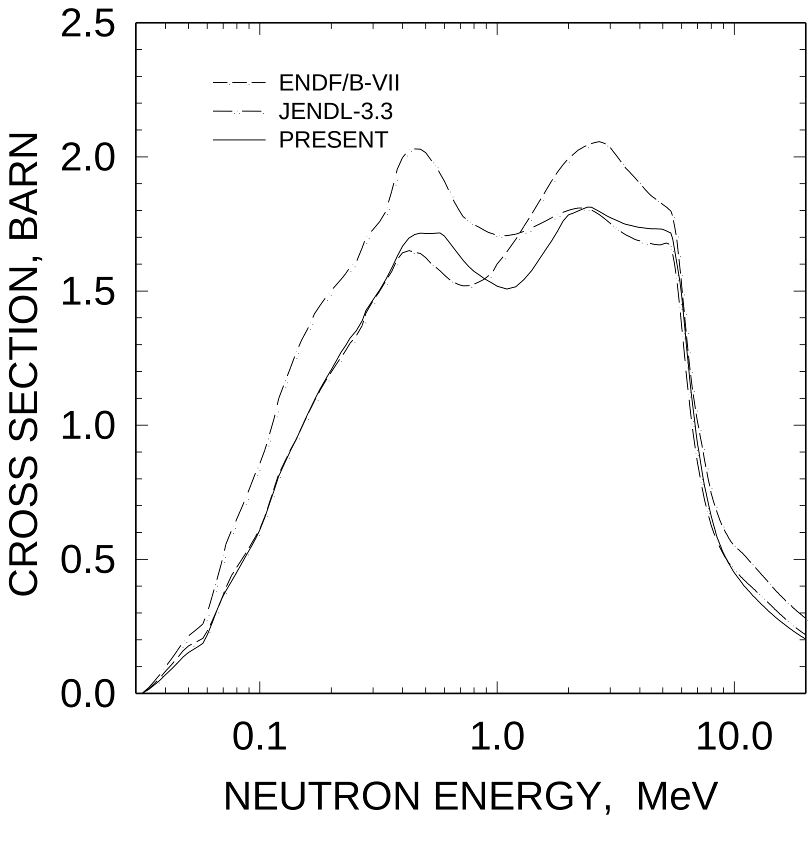

FIG. 7.11. Inelastic cross section of ^{237}Np.

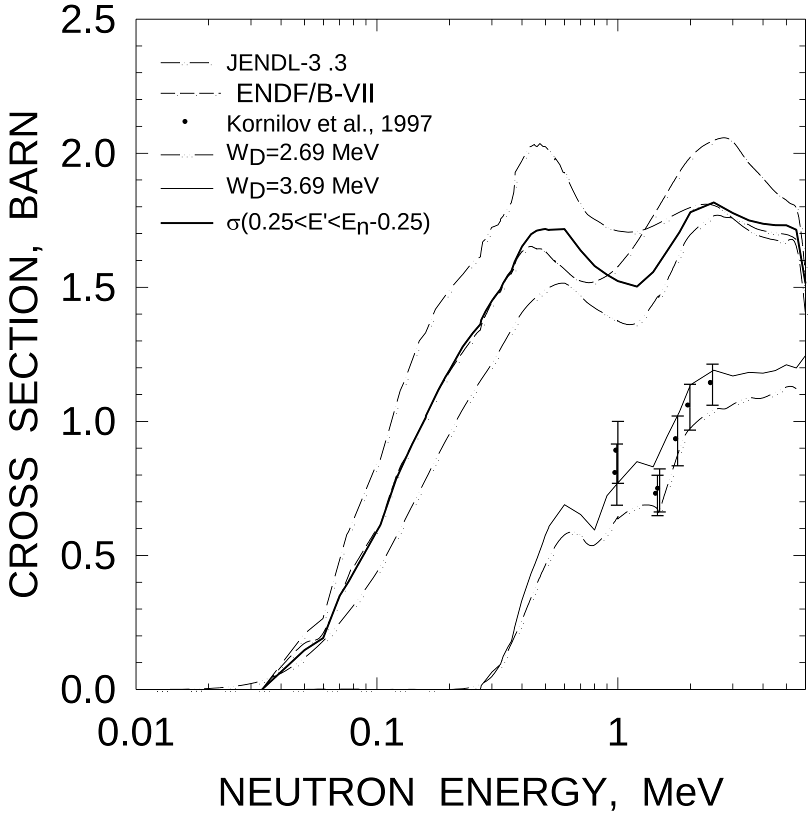

FIG. 7.12. Inelastic cross section of ^{237}Np.

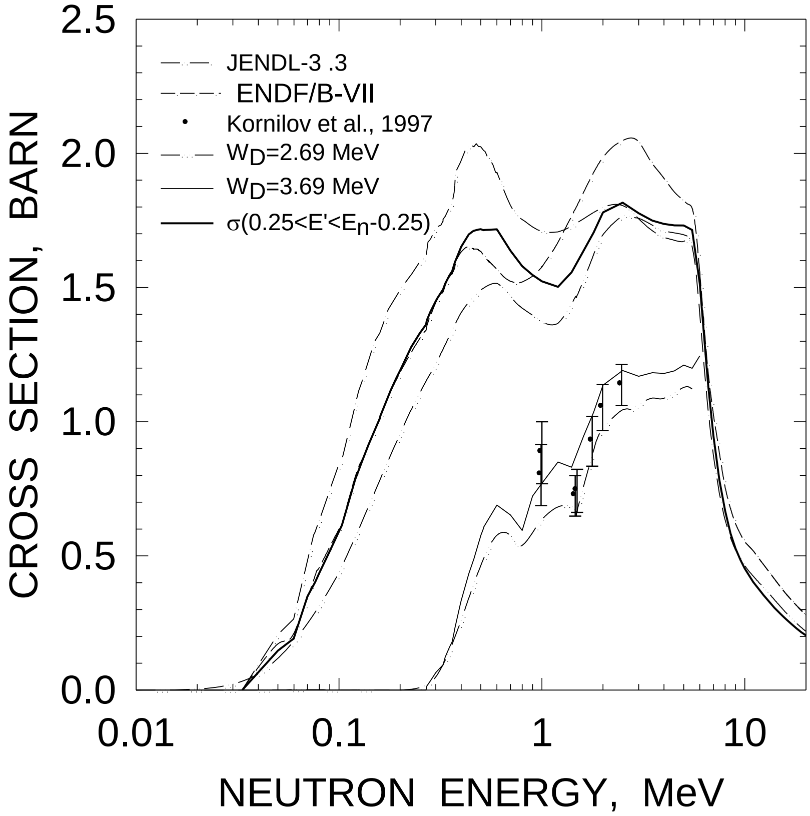

FIG. 7.13. Inelastic cross section of ^{237}Np.

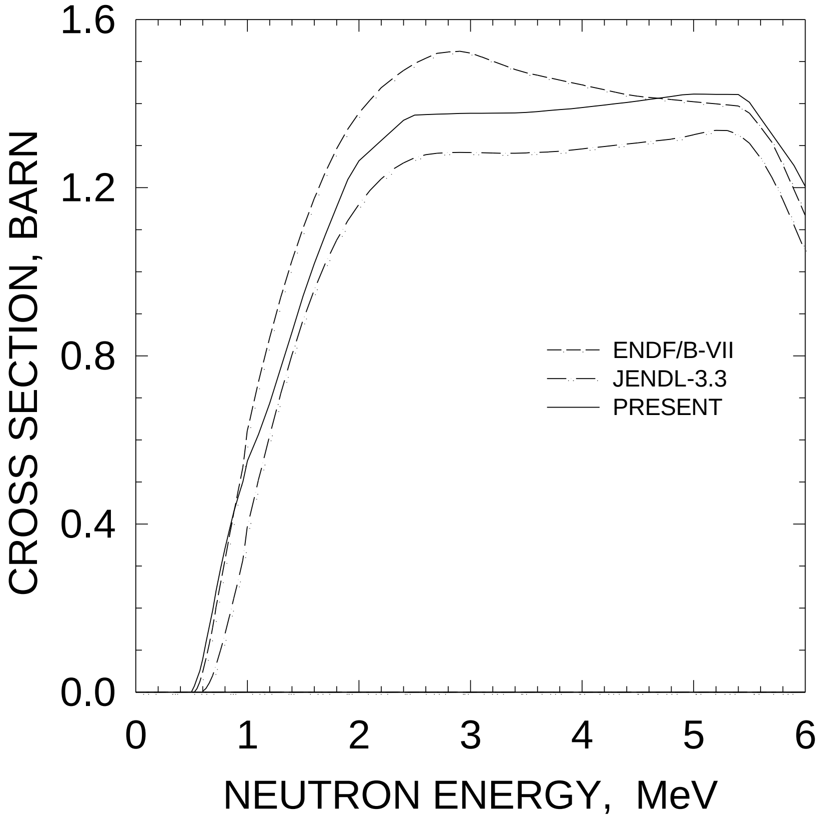

FIG. 7.14. Inelastic cross section of ^{237}Np(continuum contribution)

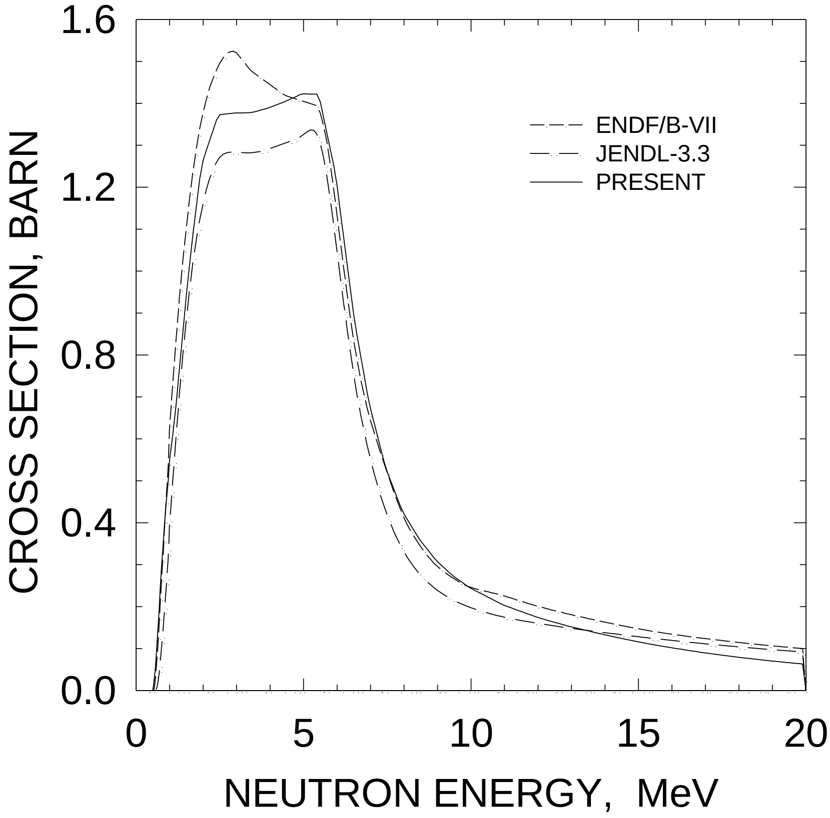

FIG. 7.15. Inelastic cross section of ^{237}Np(continuum contribution).

Then "true" capture reaction cross section (n, γγ) is defined using transmission coefficient $T_{\gamma\gamma}^{J\pi}(E)$, which is defined in a two-cascade approximation as

$$T_{\gamma\gamma}^{J\pi}(E)=\frac{2\pi C_{\gamma 1}}{3(\pi\hbar c)^2}\int_0^{E_n+B_n}\varepsilon_\gamma^2\sigma_\gamma(\varepsilon_\gamma)\sum_{I=|J-1|}^{I=J+1}\rho(U-\varepsilon_\gamma,I,\pi)\frac{\mathrm{T}_\gamma^{\mathrm{I}\pi}(U)}{\mathrm{T}_{\mathrm{f}}^{\mathrm{I}\pi}(U)+\mathrm{T}_{\mathrm{n'}}^{\mathrm{I}\pi}(U)+\mathrm{T}_\gamma^{\mathrm{I}\pi}(U)}d\varepsilon_\gamma\,. \quad (7.16)$$

The last term of the integrand describes the competition of fission, neutron emission and γ-emission at excitation energy ($U-\varepsilon_\gamma$) after emission of first γ-quanta, $C_{\gamma 1}$ is the normalizing coefficient. That means that transmission coefficients $\mathrm{T}_{\mathrm{f}}^{\mathrm{I}\pi}(U), \mathrm{T}_{\mathrm{n'}}^{\mathrm{I}\pi}(U), \mathrm{T}_\gamma^{\mathrm{I}\pi}(U)$ are defined at excitation energy ($U-\varepsilon_\gamma$). The neutron emission after emission of first γ-quanta strongly depends on the ^{237}Np residual nuclide level density at excitations around the pair-braking threshold in odd nuclide U_3. The contribution of (n, γf)-reaction [60] to the fission cross section is defined by $T_{\gamma f}^{J\pi}(E)$ value. The energy dependence of (n, γf) reaction transmission coefficient $T_{\gamma f}^{J\pi}(E)$ was calculated with the expression

$$T_{\gamma f}^{J\pi}(E)=\frac{2\pi C_{\gamma 1}}{3(\pi\hbar c)^2}\int_0^{E_n+B_n}\varepsilon_\gamma^2\sigma_\gamma(\varepsilon_\gamma)\sum_{I=|J-1|}^{I=J+1}\rho(U-\varepsilon_y,I,\pi)\frac{\mathrm{T}_f^{\mathrm{I}\pi}(U)}{\mathrm{T}_{\mathrm{f}}^{\mathrm{I}\pi}(U)+\mathrm{T}_{\mathrm{n'}}^{\mathrm{I}\pi}(U)+\mathrm{T}_\gamma^{\mathrm{I}\pi}(U)}d\varepsilon_\gamma\,. \quad (7.17)$$

Competition of (n, γn') reaction is taken into account in a similar way. Above neutron energy 5.5 MeV capture cross section is assumed to be 0.001 barn.

Trends of the measured data by Weston and Todd [50], Eshch, *et al.* [51], Kobayashi, *et al.* [52], Lindner, *et al.* [56], Buleeva, *et al.* [53] Stupegia, *et al.* [54], Trofimov, *et al.* [55] are inconsistent with each other. Measured data for the ^{237}Np(n, γ) reaction cross section [50 - 56] shown on Fig. 7.16, are scattering a lot, albeit there are a systematic shifts between different data sets. The important feedback from the consistent description of total, fission and inelastic scattering data might be the prediction of the capture cross section shape based on the estimate of radiation strength function and absorption cross section.

The sensitivities of the capture cross section to radiation strength function and absorption cross section are illustrated on Figs 4.14, 7.16 and 7.17. Fig. 4.14 [4] shows the calculated capture cross section curve, corresponding to the description of the total, fission and inelastic scattering cross section with $<\Gamma_\gamma>$ = 40.7 meV and $<D_{obs}>$ = 0.52 eV. Recent measured data [51] predict distinctly different cross section shape than the other data [50, 52 - 56]. Relatively low cross section level in 20-200 keV energy range could be reproduced with much decreased value of $<\Gamma_\gamma>$ = 30 meV or decreased by ~1 MeV value of W_D = 2.69 MeV. Combined influence of both factors brings the calculated cross section in consistency with the data by Esch, *et al.* [51] in the 4 keV–300 keV energy range. However, the resulting value of $S_o = 0.78\times10^{-4}$ appears to be much lower than the established value [18]. Obviously, the *s*-wave neutron strength function S_o value could be increased by increasing the β_2, quadrupole deformation parameter value, but after that the calculated capture cross section will again misfit the newest data [51], shown on Figs 7.15, 7.17. The high cross section level below 1 keV could be reproduced only by drastic increase of the absorption cross section, in that case the value of S_0 would increase up to 1.3x10^{-4}. That possibility also should be rejected. The shape of the capture cross section, shown on Figs 7.16, 7.17 resembles the increased competition of fission and inelastic scattering channels to the radiation capture channel. Another factor is the entrance channel, exemplified by the neutron transmission coefficients. The evaluated cross section of ENDF/B-VII.0 [3] does not reproduces the measured data in the energy range of 100-1000 keV possibly due to decreased competition of inelastic scattering or fission in the exit channels giving major contribution to the capture cross section. The increased trend of the present calculated capture cross section around E_n~1.5 MeV might be explained by the complicated competition of capture and inelastic scattering exit channels.

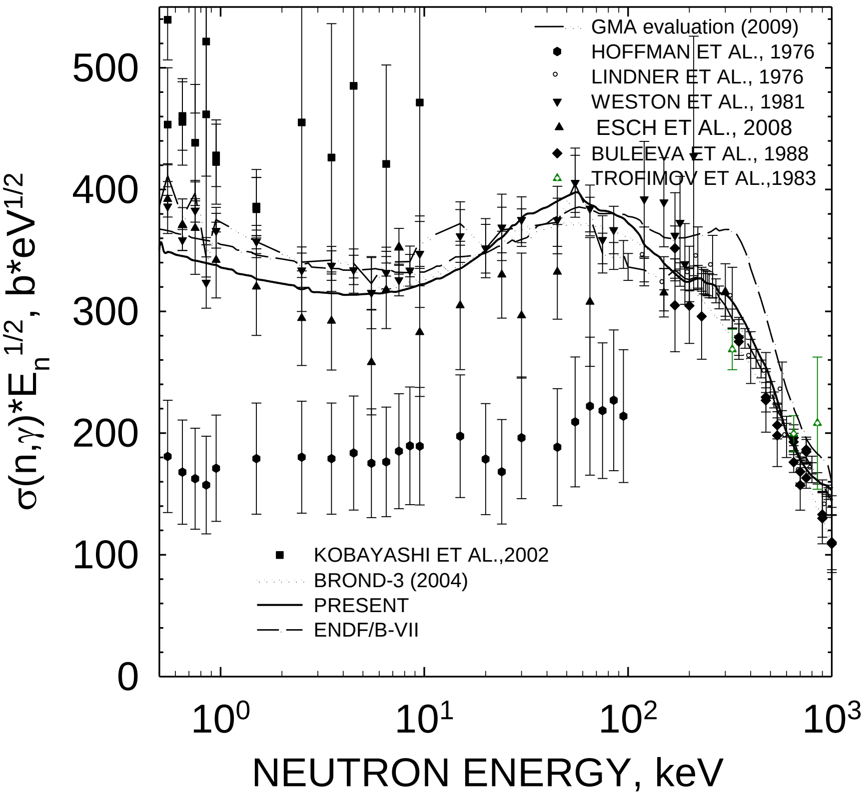

FIG. 7.16. Capture cross section of ^{237}Np.

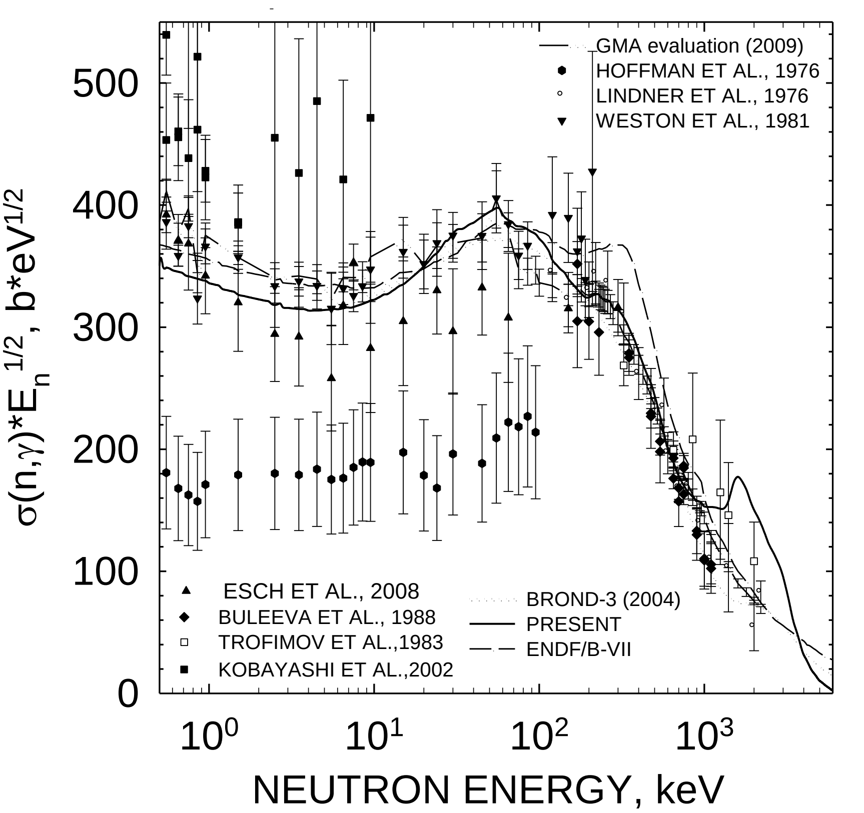

FIG. 7.17. Capture cross section of ^{237}Np.

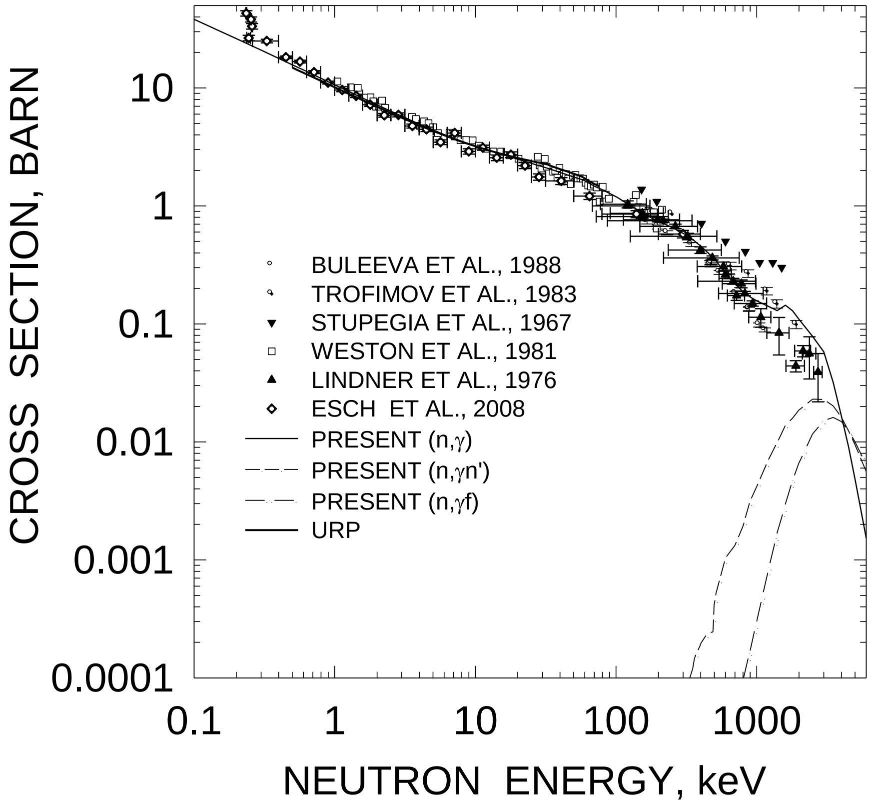

FIG. 7.18. Capture cross section of ^{237}Np.

At E_n~1.5 MeV one observes strong increase of the inelastic scattering cross section ^{237}Np(n, n') (see Fig. 7.12).

Finally, Fig. 7.18 shows calculated capture cross section and competition of ^{237}Np(n, γf) and ^{237}Np(n, γn') reactions to the "true" capture reaction ^{237}Np(n, γγ), the define the capture cross section shape at E_n≥2 MeV.

8. Fission cross section above emissive fission threshold

At incident neutron energies when fission of ^{237}Np or ^{236}Np nuclides is possible, as well as fission of ^{238}Np, after emission of 1 or 2 pre-fission neutrons, the observed ^{237}Np(n, F) fission cross section is a superposition of non-emissive or first chance fission of ^{238}Np

$$\sigma_{\mathrm{nf}}(\mathrm{E_n}) = \mathrm{q}(\mathrm{E_n})\frac{\pi\bar{\lambda}^2}{2(2I+1)}\sum_{\mathrm{lJ}\pi}(2\mathrm{J}+1)\mathrm{T_l}(\mathrm{E_n})\mathrm{P_f^{J\pi}}(\mathrm{E_n}), \tag{8.1}$$

and xth-chance fission contributions as

$$\sigma_{\mathrm{nF}}(E_n) = \sigma_{\mathrm{nf}}(E_n) + \sum_{x=1}^{X}\sigma_{\mathrm{n,xnf}}(E_n). \tag{8.2}$$

The contributions to the observed fission cross section $\sigma_{\mathrm{n,xnf}}(E_n)$, coming from (n, xnf), x= 1, 2, 3...X, fission of relevant equilibrated neptunium nuclei are weighted with a probability of x neutron emission before fission. These cross sections are calculated as

$$\sigma_{\mathrm{n,xnf}}(E_n) = \sum_{J\pi}\int_0^{U_{\max}} W_{x+1}^{J\pi}(U)P_{f(x+1)}^{J\pi}(U)dU\ , \tag{8.3}$$

where $W_x^{J\pi}$ is the population of (x+1th) nucleus at excitation energy U after emission of x neutrons, excitation energy U_{max} is defined by the incident neutron energy E_n and the energy, removed from the composite system ^{238}Np by the ^{237}Np(n, xnf) pre-fission neutrons.

Contribution of first-chance fission $\sigma_{nf}(E_n)$ is defined by the pre-equilibrium emission of the first neutron and the fission probability P_{f1} of the ^{238}Np nuclide

$$\sigma_{f1} = \sigma_c(1 - q(E))P_{f1}. \tag{8.4}$$

Once the contribution of first neutron pre-equilibrium emission $q(E)$ is fixed [81], the first-chance fission probability P_{f1} of the ^{238}Np is defined by the level densities of fissioning ^{238}Np and residual ^{237}Np nuclides. Actually, it depends on the ratio of shell correction values $\delta W_{fA(B)}$ and δW_n. Different theoretical calculations of the shell corrections as well as of the fission barriers vary by 1 – 2 MeV. The same is true for the experimental shell corrections, which are obtained with a smooth component of potential energy calculated according to the liquid-drop or droplet model. However the isotopic changes of $\delta W_{fA(B)}$ and δW_n [78] are such that P_{f1} viewed as a function of the difference $(\delta W_{fA(B)} - \delta W_n)$ is virtually independent on the choice of smooth component of potential energy. Therefore, we shall consider the adopted $\delta W_{fA(B)}$ estimates to be effective, provided that δW_n are obtained with the liquid drop model (see Table 7.1). In the first "plateau" region and at higher energies we can safely use double-humped barrier model and relevant barrier parameters (see Table 8.1).

TABLE 8.1. FISSION BARRIER PARAMETERS OF Np NUCLEI

Nuclide	E_{fA}	δE_{fA}	sym.$_A$	E_{fB}	δE_{fB}	sym.$_B$	$h\omega_A$	$\delta h\omega_A$	$h\omega_B$	$\delta h\omega_B$	δ
^{235}Np	5.1	0.5	axial	5.5	0.3	mass-asym.	1.0	0.2	0.5	0.2	0.0
^{236}Np	5.0	0.5	axial	5.4	0.3	mass-asym.	0.6	0.2	0.4	0.2	0.08
^{237}Np	5.2	0.5	axial	5.4	0.3	mass-asym.	1.0	0.2	0.5	0.2	0.00
^{238}Np	6.1	0.1	Non-axial	5.95	0.05	mass-asym.	0.6	0.05	0.4	0.2	0.08

The fission probabilities $P_{fx}^{J\pi}$ of ^{237}Np and ^{236}Np nuclides, fissioning in ^{237}Np(n, nf) and ^{237}Np(n, 2nf) reactions, respectively, could be estimated using data of fission reaction ^{236}Np(n, f) [82, 83]. A consistent description of a most complete set of measured data on the (n, F), (n, 2n), (n, 3n) and (n, 4n) reaction cross sections for the ^{238}U target nuclide up to 20 MeV [81] enables one to consider the estimates of first neutron spectra emitted from the composite ^{238}Np nuclide as fairly realistic [4, 5, 6, 84, 85]. In case of long-lived ^{236l}Np target there are neutron-induced fission data below 20 keV by Valskij, *et al.* [83], besides simulated data [82], derived using fission probability data obtained in ^{236}U(^{3}He, df) reaction. Fig. 8.1 shows neutron-induced fission cross section of ^{236}Np (J^π = 6^-) target nuclide from 0.5 keV up to 5.5 MeV. Once again, the "shoulder" is predicted in calculated fission cross section for incident neutron energies below 0.5 MeV. Fission barrier parameters of ^{237}Np fissioning nuclide were extracted by analysis of ^{237}Np(n, f) fission data above (n, nf) emissive fission threshold (see below).

Consistency of calculated ^{236l}Np(n, f) fission cross section with simulated fission data in MeV-energy region and neutron-induced fission data in keV-energy region might be considered as an indirect validation of the approach employed here.

In case of ^{237}Np(n, F) cross section, for which there are systematic discrepancies in measured data [23 - 48], which are still not removed by recent measurement by Tovesson, *et al.* [23], since the latter were normalized to the ENDF/B-VII.0 evaluation [3]. However, the overall consistency of time-of-flight data with the absolute measurements (see [23 - 48] is the indication of the 'true' cross section level. Figs 8.2-8.4 demonstrate the fission data fit from 1 keV to 20 MeV.

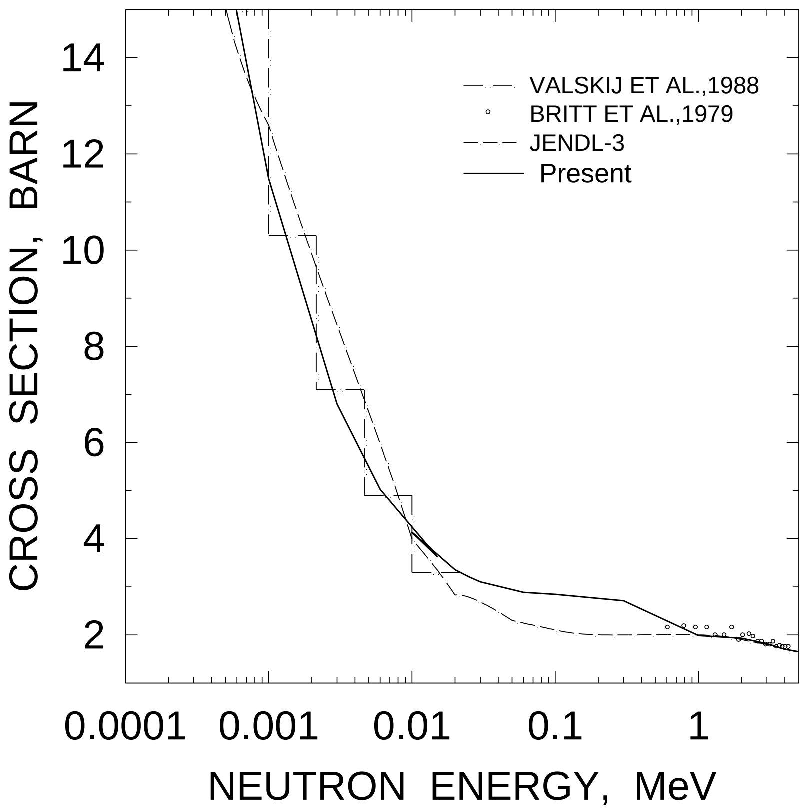

FIG. 8.1. Fission cross section of ^{236}Np.

The contributions of emissive ^{237}Np (n, nf) and ^{237}Np (n, 2nf) fission to the total fission cross section, shown on Figs 8.2 - 8.4 were further tuned within the statistical model [84, 87, 88] reproducing the ^{237}Np(n, 2n)^{236s}Np and ^{237}Np(n, F) reaction cross sections consistently. The ^{237}Np(n, 2n)^{236}Np reaction cross section is estimated using the isomer ratio of the yields of short-lived ^{236s}Np and long-lived ^{236l}Np states, calculated modeling the gamma-decay of the possible Gallaher-Moshkowski doublet states of ^{236l}Np (see below). The calculated branching ratio of yields of short-lived (1^-) and isomer (6^-) states ^{236l}Np / ^{236s}Np is “normalized” to the measured data at 14 MeV.

Fission probability of ^{237}Np, fissioning in ^{237}Np(n, nf) reaction, as will be shown below, is compatible not only with the ^{236l}Np(n, f) data [82], but with measured prompt fission neutron spectrum at 14.7 MeV [5, 6].

9. (n, 2n) and (n, 3n) cross section

The reaction chain ^{237}Np(n, 2n)^{236s}Np(β^-)^{236}Pu(α)^{232}U is one of the major sources of the accumulation of ^{232}U in the irradiated reactor fuel. The half-life of ^{236s}Np is $T^s_{1/2} = 22.5h$, the long-lived state, emerging in the reaction ^{237}Np(n, 2n) ^{236l}Np $(T^l_{1/2} = 1.55 \times 10^5 y)$ has a large thermal fission cross section [86], which may strongly influence the core neutronics. cross sections of (n, 2n) and (n, 3n) reactions are obtained from the statistical model calculations with account of pre-equilibrium neutron emission (modified STAPRE code [87] was used). Pre-equilibrium neutron emission contribution was fixed according to consistent description of (n, F) and (n, xn) reaction data for ^{238}U and ^{232}Th target nuclides [81, 88].

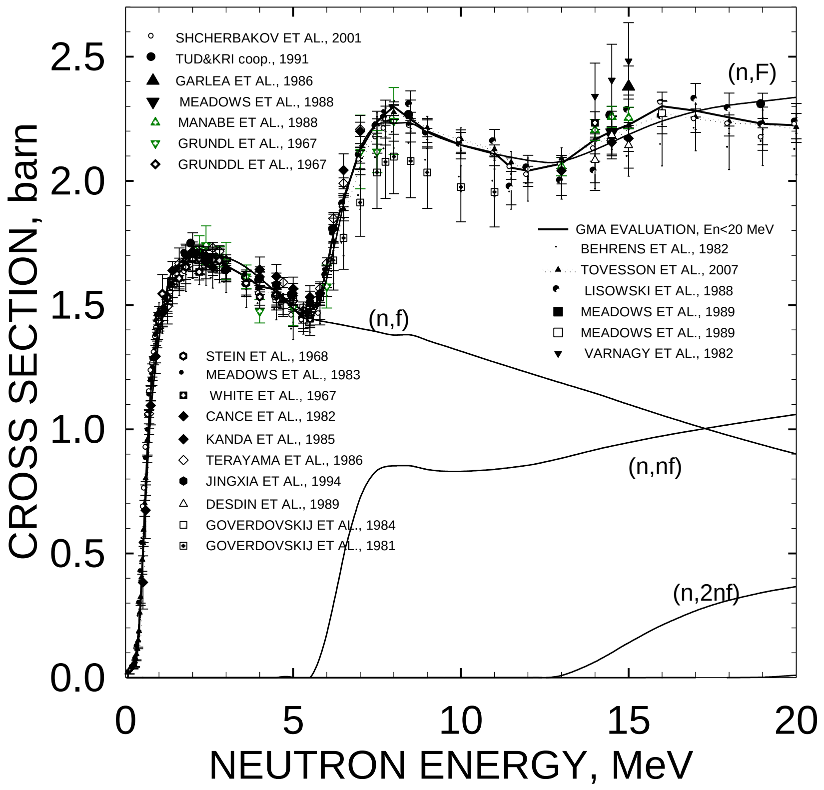

FIG. 8.2. Fission cross section of ^{237}Np.

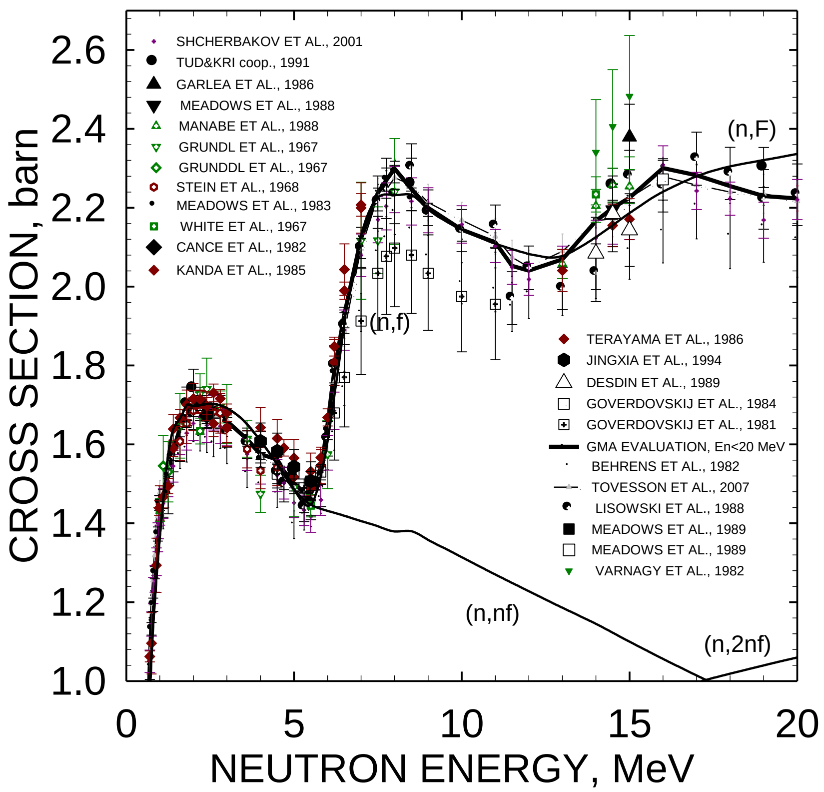

FIG. 8.3. Fission cross section of ^{237}Np.

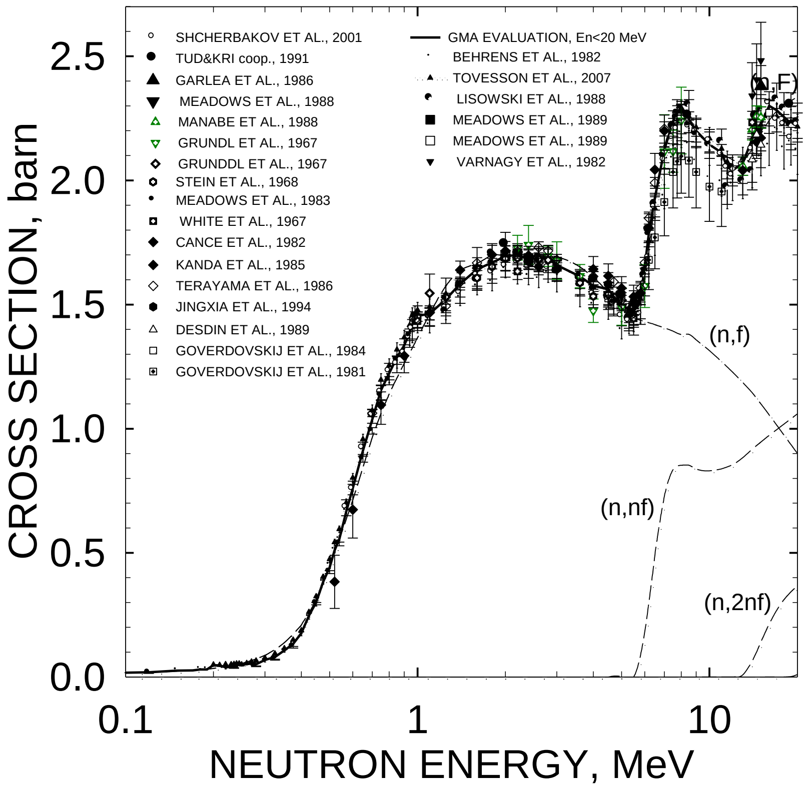

FIG. 8.4. Fission cross section of ^{237}Np.

In case of ^{237}Np(n, 2n) reaction the yield of short-lived 1^- state of ^{236s}Np is measured in the vicinity of the threshold and around 14 MeV. The ratio of the yields of short-lived (1^-) and long-lived(6^-) states

$$r(E_n) = \sigma^l_{\mathrm{n2n}}(E_n)/\,\sigma^s_{\mathrm{n2n}}(E_n), \tag{9.1}$$

measured at ~14 MeV by Myers, *et al.* [89] allows to check the compatibility of measured data on ^{237}Np(n, 2n)^{236s}Np reaction yield with the calculated cross sections of ^{237}Np(n, 2n) and ^{237}Np(n, F). That means consistent description of the data base on fission and ^{237}Np(n, 2n)^{236s}Np might be challenged at $E_n \approx 14$ MeV, at lower and higher values of E_n the predicted $r(E_n)$ might be validated. The branching ratio $r(E_n)$ is obtained by modeling the residual nuclide ^{236}Np levels. Excited levels of ^{236}Np are modeled using predicted Gallher-Moshkowski doublets by Sood [90] and Lindner, *et al.* [91]. Modeling of the ratio of the yields of short-lived (1^-) and long-lived (6^-) from threshold energy of (n, 2n) reaction up to 20 MeV, allows to infer the yield of the short- lived state ^{236s}Np as

$$\sigma^s_{\mathrm{n2n}}(E_n) = \sigma_{\mathrm{n2n}}(E_n)/(1 + r(E_n)). \tag{9.2}$$

It provides a description of ^{237}Np(n, 2n) ^{236s}Np data by Gromova, *et al.* [92], Nishi, *et al.* [93], Landrum, *et al.* [94], Paulson, *et al.* [95], Lindeke, *et al.* [96], Perkin, *et al.* [97] around $E_n \approx 14$ MeV and Daroczy, *et al.* [98] data, from ^{237}Np (n, 2n) reaction threshold up to E_n ~10 MeV.]

9.1 Branching ratio of short-lived ^{236s}Np (1^-) and long-lived ^{236l}Np (6^-) states of ^{236}Np

Myers, *et al.* [89] measured the isomer branching ratio $r(E_n) = \sigma^l_{\mathrm{n2n}}(E_n)/\,\sigma^s_{\mathrm{n2n}}(E_n)$ during the thermonuclear bomb-shot for the average beam energy of 14 MeV. In the report [99] the isomer ratio $r(E_\gamma) = \sigma^l_{\gamma n}(E_n)/\,\sigma^s_{\gamma n}(E_n)$ of 0.41 for ^{237}Np(γ, n) reaction was mentioned for the excitation energy of 9.6 MeV. That would present the evidence of the decrease of $r(E_n)$ with the increase of the incident neutron energy E_n, if not the possible influence of the entrance channel on the initial spin population of ^{236}Np residual/excited nuclide. That conclusion is supported also by the data on the isomer branching ratio for the reaction ^{238}U(d, 4n) for E_d=21 MeV [100]. In [100] it was found that the states of the residual nuclide ^{236s}Np with J = 1 are 7 times more populated than the states ^{236l}Np with spin J = 6. The modeling of the $r(E_n)$ for the ^{237}Np(n, 2n) gives more complex behavior.

The branching ratio $r(E_n)$ is defined by the ratio of the populations of the two lowest states, ^{236s}Np, with spin J = 1 and ^{236l}Np, with spin J = 6. These populations are defined by the γ-decay of the excited states of ^{236}Np. For the ^{237}Np(n, γ) reaction the γ-decay was modeled in [101]. That approach could be applied in case of ^{237}Np(n, 2n) reaction taking into account the different initial spin populations for neutron capture and (n, 2n) reactions.

The γ-decay of the excited nucleus is described by the following kinetic equation

$$\frac{\partial \omega_k(U,J^\pi,t)}{\partial t} = \sum_{J'\pi'} \int_0^{U_g} \omega_{k-1}(U',J^\pi{}',t) \frac{\Gamma_\gamma(U',J^\pi{}',U,J^\pi)}{\Gamma\,(U',J^\pi{}')} dt - \omega_k(U,J^\pi,t)\frac{\Gamma_\gamma(U,J^\pi)}{\Gamma\,(U,J^\pi)}, \qquad (9.3)$$

here $\omega_k(U,J^\pi,t)$ is the population of the state J^π at excitation U at time t, after emission of k γ-quanta; $\Gamma_\gamma(U',J^\pi{}',U,J^\pi)$ is the partial width of γ-decay from the $(U',J^\pi{}')$ to the state (U,J^π), while $\Gamma\,(U,J^\pi)$ is the total decay width of the state (U,J^π). For any state (U,J^π) with the excitation energy 0≤U≤U_g, the initial population is

$$\omega_k(U,J^\pi,t=0) = \delta_{ko}\omega_0(U,J^\pi). \qquad (9.4)$$

That equation means in the initial state we deal with the ensemble of states (U,J^π). Integrating the Eq. (9.3) over t, one gets the population $W(U,J^\pi)$ of the state (U,J^π) after emission of k γ-quanta:

$$\begin{aligned}\omega_k(U,J^\pi,\infty) - \omega_k(U,J^\pi,0) = \sum_{J'\pi'} \int_U^{U_g} \frac{\Gamma_\gamma(U',J^\pi{}',U,J^\pi)}{\Gamma\,(U',J^\pi{}')} \int_0^\infty \omega_{k-1}(U',J^\pi{}',t)dtdU' - \\ \frac{\Gamma_\gamma(U,J^\pi)}{\Gamma\,(U,J^\pi)} \int_0^\infty \omega_k(U,J^\pi,t)dt\end{aligned} \qquad (9.5)$$

Denoting the population of the state (U,J^π) after emission of k γ-quanta

$$W_k(U,J^\pi) = \frac{\Gamma_\gamma(U,J^\pi)}{\Gamma\,(U,J^\pi)} \int_0^\infty \omega_k(U,J^\pi,t)dt\ , \qquad (9.6)$$

and taking into account the condition that $\omega_k(U,J^\pi,\infty) = 0$ for any state, belonging to ensemble (U,J^π), Eq. (9.5) could be rewritten as

$$W_k(U,J^\pi) = \sum_{J'\pi'} \int_U^{U_g} \frac{\Gamma_\gamma(U',J^\pi{}',U,J^\pi)}{\Gamma\,(U',J^\pi{}')} W_{k-1}(U',J^\pi{}')dU' + \omega_k(U,J^\pi,0). \qquad (9.7)$$

The population of any state (U,J^π) after emission of any number of γ-quanta is

$$W(U,J^\pi) = \sum_k W_k(U,J^\pi), \qquad (9.8)$$

then from Eq. (9.6) one easily gets

$$W(U,J^{\pi}) = \sum_{J'\pi'} \int_{U}^{U_g} \frac{\Gamma_{\gamma}(U',J^{\pi}{}',U,J^{\pi})}{\Gamma(U',J^{\pi}{}')} W(U',J^{\pi}{}')dU' + W_0(U,J^{\pi}) \,. \tag{9.9}$$

The integral equation (9.7) in the code STAPRE [87] is solved as a system of linear equations, the integration range (U,U_g) is binned, in the assumption that there are no γ-transitions inside the bins.

The isomer branching ratio depends mostly on the low-lying levels scheme and relevant γ-transitions probabilities. The latter data are missing for the ^{236}Np nuclide. As regards the low-lying levels of odd-odd nuclides like ^{236}Np, extensive experimental data are available only for ^{238}Np, ^{242}Am, ^{244}Am and ^{250}Bk [101]. It was established for the ^{236l}Np [91, 101], that the decay of ^{236s}Np(β$^-$)^{236}Pu yields $J^{\pi} = 6^{+}$ states, while in e-capture the yield of $J^{\pi} = 6^{+}$ states of ^{236}U is observed. That is a strong argument, that the long-lived state has $J_l^{\pi} = 6^{-}$. It was established for the ^{236s}Np [91, 105 - 108], that the decay ^{236s}Np(β$^-$)^{236}Pu yields $J^{\pi} = 0^{+}, 2^{+}$ states, while in e-capture the yield of $J^{\pi} = 0^{+}, 2^{+}, 2^{-}$ states of ^{236}U is observed. That is a strong argument, that for the short-lived state $J_s = 1$, while the parity of the low-spin short-lived state is undefined. With these arguments one may stay assured that the spins of the two low-lying states of ^{236}Np are fixed. What are the energies of the ^{236s}Np and ^{236l}Np states is uncertain also. There is no experimental data about the other low-lying levels of ^{236}Np, with the exception of $J^{\pi} = 3^{-}$, which was observed in [108] when investigating the enhanced α-decay of ^{240}Am.

Modeling of low-lying levels of in [90, 91] is accomplished based on the assumption that ground and first few excited states are of two-quasi-particle nature. For actinides with quadrupole deformations the superposition principle is usually adopted, the band-head energies of the doubly-odd nucleus are generated by adding to the each unpaired configuration (Ω_p,Ω_n), as observed in the isotopic/isotonic (A-1) nucleus, the rotational energy contribution and residual n-p interaction energy contribution. The angular momenta of neutron and proton quasi-particles could be parallel or anti-parallel. In the independent quasi-particle model the two-quasi-particle states, $K^{+} = \left|K_n + K_p\right|$ and $K^{-} = \left|K_n - K_p\right|$, are degenerate. Gallaher-Moshkowski doublets [90, 91] appear because of n-p residual interaction. Fig. 9.1 (left) shows the predicted in [67] band-head energies for the two-quasi-particle states expected up to 400 keV in the odd-odd nuclide ^{236}Np. The spectroscopic properties of two pairs of proton and neutron single particle states were derived from those experimentally observed in the isotopic (Z=93) and isotonic (N=143) odd-mass nuclei with mass (A-1). Fig. 9.1 (right) shows levels expected up to 250 keV of [90]. Obviously, the relative placement of LSI (low spin isomer), as well as its parity are different, though the underlying proton and neutron single particle states are similar. In short, in [90] LSI $J^{\pi} = 1^{-}$ is just below $J^{\pi} = 1^{+}$ counterpart, while in [91] the predicted LSI $J^{\pi} = 1^{+}$ is lying much lower than the $J^{\pi} = 1^{-}$ counterpart. However, the splits of LSI and HSI of [90] and [91] are quite different. For the band-heads, shown on Fig. 9.1, the rotational bands were generated as

$$E_{JK\pi} = E_{JK} + 5.5\left[J(J+1) - K(K+1)\right]. \tag{9.10}$$

Obviously, neither of the schema presented on Fig. 9.1 represents a complete set to allow the calculation of absolute yields of ^{237}Np(n, 2n)^{236s}Np and ^{237}Np(n, 2n)^{236l}Np reactions. However, both were attributed rotational bands were constructed up to 700 keV, modeling levels with spins $J^{\pi} \le 10$, in total up to 70 levels. It was shown in [15], that simple estimate of the number of levels in odd-odd nuclei as

$$N(U) = e^{2\Delta_0/T}(e^{U/T} - 1)\,, \tag{9.11}$$

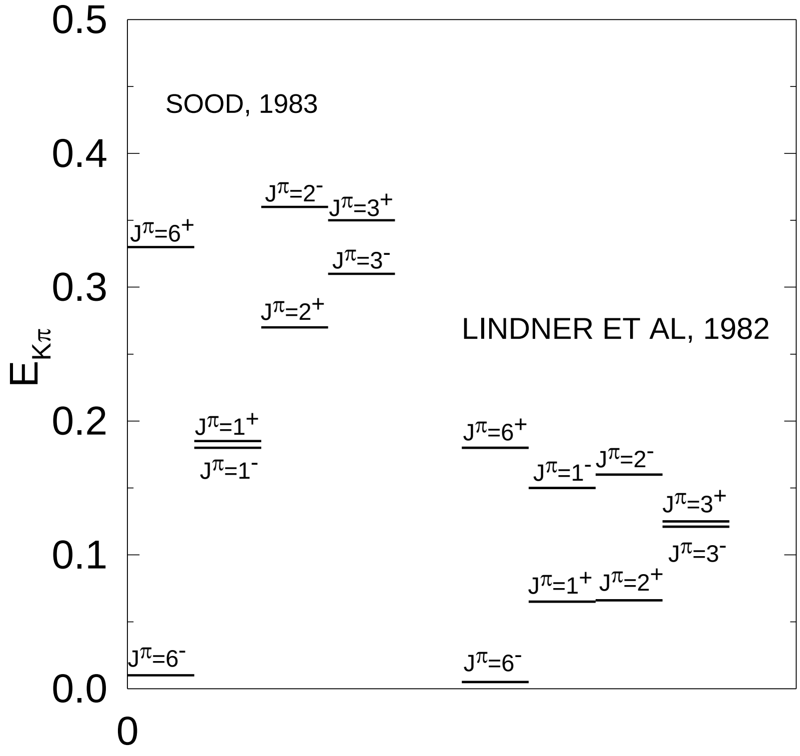

FIG. 9.1. Levels of ^{236}Np.

predicts up to 280 level at *U*~700 keV, *T*=0.388 MeV, $\Delta=12/A^{1/2}$, MeV. We assume that the modeled angular momentum distribution would not be much different from more realistic estimates. Since the data on the γ-transitions are missing, we assumed the simple decay scheme: only E1, E2 and M1 transitions are allowed in a continuum excitation energy range. Inter-band transitions are not allowed, i.e., only γ-transitions within the rotational bands are possible. In that approach the populations of the lowest four level doublets could be calculated. Then we assumed that the transition to the ground state $J^{\pi}=6^{-}$ or low-spin, short-lived isomer state $J^{\pi}=1^{-}$ [90] or $J^{\pi}=1^{+}$ [91] is defined by the "minimal multipolarity" rule. That means the states with spins $J>3$ should populate the ground state, while those with $J\leq 3$ should feed the isomer state. Then the branching ratio could be obtained as the ratio of the populations, derived from Eq. (9.9):

$$r(E_n)=\frac{\sum\limits_{J>(J_l+J_s)/2} W(U,J^{\pi})}{\sum\limits_{J\leq(J_l+J_s)/2} W(U,J^{\pi})} \qquad (9.12)$$

Fig. 9.2 shows the branching ratios, calculated for the level schema of [90] and [91], presented at left and right panels of Fig. 9.1. The level scheme of [90] appears to be quite compatible with the measured data for $r(E_n)=\sigma^{l}_{\mathrm{n2n}}(E_n)/\sigma^{s}_{\mathrm{n2n}}(E_n)$ at 14 MeV [89], while the branching ratio for the level scheme of [91] has a similar shape of $r(E_n)$, but lower absolute value. The measured data of [99] and [100] for ^{237}Np(γ, n) and ^{238}U(d, 4n) reactions, respectively, sharply differ from the predicted trend. The $r(E_n)$=0.25 of JENDL-3.3 [7] is independent on the energy of incident neutron, which strongly contradicts present predicted energy dependence. The branching ratio $r(E_n)$ of ENDF/B-VII.0 [3] has similar shape as the present one, for the E_n up to 14 MeV (see Fig. 9.2). At higher energies the predicted trend on the energy of incident neutron strongly contradicts present predicted energy dependence and calculations by Hoff, *et al.* [109].

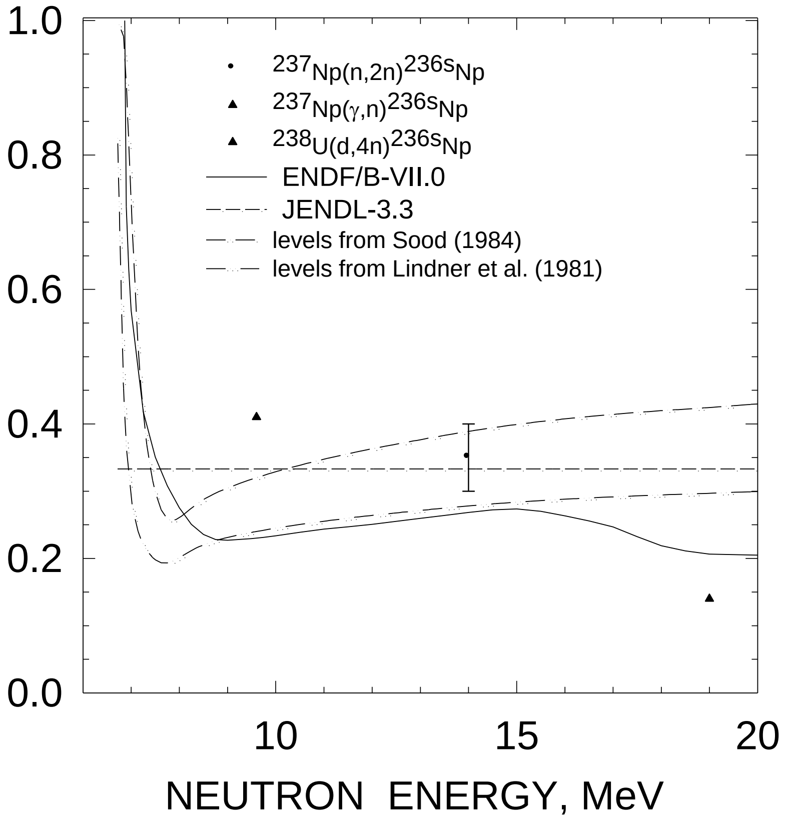

FIG. 9.2. Branching ratio of the yields of long-lived (6⁻) ^{236l}Np and short-lived (1⁻) ^{236s}Np states in ^{237}Np(n, 2n) reaction.

9.2 Yield of short-lived ^{236s}Np (1⁻) state of ^{236}Np, measured data and evaluation of ^{237}Np(n, 2n)^{236m}Np reaction cross section

Measured data base [92 - 98] should be corrected using the modern decay and cross section data standards. The decay data for the ^{236m}Np were those from [110]. The more recent evaluation by E. Browne and J.K. Tuli [111], which is in Decay Radiation Data Base [112], is consistent with the former data of [110]. The half-life, estimated in [110, 111] is $T_{1/2}$= (22.5±0.04) hours. The electron-capture and β⁻decay branching ratios of [111] equal: I_{ec} =0.52±0.01 and $I_{\beta-}$=0.48±0.01, respectively. In [112] I_{ec} = $I_{\beta-}$ =0.50±0.03. The neutron flux monitor reaction were those of ^{27}Al(n, α)^{24}Na, ^{238}U(n, 2n)^{237}U and ^{238}U(n, f), evaluated in [113], [114] and [115], respectively. It was possible to update measured data base, except data by J.L. Perkin, R.F. Coleman [97].

9.2.1 Measured data by J.H. Landrum, R.J. Nagle, M. Lindner [94]

The measurements were done at LLNL ICT with T(d, n)^{4}He reaction as a neutron source. The α-activity of ^{236}Pu in the non-irradiated Np sample was less than 0.004 decays/min. The reaction ^{237}Np(n, 2n)^{236m}Np cross section in the energy range 13.77–14.95 MeV was measured with activation technique. The reaction rate was measured with the α-activity of ^{236}Pu, emerging in ^{237}Np(n, 2n)^{236m}Np reaction, after β⁻-decay. The α-activity of ^{236}Pu in the irradiated Np sample was defined with surface barrier silicon detector. The neutron flux monitor reaction was ^{27}Al(n, α)^{24}Na. The 15-h ^{24}Na produced in aluminium foils was measured with the sodium iodine scintillation detector. The cross section of the ^{27}Al(n, α)^{24}Na reaction, as used in [94] and evaluated in [113] are given in Table 9.1.

Data of [94] were corrected (see Table 9.2) for the recommended β⁻-decay branching ratio of [111] $I_{\beta-}$ = 0.48±0.01, since initially $I_{\beta-}$ = 0.50 was used. The second correction is due to the neutron flux monitor reaction ^{27}Al(n, α)^{24}Na (see Table 9.1). The random error was increased due to uncertainty of ^{237}Np sample mass, branching ratio of the β⁻-decay and the neutron flux monitor reaction cross section.

TABLE 9.1. CROSS SECTION OF $^{27}Al(n, \alpha)^{24}Na$

E_n , MeV	σ, mbarn [94]	σ, mbarn [113]
13.77	124.0	124.33±0.52%
14.12	121.0	120.74±0.46%
14.39	118.0	117.06±0.41%
14.74	112.0	111.97±0.38%
14.95	110.0	108.86±0.44%

TABLE 9.2. CROSS SECTION OF $^{237}Np(n, 2n)^{236m}Np$ REACTION [94], ORIGINAL AND CORRECTED

E_n , MeV	σ_{orig}, mbarn	σ_{cor}, mbarn
13.77	400.0±3.6%	417.8±5.16%
14.12	340.0±4.0%	353.4±5.45%
14.39	320.0±3.5%	330.7±5.09%
14.74	280.0±3.5%	291.6±5.09%
14.95	270.0±3.7%	278.3±5.23%

9.2.2 Measured data by T. Nishi, I. Fujiwara, N. Imanshi [93]

The measurements were done at 9.6 MeV and 14.2 MeV with $^{9}Be(^{3}He, n)^{11}C$ and $T(d, n)\,^{4}H$ reactions as a neutron source, respectively. The reaction $^{237}Np(n, 2n)^{236m}Np$ cross section was measured by the ratio of α-activities of ^{236}Pu and ^{237}Np. Irradiated samples of ^{237}Np were cooled down for several weeks, till complete decay of ^{236m}Np. After that the tracers, ^{238}Pu or ^{239}Pu, were added. First the ratios of α-activities of ^{238}Pu (or ^{239}Pu) and ^{237}Np were measured. Then the ^{237}Np was removed from the sample and the ratios of α-activities of ^{236}Pu and ^{238}Pu (or ^{239}Pu) was defined. That two-step procedure allows increase the reliability of the the ratio of α-activities of ^{236}Pu and ^{237}Np. The neutron flux monitor reactions used were $^{197}Au(n, 2n)^{196}Au$, $^{203}Tl(n, 2n)^{202}Tl$ and $^{238}U(n, 2n)^{237}U$, no other information is available, so no specific correction was applied. The only correction is due to branching ratio of $I_{ec}/I_{\beta-}$ = 1.0833±0.0225 of [111], since $I_{ec}/I_{\beta-}$ = 1.08 was used in [93] (see Table 9.3).

TABLE 9.3. CROSS SECTION OF $^{237}Np(n, 2n)^{236m}Np$ REACTION [93], ORIGINAL AND CORRECTED

E_n , MeV	σ_{orig}, mbarn	σ_{cor}, mbarn
9.60	340.0±14.7%	341.04±14.7%
14.20	360.0±13.9%	361.10±13.9%

9.2.3 Measured data by K. Lindeke, S. Specht, H.J. Born [96]

The measurement was done at 15 MeV with $T(d, n)^{4}H$ reaction as a neutron source. The sample was wrapped with a cadmium foils, the initial content of ^{236}Pu in the ^{237}Np sample was negligible. The reaction $^{237}Np(n, 2n)^{236m}Np$ cross section was measured by two methods. First, γ-rays of $^{236m}Np(EC)^{236}U$ were counted. In the second method the α-activity of ^{236}Pu, emerging after β^{-}decay of ^{236m}Np, was measured after chemical separation of ^{236}Pu and ^{237}Np. The neutron flux monitor reaction was $^{27}Al(n, \alpha)^{24}Na$ [116]. The second neutron flux monitor reaction was $^{237}Np(n, f)$, for which the ^{97}Zr activity was measured. The neutron fluxes obtained $(6.77\pm0.24)\times10^{13}$ cm^{-2} and $(6.40\pm0.73)\times 10^{13}$ cm^{-2} are rather different. The branching ratio $I_{ec}/I_{\beta-}$ = 1.05 [106] was used. The cross section value 0.247±0.022 was renormalized as 0.256±0.0227, for the neutron flux monitor cross section ratio (111.09/110.30=1.00716) and $I_{ec}/I_{\beta-}$ of [111] (1.0833/1.05=1.03171).

9.2.4 Measured data by E.A. Gromova, S.S. Kovalenko, Yu.A. Nemilov [93]

The measurement was done at 14.8 MeV with T(d, n)^{4}H reaction as a neutron source. The reaction ^{237}Np(n, 2n)^{236m}Np cross section was measured by two methods. First, γ-rays of ^{236m}Np(EC)^{236}U were counted. In the second method the α-activity of ^{236}Pu, emerging after β^-decay of ^{236m}Np, was measured. Weak γ-activity of ^{236}U line E_γ = 642.3 keV (with 1% yield) was counted with the background of ^{237}Np γ-activity. Soft background (E_γ < 100 keV) was reduced with lead and cadmium filter. Hard background (E_γ = 300–400 keV) was reduced after chemical purification of ^{237}Np sample to remove ^{233}Pa before the irradiation. The γ-rays of ^{236m}Np(EC)^{236}U were counted with Ge(Li) detector. The absolute yield for E_γ=642.3 keV γ-line was I_γ = 0.98%. In [111] I_γ = (0.92±0.06)% is recommended. The neutron flux monitor reaction used was ^{238}U(n, F). The flux was renormalized, since the neutron-induced fission cross section of ^{238}U decreased from 1230±20 mbarn to 1214.52±9 mbarn [19]. The ^{237}Np(n, 2n)^{236m}Np reaction cross section was corrected for these two factors, changing from 230±50 mbarn to 241.9±52.5.

Measuring the α-activity of ^{236}Pu needs a purification of the non-irradiated ^{237}Np sample of Pu impurities, and after irradiation the ^{236}Pu should cleaned of ^{237}Np. The initial ^{236}Pu impurities are next to negligible as compared with a build-up of ^{236}Pu. After irradiation weighted amount of ^{239}Pu was added, with 10^{-2} % impurity of ^{238}Pu. Then the Pu fraction was separated, 40 % of ^{236}Pu, built-up in ^{237}Np sample, was extracted. The α-spectrometry with silicon surface barrier detector was accomplished. The ^{237}Np(n, 2n)^{236m}Np reaction cross section was corrected for the neutron flux related factor, changing from 276±14 mbarn to 272.5±14 mbarn.

9.2.5 Measured data by S. Daroczy, P. Raics, J. Csikai, N.V. Kornilov [98]

The measurement was done at 7.09–9.9 MeV energy range with D(d, n)^{3}He reaction as a neutron source. The reaction ^{237}Np(n, 2n)^{236m}Np cross section was measured by the α-activity of ^{236}Pu, emerging after β^- decay of ^{236m}Np. After irradiation weighted amount of ^{239}Pu was added, with 10^{-2} % impurity of ^{238}Pu. Then the Pu fraction was separated, the α-spectrometry with silicon surface barrier detector was accomplished. The neutron flux was monitored with the reaction cross sections, shown in Table 9.4. The factor $F_m(E_n)$ was used to correct the original cross section data shown in Table. 9.5. The cross section data of ^{237}Np(n, 2n)^{236m}Np reaction, shown in Table. 9.5 are averaged data obtained for three different flux monitors.

Fig. 9.3 shows the $\sigma^s_{\mathrm{n2n}}(E_n)$ reaction cross section and available measured data [92 - 98], normalized to modern reference cross sections and gamma-yields, as applicable. Present calculated $\sigma^s_{\mathrm{n2n}}(E_n)$, obtained with Eq. (9.2), with the branching ratio, relevant for the scheme [90], is compatible with the measured data starting from the threshold [98] and in the vicinity of 14 MeV [92 - 97]. The calculated cross section $\sigma^s_{\mathrm{n2n}}(E_n)$, corresponding for the systematically lower branching ratio $r(E_n)$ for the level scheme by Lindner, *et al.* [91] is higher than the measured data around 14 MeV and systematically higher than $\sigma^s_{\mathrm{n2n}}(E_n)$ for the scheme by Sood [90]. The evaluated $\sigma^s_{\mathrm{n2n}}(E_n)$ of JENDL-3.3 is much different from ENDF/B-VII.0 [3] and and present evaluations in the energy range of 10~13 MeV, where measured data are missing.

TABLE 9.4. CROSS SECTION OF ^{27}Al(n, α)^{24}Na, ^{238}U(n, 2n)^{238}U and ^{238}U(n, f) REACTIONS [98], ORIGINAL AND CORRECTED

E_n, MeV	^{27}Al(n,α)^{24}Na		^{238}U(n,2n)^{238}U		^{238}U(n,f)		$F_m(E_n)$
	σ, mbarn, [117]	σ, mbarn, [113]	σ, mbarn, [118]	σ, mbarn, [114]	σ, mbarn, [119]	σ, mbarn, [115]	
7.09	17.790	18.388±1.45%	524.50	509.49±1.99%	933.55	948.17±0.85%	1.006886
7.47	26.750	26.716±1.17%	824.00	822.99±1.72%	983.18	984.59±0.89%	0.999646
7.90	38.450	37.371±0.93%	1071.20	1069.84±1.51%	990.11	1001.71±0.90%	0.994128
8.32	50.820	49.124±0.86%	1211.93	1213.31±1.46%	993.28	1008.92±0.87%	0.994504
8.90	67.550	65.593±0.87%	1325.64	1326.33±1.46%	997.65	1009.06±0.88%	0.994329
9.37	79.010	77.570±0.88%	1373.31	1384.44±1.41%	992.33	1006.40±0.90%	1.001353
9.90	89.450	88.866±0.91%	1416.61	1435.67±1 39%	983.64	1002.11±0.94%	1.008568

TABLE 9.5. CROSS SECTION OF ^{237}Np(n, 2n)^{236m}Np REACTION [98], ORIGINAL AND CORRECTED

E_n , MeV	σ $_{orig}$, mbarn	σ $_{cor}$, mbarn
7.09	49.0±6.13%	49.34±7.32%
7.47	86.0±4.66%	85.97±6.15%
7.90	123.0±5.70%	122.28±6.97%
8.32	191.0±4.72%	189.95±6.19%
8.90	256.0±5.08%	254.55±6.47%
9.37	338.0±3.85%	338.46±5.56%
9.90	335.0±3.89%	337.87±5.58%

Fig. 9.4 shows the present $\sigma_{\text{n2n}}(E_n)$ reaction cross section and evaluated cross sections of ENDF/B-VII.0 [3] and JENDL-3.3 [7]. Present calculated $\sigma_{\text{n2n}}(E_n)$ cross section is defined by the fission competition and the pre-equilibrium emission contribution to the first neutron spectrum. The calculated cross section $\sigma_{\text{n2n}}(E_n)$ is systematically lower than that of JENDL-3.3 [7] in the incident energy range of 9-13 MeV, where the measured data for $\sigma^s_{\text{n2n}}(E_n)$ are missing. In case of ENDF/B-VII.0 [3] evaluation different than ours estimates of $\sigma_{\text{n2n}}(E_n)$ and $r(E_n)$ lead to similar estimates of $\sigma^s_{\text{n2n}}(E_n)$. In our approach the estimate of $\sigma^s_{\text{n2n}}(E_n)$ is based on modeling the branching ratio $r(E_n)$.

Fig. 9.5 shows the comparison of ^{237}Np(n, 3n) reaction evaluations of ENDF/B-VII.0[3] and JENDL-3.3 [7] with a present calculation. Huge discrepancies are just a reflection of the neutron absorption cross section differences. The one more conclusion which might be drawn from these discrepancies is the need to check the model approaches in case of target nuclides like ^{238}U and ^{235}U. In latter cases the (n, F), (n, 2n) and (n, 3n) are described consistently within our approach [63].

9.2.6 Measured integral data by E.A. Gromova, S.S. Kovalenko, Yu.A. Nemilov [93]

The yield of the ^{232}U in power reactors depends on the integral cross section of $\langle\sigma^s_{\text{n2n}}(E_n)\rangle_U$ for the ^{235}U(n, f) prompt fission neutron spectrum. In [95] and [120] $\langle\sigma^s_{\text{n2n}}(E_n)\rangle_U$ = 1.05 mbarn and $\langle\sigma^s_{\text{n2n}}(E_n)\rangle_U$ =2.4 mbarn, respectively, were obtained. In [95] the ratio of α-activities of ^{236}Pu and ^{238}Pu was defined for the fuel, the value of $\langle\sigma^s_{\text{n2n}}(E_n)\rangle_U$ was defined with the kinetic equations. In [120] to estimate the dependence of the ^{236}Pu build-up as dependent on the burn-up, outdated evaluation of KEDAK-4 was used. The cross section $\sigma^s_{\text{n2n}}(E_n)$ of KEDAK-4 is much higher than present evaluation in the incident neutron energy range of 7≤ E_n ≤13 MeV (see [85]). Another systematic uncertainty of $\langle\sigma^s_{\text{n2n}}(E_n)\rangle_U$ [95] is due to usage of prompt fission neutron spectrum of [121] to represent neutron spectrum in the reactor. It was concluded in [120], that $\langle\sigma^s_{\text{n2n}}(E_n)\rangle_U$ =2.4 mbarn overestimates the build-up of ^{236}Pu as dependent on the burn-up by ~20% at least. Present estimate of $\langle\sigma^s_{\text{n2n}}(E_n)\rangle_U$ =1.8144 mbarn is consistent with that trend. The prompt fission neutron spectrum of ^{235}U(n_{th},f) used was calculated in [2] (see discussion below).

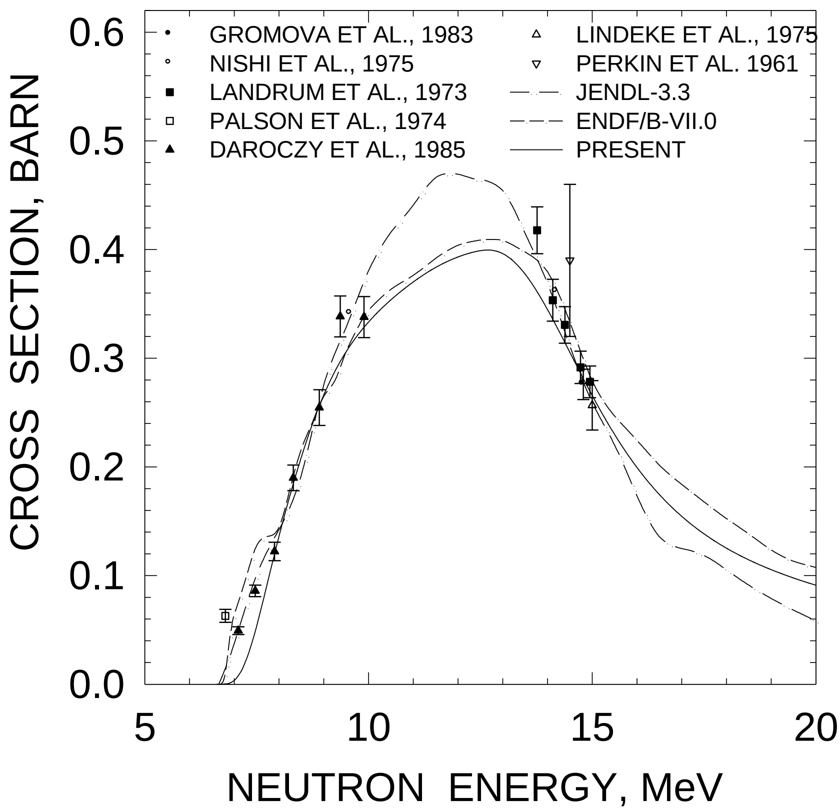

FIG. 9.3. Cross section of ^{237}Np(n, 2n)^{236s}Np reaction

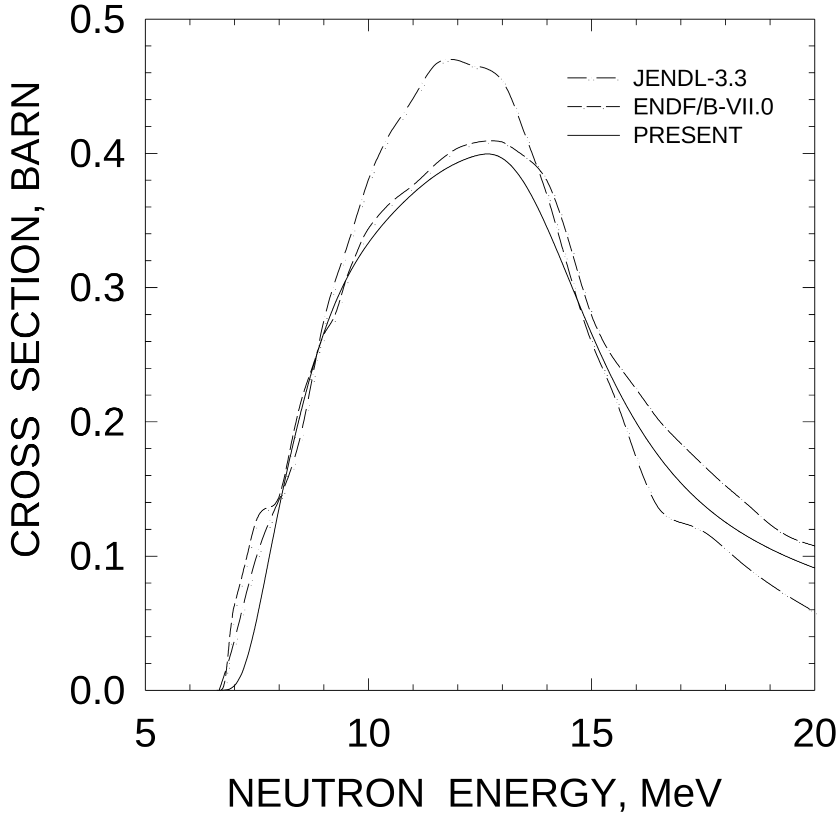

FIG. 9.4. Cross section of ^{237}Np(n, 2n) reaction.

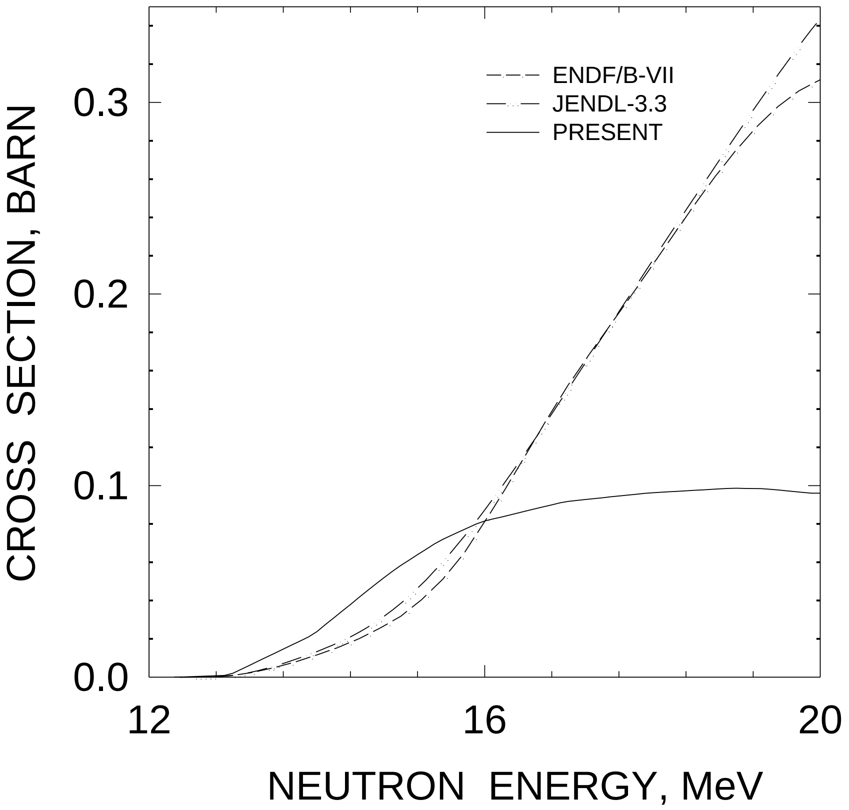

FIG. 9.5. Cross section of ^{237}Np(n, 3n) reaction.

The integral cross section of $\left\langle \sigma^{s}_{\mathrm{n2n}}(E_n) \right\rangle_{Cf}$ =4.66±0.47 mbarn for the ^{252}Cf(sf) spontaneous fission neutron spectrum was measured by Gromova, *et al.* [122]. The ^{237}Np(n, 2n) ^{236m}Np reaction cross section was measured by the α-activity of ^{236}Pu, emerging after β¯-decay of ^{236m}Np. After irradiation weighted amount of ^{239}Pu was added, with 10^{-2} % impurity of ^{238}Pu. Then the Pu fraction was separated, the α-spectrometry with silicon surface barrier detector was accomplished. The neutron flux monitor reactions used were ^{27}Al(n, α)^{24}Na, ^{27}Al(n, p)^{27}Mg, ^{48}Ti(n, p)^{48}Sc, ^{58}Ni(n, p)^{58}Co and ^{197}Au(n, 2n)^{196}Au. The relevant reaction rates were measured with the γ-activity of the reaction products, using Ge(Li) detector. The relevant decay data are given in Table 9.6. The original data [122] should be corrected for the neutron flux monitor reactions only (see Table 9.7, factor F_c). The neutron flux was measured by replacing the container with ^{237}Np by container with the monitor reactions. The possible corrections for the decay data are negligible, as shows factor F_γ in Table 9.6. Obviously, $F_m = F_\gamma F_c$, $\left\langle F_m \right\rangle$ = 1.009571, eventually $\left\langle \sigma^{s}_{\mathrm{n2n}}(E_n) \right\rangle_{Cf}$ =4.70±0.47 mbarn. Present estimate of $\left\langle \sigma^{s}_{\mathrm{n2n}}(E_n) \right\rangle_{Cf}$ =2.9027 mbarn is inconsistent with the measured data, when the ^{252}Cf(sf) spontaneous fission neutron spectrum is taken from [125]. In [126] the integral fission cross section of ^{237}Np equals $\left\langle \sigma_{\mathrm{nF}}(E_n) \right\rangle_{Cf}$ =1361 mbarn was estimated. Since the ^{237}Np sample is rather massive, 10000 times as that of ^{252}Cf, and the cross section $\left\langle \sigma^{s}_{\mathrm{n2n}}(E_n) \right\rangle_{Cf}$ is rather small, the prompt fission neutrons of neutron-induced fission of ^{237}Np may essentially increase the neutron flux. That may explain the large difference of present calculated and measured values of $\left\langle \sigma^{s}_{\mathrm{n2n}}(E_n) \right\rangle_{Cf}$.

TABLE 9.6. DECAY DATA FOR THE NEUTRON FLUX MONITOR REACTIONS

Flux monitor	$T_{1/2}$		E_γ, keV	I_γ, %		F_γ
	[124]	[112]		[124]	[112]	
^{27}Al(n,α)^{24}Na	14.659±0.004 H	14.997±0.012 H	1368.63	100.0	99.9936±0.0016	0.999936
^{27}Al(n,p)^{27}Mg	9.462±0.011 M	9.458±0.012 M	843.76	73.0	71.8±0.4	0.983562
^{48}Ti(n,p)^{48}Sc	43.704±0.096 H	43.67±0.09 H	983.5 1037.5 1312.1	100.0 97.5±0.3 100.0	100.1±0.6 97.6±0.7 100.1±0.7	1.001009
^{58}Ni(n,p)^{58}Co	70.916±0.015 D	70.86±0.06 D	810.76	99.5±0.3	99.45±0.01	0.999497
^{197}Au(n,2n)^{196}Au	6.183±0.010 D	6.1669±0.0006 D	333.0 355.7	22.9±0.5 87.0	22.9±0.9 87.0±0.2	1.000000

TABLE 9.7. CROSS SECTION DATA FOR THE NEUTRON FLUX MONITOR REACTIONS

Flux monitor	σ, mbarn [123]	σ, mbarn [124]	F_c	F_m
^{27}Al(n,α)^{24}Na	1.004±1.90%	1.016±1.47%	1.011952	1.011887
^{27}Al(n,p)^{27}Mg	4.825±3.20%	4.880±2.14%	1.011399	0.994773
^{48}Ti(n,p)^{48}Sc	0.4202±2.20%	0.4247±1.89%	1.010709	1.011729
^{58}Ni(n,p)^{58}Co	115.0±1.70%	117.5±1.30%	1.021739	1.021226
^{197}Au(n,2n)^{196}Au	5.461±2.20%	5.506±1.83%	1.008240	1.008240

10. Evaluation of prompt neutron yield in ^{237}Np fission

GMA code [21] was used for evaluation of the prompt fission neutron yield ν_p for ^{237}Np+n interaction. For the least-squares fit we have not used any prior model function. The measured data were reduced to the energy nodes chosen for the evaluation (with a mesh-size of 0.5 MeV below 10 MeV and a mesh-size of 1 MeV for the energy range of 10 to 15 MeV). The list of experimental data [127 - 133], selected for the evaluation is given in Table 10.1. All data are obtained in the measurements in which ^{252}Cf(sf) prompt fission neutron yield was used as standard. The data were renormalized to new ^{252}Cf(sf) standard value [19]. Since the uncertainty of the evaluated standard is 0.013 %, all measurements have been considered as absolute ones.

The following data sets were excluded from the fit:

1) data by Iyer, *et al.* [134], because data obtained by summation method is incomplete (partial) prompt neutron yield;

2) data by Kornilov, *et al.* [135], because the measured quantity was the product of the average ν_p and fission cross section; the energy dependence of the average ν_p [135] is discrepant with other experimental data.

The least squares fit of ν_p shows that fitted experimental data are mutually consistent and the chi-squared value per degree of freedom is below unity. The result of fit together with the experimental data and a prior used in the fit (ENDF/B-VII.0) evaluation are shown in Fig. 10.1. The GMA evaluation is very close to the evaluation of ENDF/B-VII.0. The linear function is often used for a “smoothing”, or as a “model” curve in the prompt fission multiplicity ν_p fit for the first-chance fission. This procedure cannot be followed on for a wider incident neutron energy region. A simple estimate shows that the “step” in the ν_p due to the opening of the (n, nf) channel and explicit contribution of pre-fission neutron to the fission neutron multiplicity could amount to ~3%. Because of that reason the linear smoothing (fits) of GMA’ estimates have been done separately for energy regions of 0–5 MeV (first-chance fission), 8–15 MeV (second- and third-chance fission) and 5–8 MeV (transitional region, where contribution of (n, nf) reaction reaches maximum). The curve, obtained with that “smoothing” procedure is shown in Fig. 10.1 together with GMA evaluation (symbols given in the nodes of the evaluation, error bars correspond to its uncertainty). The step in the energy dependence due to the opening of (n, nf) fission reaction at E_n= 8 MeV is around 2.3 %.

TABLE 10.1. EXPERIMENTAL DATA USED IN THE EVALUATION OF THE PROMPT nu-bar FOR ^{237}Np FISSION.

EXFOR sub-entry	First author (year)	Data type	Energy range, MeV	Comment
10646002	L.R. Veeser (1978) [128]	absolite prompt neutron yield with ^{252}Cf(sf) used for normalization	1 – 14.7	^{252}Cf(sf) ν_p =3.733 value was used, renormalized to the latest value of ν_p =3.7606 ± 0.0048
21785002	J. Frehaut (1982) [129]	absolute prompt neutron yield with ^{252}Cf(sf) used for normalization	1.14 – 14.7	^{252}Cf(sf) ν_p =3.733 value was used, renormalized to the latest value of ν_p =3.7606 ± 0.0048
21834021	R. Mueller (1981)[130]	absolute prompt neutron yield with ^{252}Cf(sf) used for normalization	0.8; 5.5	No information about the value of ^{252}Cf(sf) ν_p used for detector calibration. Because the uncertanty of the results is substantially larger than changes of the standard value, the data were taken as they are given by authors.
4066402	V.V. Malinov-skyj (1983[131])	absolute prompt neutron yield with ^{252}Cf(sf) used for normalization	0.98 – 5.9	^{252}Cf(sf) ν_p =3.733 value was used, renormalized to the latest value of ν_p =3.7606 ± 0.0048
41171003	G.S. Boykov (1994)[133]	absolute prompt neutron yield with ^{252}Cf(sf) used for normalization	2.9; 14.7	^{252}Cf(sf) ν_p =3.757 value was used, renormalized to the latest value of ν_p =3.7606 ± 0.0048
41378003	Yu.A. Khokhlov (1994)[127]	absolute prompt neutron yield with ^{252}Cf(sf) used for normalization	0.51 - 11.67	^{252}Cf(sf) ν_p =3.756± 0.0075 value was used, renormalized to the latest value of ν_p =3.7606 ± 0.0048
21651003	H. Thierrens (1980)[132]	absolute total neutron yield	thermal neutrons	uncertainty of measurements is at the level of 6% because of low thermal ^{237}Np fission cross sections

There is a single direct measurement of the average ν_p for thermal neutron spectrum [132]. The value obtained in the measurements was 2.47±0.14. Although it is difficult to expect in case of sub-threshold fission, where there is no good averaging over compound resonances, that the linear dependence in ν_p is preserved for sub-threshold region, it was decided to use at thermal point the value obtained by extrapolation of the linear fit coming from 0.5–8 MeV region.

This value of ν_p equals 2.6343 with an assigned uncertainty ~5.9 %, which makes this value consistent with the result of measurement [132]. The linear extrapolation of the linear fit in the energy range of 8–15 MeV was extended from 15 MeV up to 20 MeV, where no experimental data are available. In a wider energy range the increase of ν_p with energy is weaker than a linear rate. The quadratic power fit in 8–15 MeV range which produces weaker than linear rate increase of ν_p with energy, it was used for the estimation of uncertainties. The uncertainty of evaluated ν_p values in 15-20 MeV energy range were obtained as a difference between linear and quadratic fit of data in 8-15 MeV energy range, extrapolated to higher energies.

Because the linear smoothing (fit) was used for final presentation of evaluated data in three energy regions, the data can be very easily presented in the file with use of LAW=2 for linear interpolation between energy points: uncertainties of evaluated data are shown in the Table 10.2. The correlation matrix of evaluated data has no correlations between thermal point and all the other data points. Due to the limited number of available experimental data, the correlations of evaluated uncertainties are higher at low energies and lower at higher energies. Between 15 and 20 MeV, where the extrapolation was used for evaluation, the uncertainties are estimated assuming only statistical component.

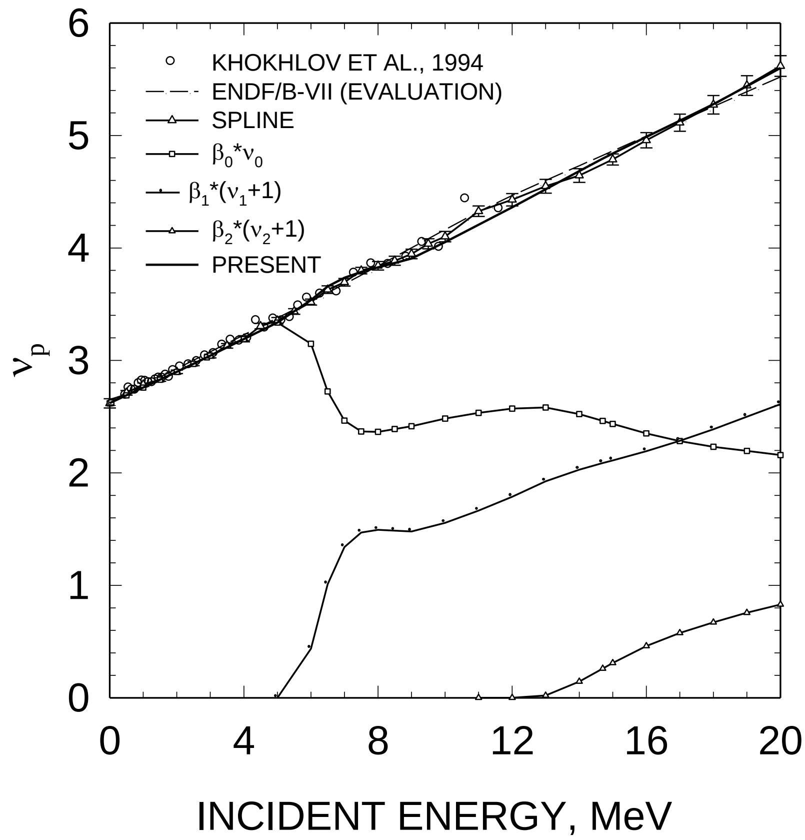

FIG. 10.1. Multiplicity of prompt fission neutrons in ^{237}Np(n, F) reaction.

TABLE 10.2. EVALUATED VALUES OF ν_p WITH LINEAR INTERPOLATION BETWEEN POINTS. UNCERTAINTIES ARE GIVEN FOR THE DIAGONAL OF COVARIANCE MATRIX.

E_n, eV	ν_p	Uncertainty %
1.0E-05	2.6343	5.9
0.0253	2.6343	5.9
5.0E+6	3.3470	1.0
8.0E+6	3.8610	1.5
1.5E+7	4.8094	1.3
2.0E+7	5.4880	12.1

We applied more complicated theoretical approach, than just linear extrapolation of ν_p, with incorporation of the pre-fission neutron emission and fission chances. At incident neutron energies above emissive fission threshold the number of prompt fission neutron ν_p was calculated as

$$\nu(E_n) = \sum_{x=1}^{X} \left(\nu_x(E_{nx}) + (x-1)\right) \cdot \beta_x(E_n), \tag{10.1}$$

here x =1, …X is the multiplicity for the x-chance fission of the nuclei A+1, A, A-1, A-2 after emission of (x-1) pre-fission neutrons, $\beta_x(E_n)$ is the x-chance contribution to the observed fission cross section, $\nu_x(E_{nx})$ - prompt neutron multiplicity for i-th fissioning nucleus. The excitation energy of A, A-1, A-2 nuclides, which emerge after emission of (x-1) pre-fission neutrons is defined as

$$E_{nx} = E_n - \sum_j B_{nj} - \langle E_{xj} \rangle, \qquad (10.2)$$

here B_{nj} - neutron binding energy for the (A+1-j), j=1, 2, 3, nucleus, $\langle E_{xj} \rangle$ - average energy of j-th pre-fission neutron. The incident neutron energy dependence of neutron multiplicity in the energy range $E_n \leq$ 6 MeV for all fissioning ^{238,237,236,235}Np nuclei was taken from evaluation by Malinovskij [136], with slight modifications, tuned to reproduce the measured data on ν_p (see Table 10.3). We assumed that excitation energy E_{nx} is brought into A_j nuclide with the reaction: n+(A_j -1) →fission . Incident neutron energy in this hypothetical reaction equals to $(E_{nj} - B_{nAj})$. In this way the $\nu_x(E_{nx})$ functions for all nuclides in the mass chain ^{238,237,236,235}Np were calculated. Energy dependence of ν_p versus incident neutron energy estimated with this equations compared on Fig. 10.2 with previous present GMA-evaluation and previous evaluations. Relevant partial contributions to ν_p are shown on Fig. 10.1. Bump in ν_p around (n, nf) reaction threshold is due to the pre-fission neutrons, emitted in ^{237}Np(n, nf) reaction. The similar behavior was evidenced in measured data for ^{232}Th(n, F) and ^{238}U(n, f), it was reproduced with the present model [88].

TABLE 10.3. EVALUATED FIRST CHANCE ν_p –VALUES FOR ^{237,236,235}Np TARGET NUCLIDES.

Target	ν_p^{th}	ν_p(E_n MeV)	ν_p(6 MeV)
^{237}Np	2.619	2.950 (2.37)	3.484
^{236}Np	2.922	2.869 (1.06)	3.987
^{235}Np	2.818	2.908 (2.13)	3.861

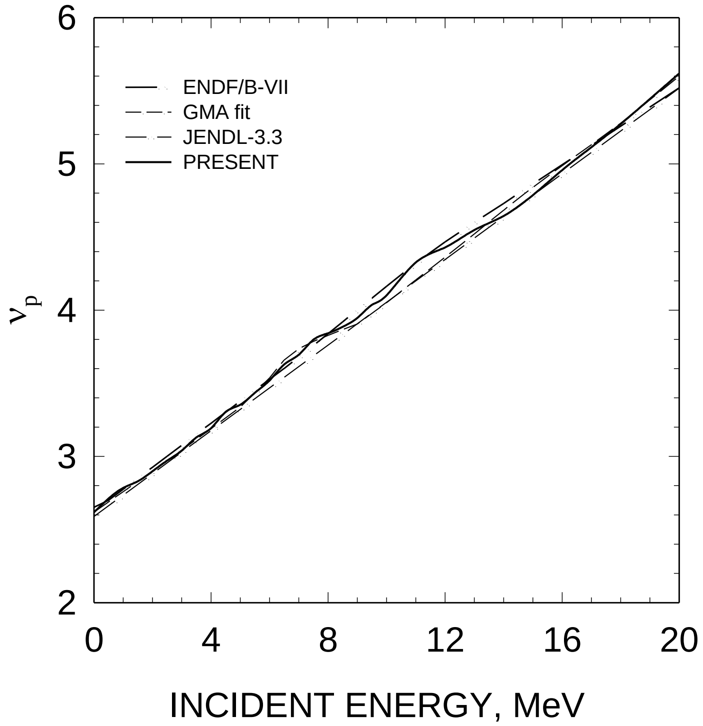

FIG. 10.2. Multiplicity of prompt fission neutrons in ^{237}Np(n, F) reaction.

11. Evaluation of averaged delayed neutron yield for ^{237}Np(n, f)

The energy dependence of the averaged delayed fission neutron yields in the evaluated data files is given usually as a step function (see Figs 11.1, 11.2) with a sharp drop due to the (n, nf) fission reaction. The phenomenological parameterization based on summation of the contributions to the observed yield from all precursors [137, 138] had shown, that the strongest influence on the energy dependence of delayed neutron yield has the prompt fission neutron emission. It defines the probability of the formation of precursors, contributing to the delayed neutron yield. The account of four most important factors (see [137, 138]) predicts rather smooth energy dependence of the delayed neutron yields. However, in the first-chance fission domain local increase for Z-even targets is possible. Because there is still no reasonable physical model for the prediction of the energy dependence of ν_d, a simple polynomial fits were used in the evaluation of data in two energy regions: below 5 MeV and above 4 MeV. The evaluated curve is shown in Figs 11.1, 11.2. Energy point E_n =4.4 MeV was taken as a matching point between the two fits, because both give virtually the same ν_d -value at this energy point. The data of different measurements at thermal neutron energy, two averaged fission neutron spectrum measurements (shown at E_n =1.4 and E_n=1.5 MeV), measurement by Bobkov, *et al.* [139] at 14.7 MeV and measurements in a wide energy range from 0.37 to 4.7 MeV by Piksaikin, *et al.* [140]. The evaluated data uncertainties present the conservative estimate for a wide energy groups with account of uncertainty of reference data used for normalization. The detailed analysis of ν_d uncertainties was accomplished. There are no cross-energy correlations in the covariance matrix of the evaluated uncertainties. The evaluated ν_t –values were obtained by summing up of ν_p and ν_d yields. The covariance matrix of uncertainties of total fission neutron yield is a sum of covariance matrices of uncertainties for prompt ν_p and delayed ν_d neutron yields.

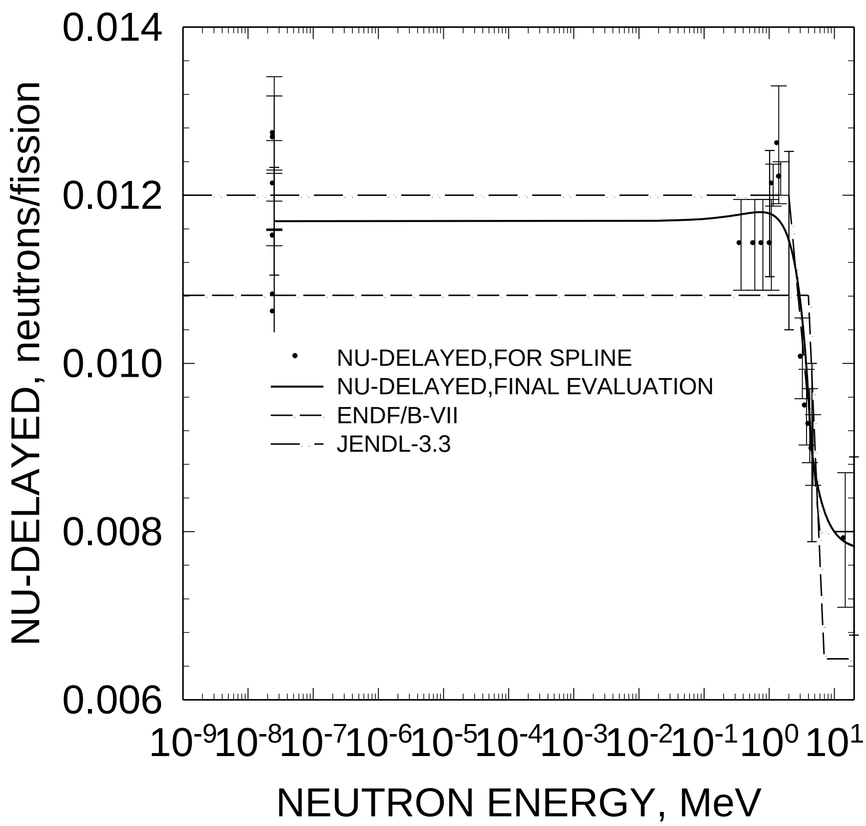

FIG. 11.1. Multiplicity of delayed fission neutrons in ^{237}Np(n, F) reaction.

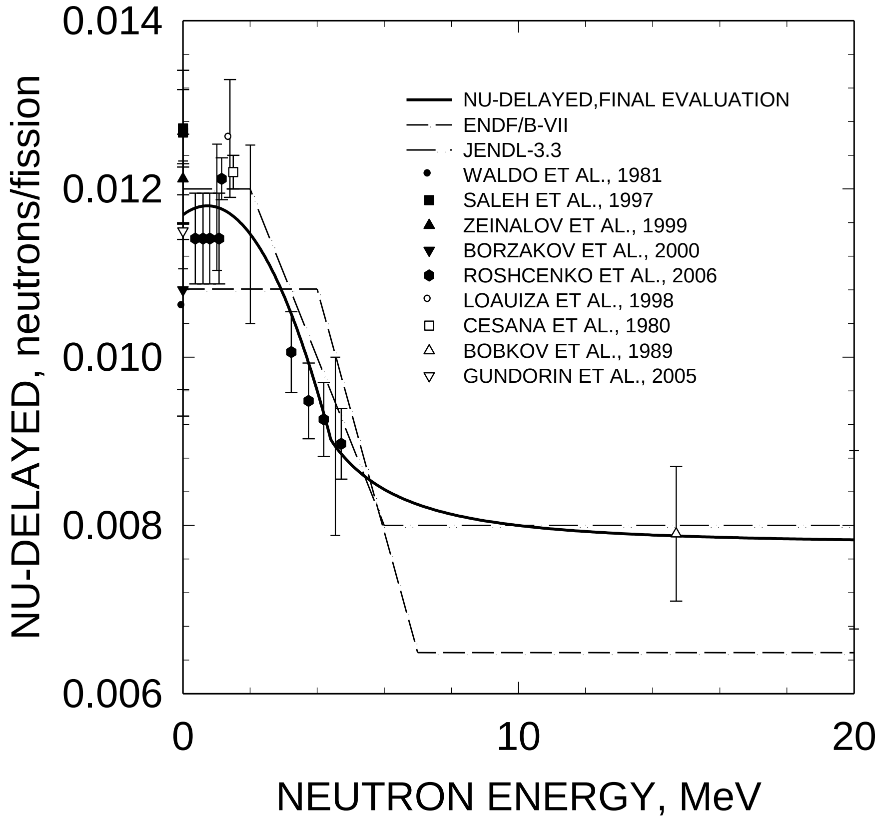

FIG. 11.2. Multiplicity of delayed fission neutrons in ^{237}Np(n, F) reaction.

12. Energy distributions of secondary neutrons

Energy distributions for (n, 2n), (n, 3n) and (n, n') reactions were calculated with a Hauser-Feshbach statistical model of cascade neutron emission [88, 148, 149], taking into account exclusive pre-fission (n, xnf) and (n, xnγ) neutron spectra, with the allowance of pre-equilibrium emission of first neutron.

Prompt fission neutron spectra (PFNS) were calculated with a phenomenological model, developed for the first-chance fission by Kornilov, *et al.* [150] and extended to emissive fission domain by Maslov, *et al.* [2, 4, 5, 6, 88, 151, 152] with inclusion of exclusive prefission neutron spectra. Exclusive pre-neutron spectra of (n, xnf) reactions, either equilibrium and pre-equilibrium spectra of pre-fission (n, xnf) neutrons are strictly correlated with (n, F) and (n, xn) reaction cross sections. This approach was used previously for the description of the PFNS and neutron emission spectra for ^{238}U+n [81, 88, 148], ^{235}U+n [2, 151] and ^{232}Th+n [88, 149] interactions. A number of experimental signatures were revealed and correlated with the exclusive pre-fission (n, xnf) and (n, xnγ) neutron spectra. The major constraint was the description of (n, F) and (n, xn) reaction cross sections. Important point is that the contributions of (n, nf) and (n, 2nf) to the observed fission cross sections (n, F) are consistent with the neutron-induced fission cross sections of the unstable target nuclides like ^{237}U or ^{231}Th, fissilities of which are probed in ^{238}U(n, nf) or ^{232}Th(n, nf) reaction channels. The fission cross section of ^{237}U(n, F), calculated based on consistent description of ^{238}U(n, F), ^{238}U(n, 2n), ^{238}U(n, 3n) and PFNS for n+^{238}U interaction for emissive fission domain [88, 148, 152, 153] were proved by ratio surrogate measurements [154, 155]. For ^{232}Th+n interaction the situation is more complex, mainly because of data scarcity on PFNS (see [88, 149]), missing of data on ^{232}Th(n, 3n) and inconsistency of surrogate data on ^{231}Th(n, f) [156, 157] and recent ratio surrogate data on ^{231}Th(n, F) [158]. However, the surrogate data on ^{231}Th(n, f) [156, 157] are consistent with the ^{231}Th(n, F), ^{232}Th(n, 2n) [88] and PFNS for n+^{232}Th interaction for emissive fission domain (E_n=14.7 MeV and E_n=18.8 MeV [88, 149]). Signatures in the measured PFNS were revealed, which are correlated with pre-fission neutron spectra and neutrons from chance-fission contributions.

This validated approach is used for the ^{237}Np(n, F), ^{237}Np(n, 2n)^{236s}Np and PFNS for n+^{237}Np interaction for non-emissive and emissive fission domain. Average energies of PFNS would predict distinct lowering in the vicinity of (n, nf) and (n, 2nf) reaction thresholds [4, 5, 6] probed in measured PFNS shapes by Taieb, *et al.* [159] at E_n=1-200 MeV. Obviously, in such approach we can describe/predict the PFNS shape variation with the increase of the excitation energy of the composite nuclide, using the average energy for the lowest incident neutron energy E_n=0.52 MeV [65].

12.1. (n, xnγ) and (n, xnf) neutron emission spectra

Exclusive (n, xnγ) and (n, xnf) neutron emission spectra for x = 1, 2, 3, reactions are calculated with Hauser-Feshbach model taking into account fission and gamma-emission competition to neutron emission, actually neutron spectra are calculated simultaneously with fission and (n, xn) reaction cross sections. The pre-equilibrium emission of first neutron is fixed by the description of high energy tails of (n, 2n) reaction cross sections and (n, F) reaction cross sections for ^{235}U, ^{238}U and ^{232}Th target nuclides [88, 151].

First neutron spectrum of the ^{237}Np(n, nf) or ^{237}Np(n, nγ) reactions is the sum of evaporated and pre-equilibrium emitted neutron contributions. Second and third neutron spectra for ^{237}Np(n, xnf(γ)) reactions are assumed to be evaporative. Pre-fission neutron spectrum of ^{237}Np(n, nf) reaction, especially its hard energy tail, is sensitive to the description of fission probability of ^{237}Np nuclide near fission threshold (see below).

Partial neutron spectra are shown on Figs 12.1 - 12.8. Components of first neutron spectra for E_n = 20, 14.7, 8 MeV are shown on Figs 12.1, 12.2, 12.3. Components of second neutron spectra for E_n = 20, 14.7, 8 MeV are shown on Figs 12.4, 12.5, 12.6. Components of third neutron spectra for E_n = 20, 14.7 MeV are shown on Figs 12.7, 12.8.

12.1.1 First neutron spectra

The first neutron spectra are calculated within a Hauser-Feshbach theory of nuclear reactions [87, 88] as

$$\frac{d\sigma^1_{nnx}}{d\varepsilon} = \sum_{J,\pi} W^A(E_n - \varepsilon, J^\pi)\,. \tag{12.1}$$

Here, $W^A(E_n - \varepsilon, J^\pi)$ is the population of the excited states in the first residual (target) nuclide A, ^{237}Np, formed after emission of first neutron, with spin J and parity π at excitation energy $U = E_n$-ε. For the compound nucleus A+1, ^{238}Np, the excitation energy equals $U = E_n+B_n$. First neutron spectrum contains the contribution of the pre-equilibrium neutron emission, for details of pre-equilibrium model calculations see [87]. Present statistical model of fission reaction assumes fission/neutron evaporation competition during decay of the excited compound nucleus, which is formed after the first-chance emission of pre-equilibrium neutron [87, 88], treated with a simple version of exciton model (see references in [87]). The equilibration is treated with a set of master-equations, describing the evolution of the excited nucleus states, classified by the number of particles plus number of holes [65].

To simplify the equations, we will omit spin and parity indices for fission Γ_f, neutron Γ_n, γ-emission Γ_γ and total $\Gamma = \Gamma_f + \Gamma_n + \Gamma_\gamma$ widths, as well as summations either over J and π, made according to the spin and parity conservation laws in neutron emission cascades. Neutron spectrum $\frac{d\sigma^1_{nnf}}{d\varepsilon}$ of the (n, nf)[1] reaction could be calculated using the first neutrons spectrum of (n, nx) reaction, i.e., (n, nx)[1], multiplied by the fission probability of the A, ^{237}Np, nuclide:

$$\frac{d\sigma^1_{nnf}}{d\varepsilon} = \frac{d\sigma^1_{nnx}(\varepsilon)}{d\varepsilon}\frac{\Gamma^A_f(E_n - \varepsilon)}{\Gamma^A(E_n - \varepsilon)}. \tag{12.2}$$

The hard-energy tail of the neutron spectrum of the (n, nf)[1] reaction would resemble the fission probability shape of nuclide A, ^{237}Np.

Spectrum of the first neutrons $\frac{d\sigma^1_{n2nx}}{d\varepsilon}$ of (n, 2nx) reaction, we will denote it as (n, 2nx)[1], could be obtained using the first neutrons spectrum of (n, nx) reaction, i.e., (n, nx)[1], (see Eq. (12.1)), multiplied by the neutron emission probability of A, ^{237}Np, nuclide:

$$\frac{d\sigma^1_{n2nx}}{d\varepsilon} = \frac{d\sigma^1_{nnx}(\varepsilon)}{d\varepsilon}\frac{\Gamma^A_n(E_n-\varepsilon)}{\Gamma^A(E_n-\varepsilon)} \tag{12.3}$$

Spectrum of the first neutrons $\frac{d\sigma^1_{n2nf}}{d\varepsilon}$ of (n, 2nf) reaction, i.e. (n, 2nf)[1] is obtained integrating the first neutrons spectrum of (n, 2nx) reaction, i.e., (n, 2nx)[1], multiplied by the fission probability of nuclide (A-1), ^{236}Np:

$$\frac{d\sigma^1_{n2nf}}{d\varepsilon} = \int_0^{E_n-B^A_n} \frac{d\sigma^1_{n2nx}(\varepsilon)}{d\varepsilon}\frac{\Gamma^{A-1}_f(E_n-B^A_n-\varepsilon-\varepsilon_1)}{\Gamma^{A-1}(E_n-B^A_n-\varepsilon-\varepsilon_1)}d\varepsilon_1 \tag{12.4}$$

Spectrum of the first neutrons $\frac{d\sigma^1_{n3nx}}{d\varepsilon}$ of (n, 3nx) reaction, we will denote it as (n, 3nx)[1], is obtained integrating the first neutrons spectrum of (n, 2nx) reaction, i.e., (n, 2nx)[1] (see Eq. (12.3)), using the neutron emission probability of (A-1) nuclide ^{236}Np as:

$$\frac{d\sigma^1_{n3nx}}{d\varepsilon} = \int_0^{E_n-B^A_n} \frac{d\sigma^1_{n2nx}(\varepsilon)}{d\varepsilon}\frac{\Gamma^{A-1}_n(E_n-B^A_n-\varepsilon-\varepsilon_1)}{\Gamma^{A-1}(E_n-B^A_n-\varepsilon-\varepsilon_1)}d\varepsilon_1 \tag{12.5}$$

Then, having the spectrum of first neutron of the (n, 3nx) reaction, $\frac{d\sigma^1_{n3nf}}{d\varepsilon}$ - spectrum of first neutrons of (n, 3nf) reaction, i.e. (n, 3nf)[1], is obtained integrating the first neutrons spectrum of (n, 3nx) reaction, i.e., (n, 3nx)[1] (see Eq. (12.5)), multiplied by the fission probability of (A-2) nuclide ^{235}Np as

$$\frac{d\sigma^1_{n3nf}}{d\varepsilon} = \int_0^{E_n-B_n-B^{A-1}_n} \frac{d\sigma^1_{n3nx}(\varepsilon)}{d\varepsilon}\frac{\Gamma^{A-2}_f(E_n-B^A_n-B^{A-1}_n-\varepsilon-\varepsilon_1-\varepsilon_2)}{\Gamma^{A-2}(E_n-B^A_n-B^{A-1}_n-\varepsilon-\varepsilon_1-\varepsilon_2)}d\varepsilon_2 \tag{12.6}$$

The latter equation is actually a double integral, which is obtained after substitution of Eq. (12.5) into Eq. (12.6), the integrations are maintained over the energies of partial neutrons of (n, 3nf)[1] reaction.

The fissilities of ^{238,237,236,235}Np are relatively higher than those of U and Th nuclei, considered earlier. At E_n = 20 and 14.7 MeV major contributions to the first neutron spectrum comes from (n, nf)[1] and (n, 2nf)[1] reactions spectra (see Figs 12.1 and 12.2), at lower energy of E_n = 8 MeV major contribution comes from (n, nf) reaction (see Fig. 12.3). That is obviously correlated with the neutron emission/fission competition for the n+^{237}Np interaction. Relative contributions of the (n, nf)[1] and (n, 2nf)[1] reactions spectra are correlated with the emissive/non-emissive fission chances structure of the observed fission cross sections and are evidenced in measured prompt fission neutron spectra. The contribution of (n, 2nf)[1] reaction spectrum to the first neutron spectrum of n+^{237}Np interaction is systematically lower than that of (n, nf) spectrum (see Figs 12.1 and 12.2). These relative contributions are much different as dependent on the fissilities of the initial composite nuclide and nuclides which emerge in emissive fission reactions.

In case of n+^{238}U and n+^{232}Th interactions the major partial components of the first neutron spectrum are those of (n, 2n)[1] and (n, 3n)[1] [88, 148, 149]. Shapes of the (n, nf)[1] spectra $\frac{d\sigma^1_{nnf}}{d\varepsilon}$ for ^{238}U(n, f) and ^{232}Th(n, f) reactions are defined by the fission probabilities of ^{238}U and ^{232}Th nuclides, respectively. Figs 1 and 2 of [88] demonstrate that contributions of (n, nf) second-chance fission reaction to the observed fission cross sections are rather different in case of ^{238}U and ^{232}Th target nuclides. Cross section shape of $^{238}U(n, nf)$ reaction is rather flat above the relevant threshold E_{nnf}, while that of $^{232}Th(n, nf)$ reaction demonstrates rather strong dependence on the incident neutron energy. Broad peak in $^{232}Th(n, nf)^1$ reaction cross section is pronounced in the neutron spectrum of (n, nf) reaction. Sharp decrease of $^{232}Th(n, nf)^1$ reaction spectrum for emitted first neutron energies $\varepsilon \geq E_n - B_f$ is evidenced in measured prompt fission neutron spectrum (see [88]).

In case of ^{238}U+n interaction, $(n, 2nf)^1$ spectrum $\dfrac{d\sigma^1_{n2nf}}{d\varepsilon}$ contribution is lower than that of $(n, nf)^1$ reaction up to $\varepsilon \approx 5$ MeV, for $\varepsilon \geq 5$ MeV it turns out to be higher. Contribution of $(n, 2nf)^1$ reaction spectrum to the first neutron spectrum of ^{232}Th +n interaction is systematically higher than that of $(n, nf)^1$ spectrum for $\varepsilon \leq 8$ MeV.

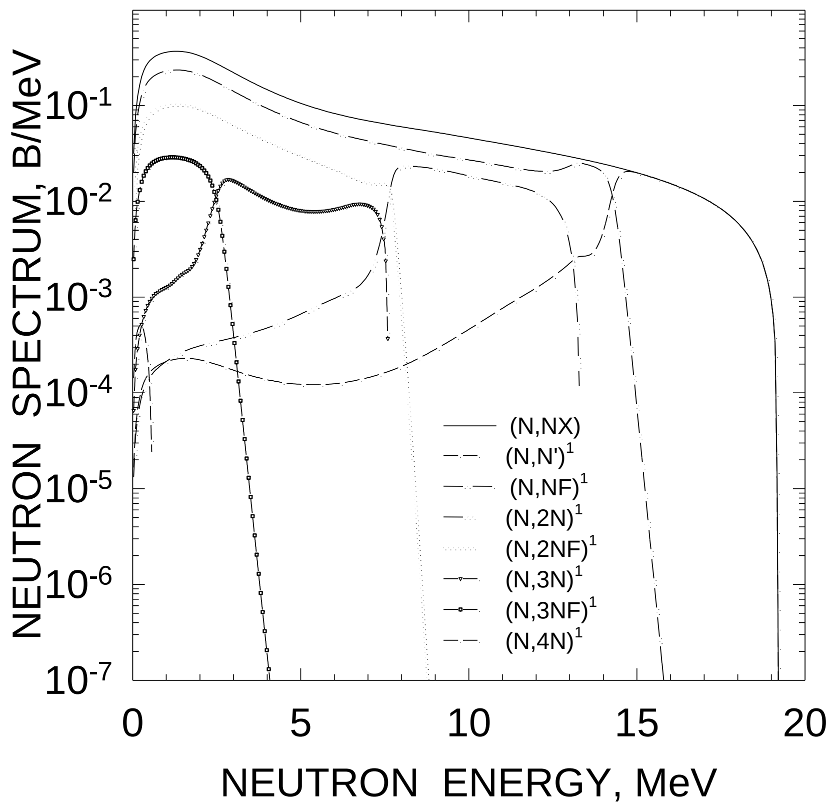

FIG. 12.1. Components of first neutron spectrum of ^{237}Np+n interaction for incident neutron energy 20 MeV.

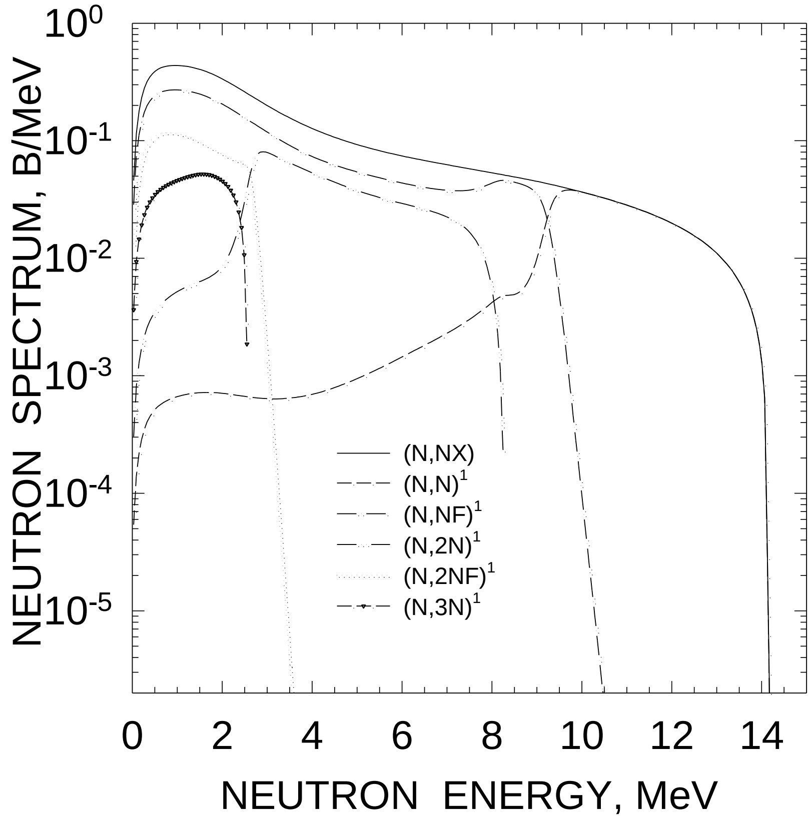

FIG. 12.2. Components of first neutron spectrum of ^{237}Np+n interaction for incident neutron energy 14.7 MeV.

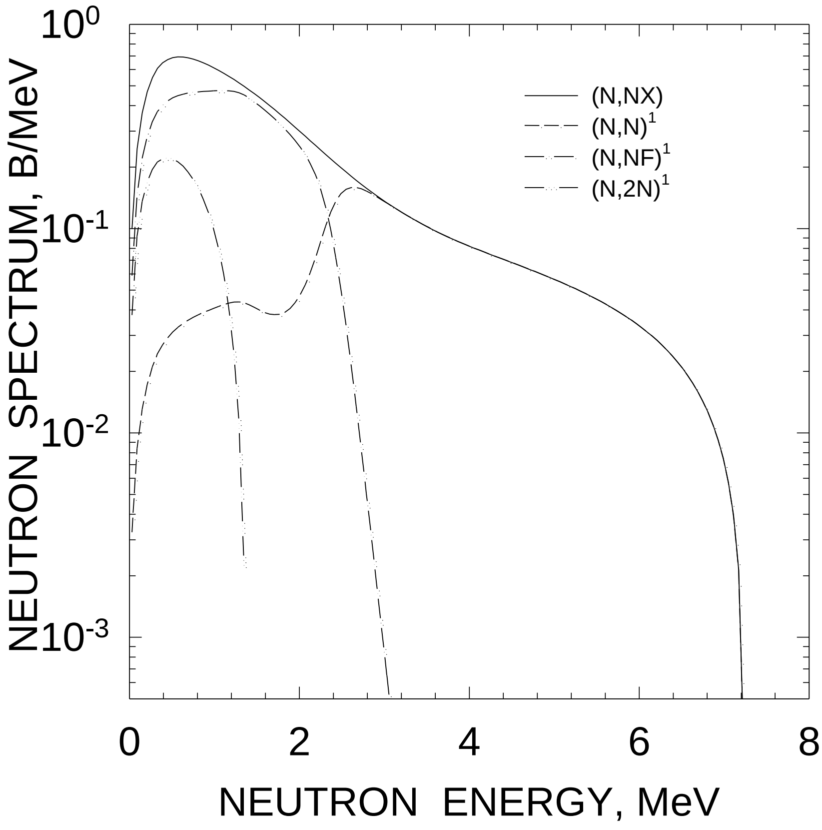

FIG. 12.3. Components of first neutron spectrum of ^{237}Np+n interaction for incident neutron energy 8 MeV.

In case of ^{238}U target nuclide contribution of (n, 3nf)^1 reaction spectra $\frac{d\sigma^1_{n3nf}}{d\varepsilon}$ to the first neutron spectrum is comparable with those of lower chance fission reactions for ε≤3 MeV, while in case of ^{232}Th target nuclide it is much lower (see [88]).

The components of the first neutron spectrum for n+^{237}Np interaction at E_n = 8 MeV are shown on Fig. 12.3. The contribution of (n, nf)^1 reaction is much higher than those of (n, n)^1 and (n, 2n)^1.

Spectrum of (n, nγ) ((n, n)^1) reaction actually is just hard energy tail of the pre-equilibrium component of the first neutron spectrum. Shapes of the first neutron spectra of (n, nγ) and (n, 2nγ) reactions at E_n=20 (Fig. 12.1) and 14 MeV (Fig. 12.2) are rather similar, soft part being defined by neutron emission competition of higher neutron multiplicity reactions. This lowering of soft part of first neutron spectrum of (n, 2nγ) reaction disappears for E_n=8 MeV (see Fig. 12.3).

That is a simple illustration of the strong dependence of the partial contributions of the exclusive first neutron spectra on the fissilities of the composite (A+1) nuclides as well as relative fissilities of A, A-1, A-2 nuclides.

12.1.2. Second neutron spectra

Second neutron spectrum of the (n, 2nx) reaction, (n, 2nx)^2 , i.e. emission spectrum of the second neutrons or neutrons, emitted from residual nuclide A, ^{237}Np, is calculated integrating over first neutron spectrum (n, nx)^1 of the (n, nx) reaction (see Eq. (12.1)) using the neutron emission probability of A, ^{237}Np, nuclide as

$$\frac{d\sigma^2_{n2nx}}{d\varepsilon} = \int_0^{E_n - B_n^A} \frac{d\sigma^1_{n2nx}(\varepsilon)}{d\varepsilon} \frac{\Gamma_n^A(E_n - B_n^A - \varepsilon - \varepsilon_1)}{\Gamma^A(E_n - B_n^A - \varepsilon - \varepsilon_1)} d\varepsilon_1 \qquad (12.7)$$

Second neutron spectrum of the (n, 2nf) reaction, we will denote it as (n, 2nf)^2, would be expressed as a double integral. It would be obtained using Eq. (12.7), which defines second neutron spectrum of (n, 2nx) reaction, i.e., (n, 2nx)^2 and fission probability of (A-1),^{236}Np, nuclide as

$$\frac{d\sigma^2_{n2nf}}{d\varepsilon} = \int_0^{E_n - B_n^A} \frac{d\sigma^2_{n2nx}(\varepsilon)}{d\varepsilon} \frac{\Gamma_f^{A-1}(E_n - B_n^A - \varepsilon - \varepsilon_1)}{\Gamma^{A-1}(E_n - B_n^A - \varepsilon - \varepsilon_1)} d\varepsilon_1 . \qquad (12.8)$$

Obviously, boundary energies of first and second neutrons of (n, 2nf) reactions coincide.

Second neutron spectrum of the (n, 3nx) reaction, we will denote it as (n, 3nx)^2, also would be a double integral, it is defined using second neutron spectrum of (n, 2nx) reaction, i.e., (n, 2nx)^2 (see Eq. (12.7)) and neutron emission probability of (A-1), ^{236}Np nuclide, as

$$\frac{d\sigma^2_{n3nx}}{d\varepsilon} = \int_0^{E_n - B_n^A} \frac{d\sigma^2_{n2nx}(\varepsilon)}{d\varepsilon} \frac{\Gamma_n^{A-1}(E_n - B_n^A - \varepsilon_1 - \varepsilon_2)}{\Gamma^{A-1}(E_n - B_n^A - \varepsilon_1 - \varepsilon_2)} d\varepsilon_2 . \qquad (12.9)$$

Second neutron spectrum of the (n, 3nf) reaction, we will denote it as (n, 3nf)^2, is calculated integrating second neutron spectrum of (n, 3nx) reaction, (n, 3nx)^2, which is a double integral, and a fission probability of (A-2), ^{235}Np nuclide, as

$$\frac{d\sigma^2_{n3nf}}{d\varepsilon} = \int_0^{E_n - B_n - B_n^{A-1}} \frac{d\sigma^2_{n3nx}(\varepsilon)}{d\varepsilon} \frac{\Gamma_f^{A-2}(E_n - B_n^A - B_n^{A-1} - \varepsilon_1 - \varepsilon_2 - \varepsilon_3)}{\Gamma^{A-2}(E_n - B_n^A - B_n^{A-1} - \varepsilon_1 - \varepsilon_2 - \varepsilon_3)} d\varepsilon_3 \qquad (12.10)$$

The latter expression is a triple integral over excitation energies of the (A-2), (A-1) and A residual nuclides, or, equivalently, over partial neutron energies of (n, 3nf) reaction. The latter expression is a triple integral over excitation energies of the (A-2), (A-1) and A residual nuclides, or, equivalently, over partial neutron energies of (n, 3nf) reaction.

At E_n = 20 MeV major contribution to the second neutron spectrum (up to ε ≈ 8 MeV) comes from (n, 2nf) ^{2} reaction (see Fig. 12.4). Soft parts of the second neutron spectra of (n, 2nγ)^2 and (n, 3nγ)^2 reactions are comparable. At lower incident neutron energy E_n = 14 MeV major contribution to the second neutron spectrum comes from (n, 2nγ)^2 reaction (see Fig. 12.5).

At lower energy E_n = 8 MeV major contribution to the second neutron spectrum, obviously, comes from (n, 2n)^2 reaction (see Fig. 12.6). In case of n+^{238}U and n+^{232}Th interactions the major partial components of the second neutron spectrum are those of (n, 2n)^1 partial contributions of the exclusive second neutron spectra on the fissilities of the composite (A+1) nuclides as well as relative fissilities of A, A-1, A-2 nuclides.

12.1.3. Third neutron spectra

Third neutrons spectrum of the (n, 3nx) reaction, (n, 3nx)^3, is obtained from (n, 2nx)^2 (see Eq. (12.7)) reaction spectrum using neutron emission probability from (A-1) nuclide as

$$\frac{d\sigma^3_{n3nx}}{d\varepsilon} = \int_0^{E-B_n^A-B_n^{A-1}} \frac{d\sigma^2_{n2nx}(\varepsilon)}{d\varepsilon}\frac{\Gamma_n^{A-1}(E_n-B_n^A-\varepsilon_1-\varepsilon_2)}{\Gamma^{A-1}(E_n-B_n^A-\varepsilon_1-\varepsilon_2)}d\varepsilon_2 . \qquad (12.11)$$

The latter spectrum is a double integral over excitation energies of A and (A-1) residual nuclides, or, equivalently, over partial neutron energies of (n, 3nx) reaction.

Third neutrons spectrum (n, 3nf)^3 is obtained using the third neutrons spectrum of (n, 3nx) reaction, (n, 3nx)^3, and fission probability of (A-2) nuclide as

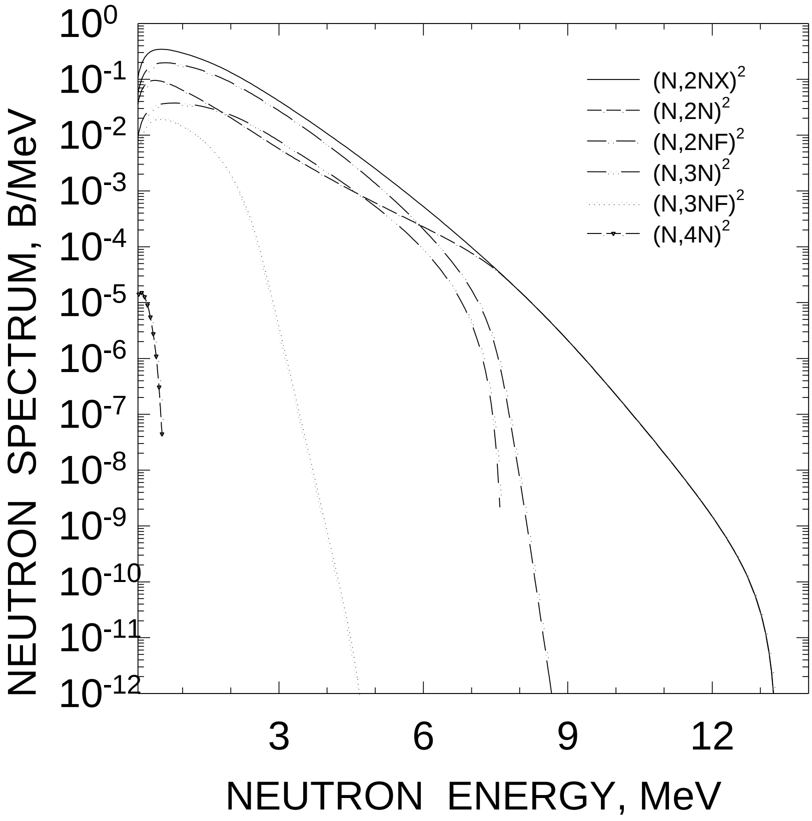

FIG. 12.4. Components of second neutron spectrum of ^{237}Np+n interaction for incident neutron energy 20 MeV.

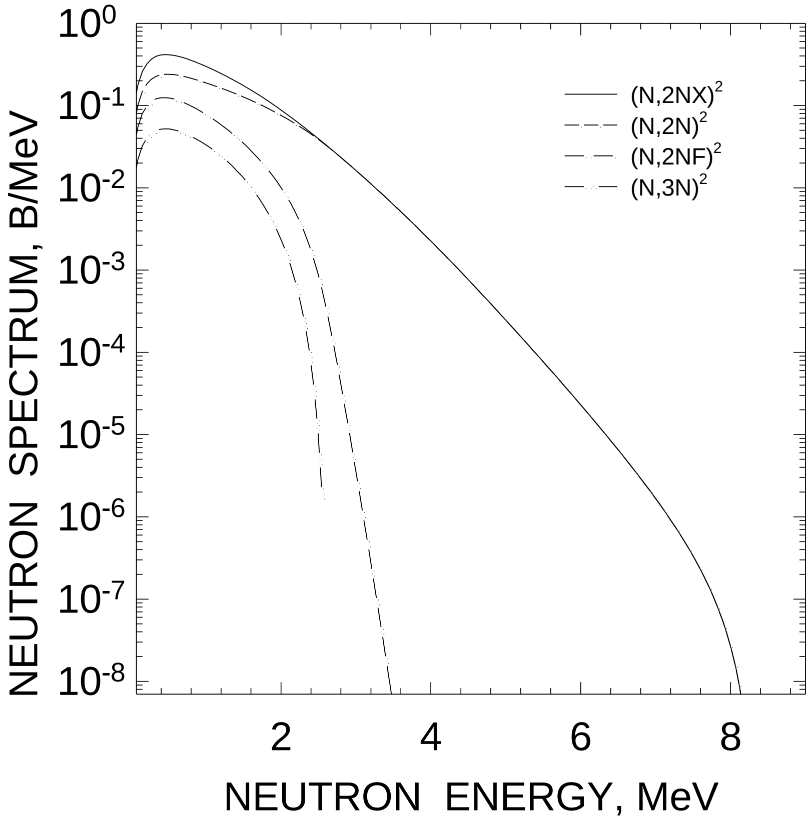

FIG. 12.5. Components of second neutron spectrum of ^{237}Np+n interaction for incident neutron energy 14.7 MeV.

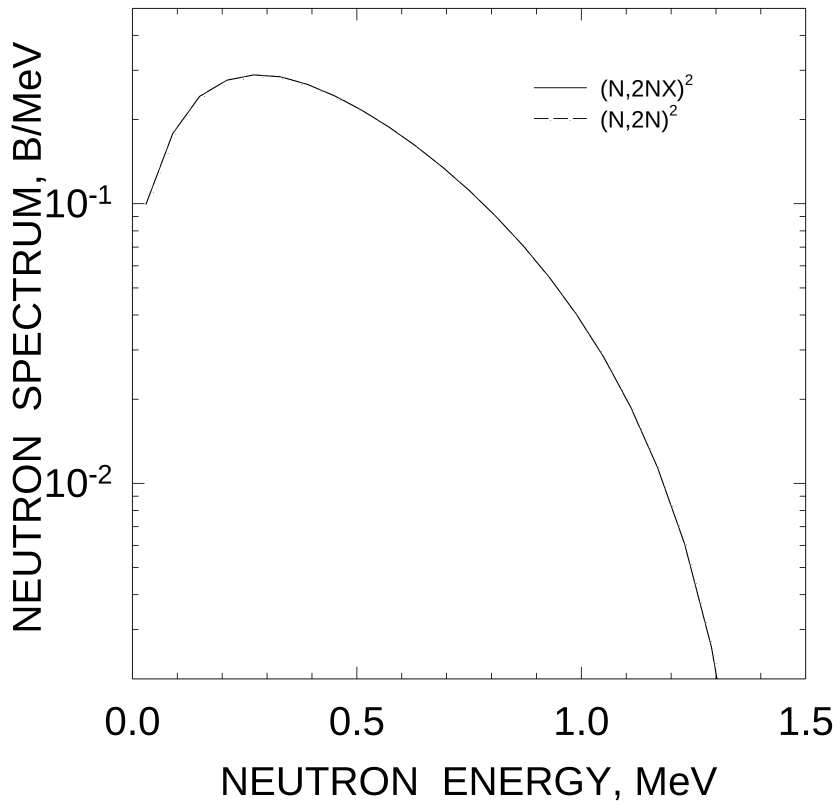

FIG. 12.6. Components of second neutron spectrum of ^{237}Np+n interaction for incident neutron energy 8 MeV.

$$\frac{d\sigma^3_{n3nf}}{d\varepsilon} = \int_0^{E-B_n^A-B_n^{A-1}} \frac{d\sigma^3_{n3nx}(\varepsilon)}{d\varepsilon} \frac{\Gamma_f^{A-2}(E_n - B_n^A - B_n^{A-1} - \varepsilon_1 - \varepsilon_2 - \varepsilon_3)}{\Gamma^{A-2}(E_n - B_n^A - B_n^{A-1} - \varepsilon_1 - \varepsilon_2 - \varepsilon_3)} d\varepsilon_3 . \qquad (12.12)$$

At E_n = 20 MeV most contribution to the third neutron spectrum comes from (n, 3nγ) reaction (see Fig. 12.7), that of the (n, 3nf) reaction being rather low. Similar partitioning is predicted in case of n+^{238}U and n+^{232}Th interactions [88, 141, 142]. Main contribution to the third neutron spectrum (n, 3nf)^3 comes from (n, 3n)^3 reaction for both target nuclei. The contribution of (n, 3nf)^3 is higher in case of ^{238}U target than in case of ^{232}Th. Because of the lowering of excitation energy after emission of 1st and 2nd neutrons, influence of relevant nuclei level density and fission barrier parameters for the 3d neutron spectra is much higher, than in case of first or second neutron emission.

Summarizing, we anticipate that partial (n, xnf) pre-fission neutron spectra for ^{237}Np target nuclide would be pronounced in observed PFNS to a different extent as compared with n+^{238}U and n+^{232}Th interactions. Present estimates of the partial pre-fission neutron spectra, calculated simultaneously with consistent reproduction of (n, F) and (n, xn) reaction cross sections, are more reliable than various previous estimates, based on Weisscopf-Ewing approach [160, 161], or more ambiguous phenomenological estimates of pre-fission neutron spectra, which are used in previous PFNS analyses [3, 7].

12.2 Prompt Fission Neutron Spectra

PFNS from fission fragments are calculated as a superposition of two Watt distributions for heavy and light fission fragments (FF), the partial contributions being equal, while the temperatures of the fragments are different [150]. Fission fragments' kinetic energy is the superimposed phenomenological parameter, generally lower, than total kinetic energy (TKE) of

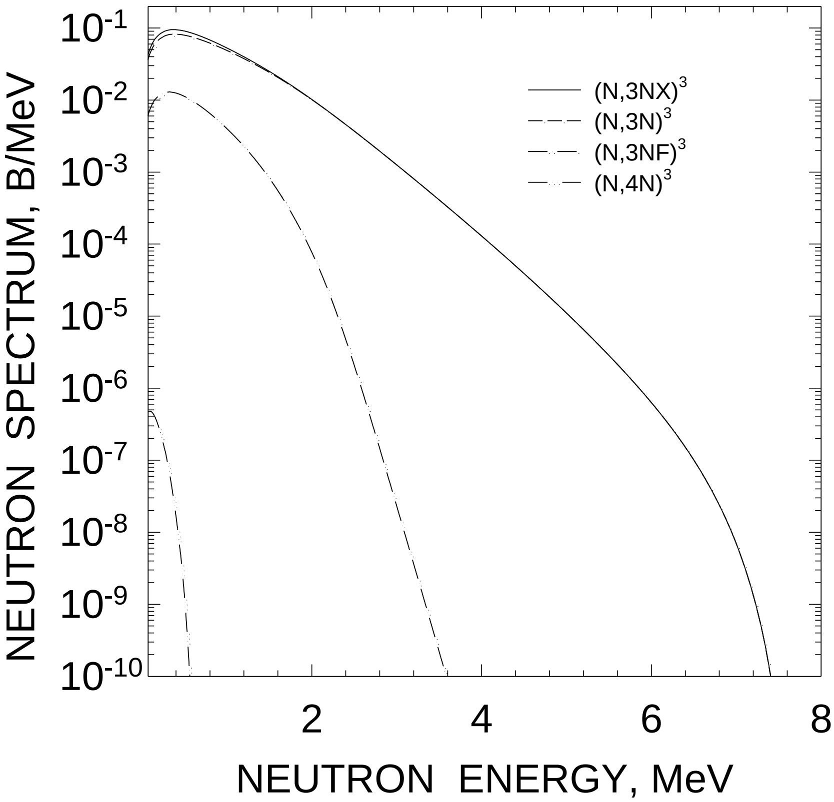

FIG. 12.7. Components of third neutron spectrum of ^{237}Np+n interaction for incident neutron energy 20 MeV.

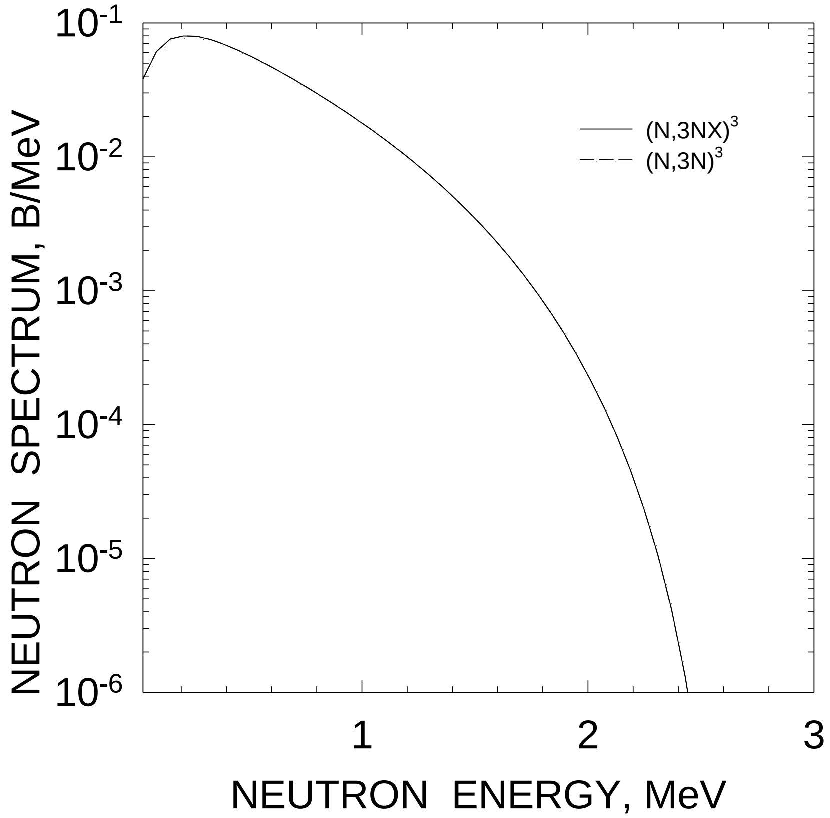

FIG. 12.8. Components of third neutron spectrum of ^{237}Np+n interaction for incident neutron energy 14.7 MeV

accelerated fission fragments. That peculiarity roughly reflects its dependence on the moment of prompt fission neutron emission [150].

That approach appeared to be quite flexible to reproduce the measured data base for the prompt fission neutron spectrum of the n+^{235}U system [2]. The evaluated ^{235}U(n, f) thermal neutron spectrum describes the newest data by Hambsch, *et al.* [162, 163]. The longstanding problem of inconsistency of integral thermal data testing and differential prompt fission neutron spectra data (PFNS) for major fissile nuclide ^{235}U seems to be resolved. The problem had emerged mostly due to rather poor fits of differential PFNS data in major data libraries. A phenomenological approach, developed by Kornilov, *et al.* [150] for the first-chance fission and extended for the emissive fission domain by Maslov, *et al.* [88, 151] was normalized at E_{th} to reproduce for ^{235}U(n, F) both the PFNS average energy $\langle E \rangle$ and measured PFNS up to 20 MeV [2].

In case of n+^{237}Np system for normalization purposes the point of $E_n \approx 0.52$ MeV [65] would be used as that is the lowest incident neutron energy at which measured PFNS data are available. The prompt fission neutron spectrum $S\ (\varepsilon, E_n)$ is calculated as a sum of two Watt [164] distributions, modified to take into account the emission of prompt fission neutrons before full acceleration of fission fragments. The neutrons, emitted from heavy and light fission fragments are included with equal weights:

$$S(\varepsilon, E_n) = 0.5 \cdot \sum_{j=l,h} W_j(\varepsilon, E_n, T_j(E_n), \alpha), \tag{12.13}$$

$$W_j(\varepsilon, E_n, T_j(E_n), \alpha) = \frac{2}{\sqrt{\pi} T_j^{3/2}} \sqrt{\varepsilon} \exp\left(-\frac{\varepsilon}{T_j}\right) \exp\left(-\frac{E_{vj}}{T_j}\right) \frac{sh(\sqrt{b_j \varepsilon})}{\sqrt{b_j \varepsilon)}}, \tag{12.14}$$

$$b_j = \frac{4E^0_{vj}}{T^2_j},\ T_j = k_j\sqrt{E^*_j} = k_j\sqrt{E_r - TKE + E_n + B_n}\ , \tag{12.15}$$

$$E^0_{vl} = \frac{A_h}{A_l A}\cdot\alpha\cdot TKE\ ,E^0_{vh} = \frac{A_l}{A_h A}\cdot\alpha\cdot TKE\ . \tag{12.16}$$

The coefficient α is the ratio of the kinetic energies of the fragments at the moment of neutron emission to the kinetic energy of fully accelerated fragments and is, in fact, a free parameter. The ratio of the temperatures of the light and heavy fragment $r=T_l/T_h$ is another free parameter, which ensures the model [150] flexibility to reproduce the soft and hard tails of the PFNS. The parameters α=0.808 and r=1.248 were fixed in [150] by fitting, in fact, the PFNS for n+^{237}Np system at E_n=7.8 MeV [165]. However, these model parameters allow reproduce quite well the shape of PFNS and/or PFNS average energy $\langle E\rangle$, measured at 0.52 MeV by Kornilov, *et al.* [65], at 2.9 MeV by Boikov, *et al.* [133] and at 4.9 MeV by Trufanov, *et al.* [165] (see Figs 12.9-12.11). The evaluation of ENDF/B-VII.0 poorly describes the data shape, introducing strange step-wise structures at E_n = 0.52 MeV for emitted neutron energies ε≤1 MeV.

The phenomenological approach, developed in [150], was extended towards the emissive fission up to E_n = 20 MeV [88, 151]. The analysis of the measured PFNS for neutron-induced fission of ^{232}Th, ^{235}U and ^{238}U showed that a number of data peculiarities are correlated with the influence of (n, xnf) pre-fission neutrons on the observed prompt fission neutron spectra.

Fortunately, in case of ^{237}Np(n, F) the partial ^{237}Np (n, xnf) contribution could be fixed almost unambiguously. Exclusive (n, xnf) pre-fission neutron spectra, as described above, are calculated consistently with the ^{237}Np(n, F) and ^{237}Np(n, 2n)^{236s}Np neutron cross sections. At E_n higher than the emissive fission threshold $S\ (\varepsilon, E_n)$ is calculated as a superposition of pre-

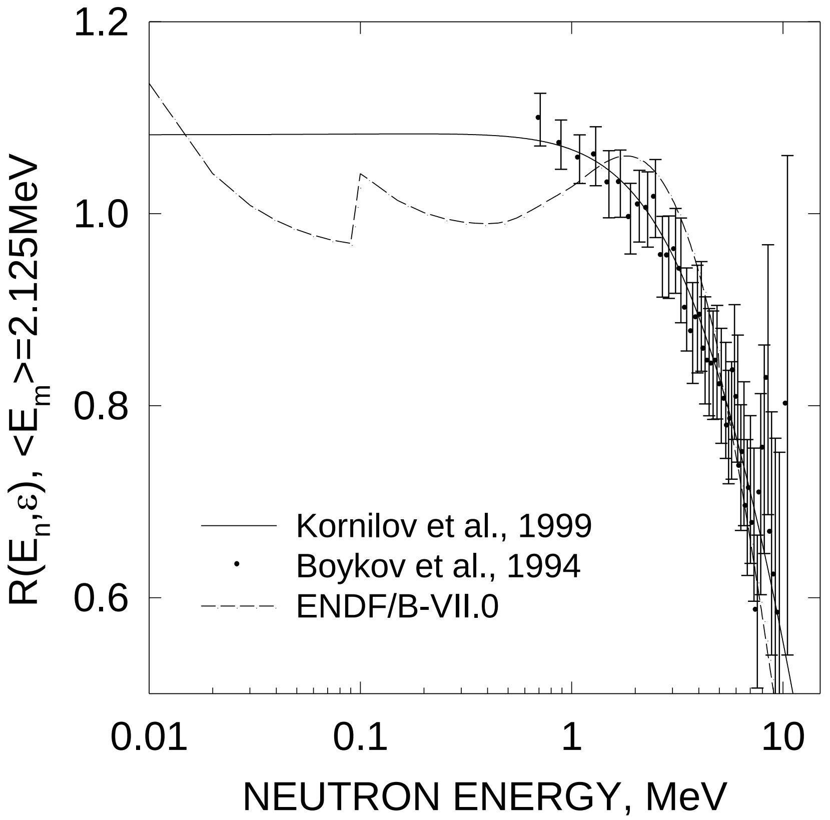

FIG. 12.9. Prompt fission neutron spectra for ^{237}Np(n, F), incident neutron energy 0.52 MeV. The spectrum is plotted as a ratio to Maxwellian with average energy of $<E_m>$=2.125 MeV.

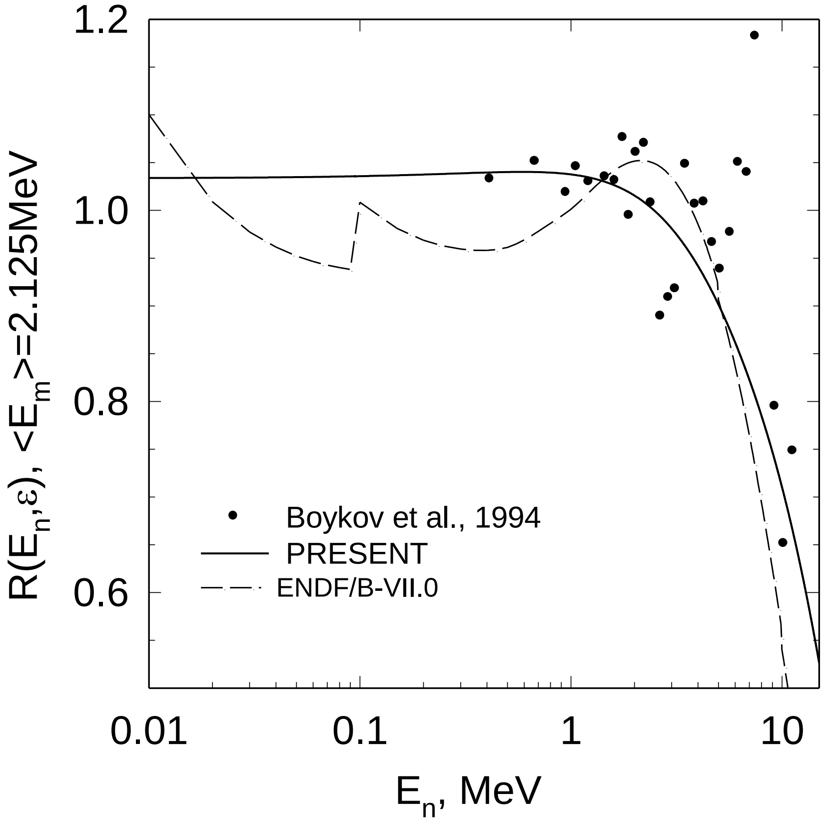

FIG. 12.10. The same as in Fig. 12.9 for E_n= 2.9 MeV. The spectrum is plotted as a ratio to Maxwellian with average energy of $<E_m>$=2.125 MeV.

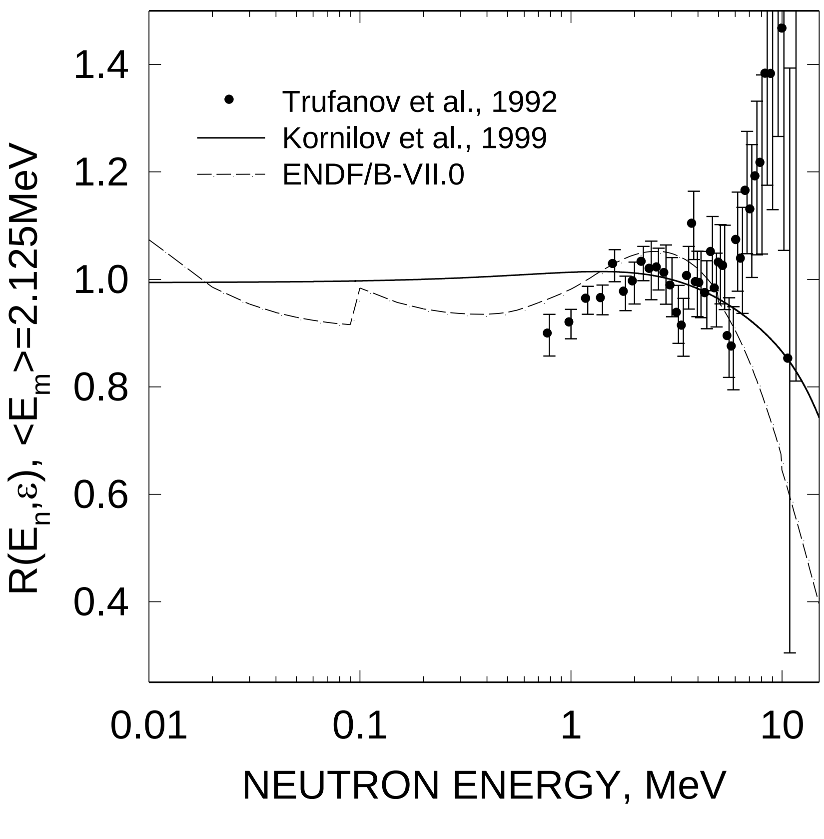

FIG. 12.11. The same as in Fig. 12.9 for E_n= 4.9 MeV. The spectrum is plotted as a ratio to Maxwellian with average energy of $<E_m>$=2.125 MeV.

fission (n, xnf) neutrons $-d\sigma^k_{nxnf}/d\varepsilon$ (x=1, 2, 3, 4; k=1,…,x) and post-fission spectra $S_{A+2-x}(\varepsilon, E_n)$ of the neutrons from the fission fragments:

$$
\begin{aligned}
& S(\varepsilon,E_n)=\tilde{S}_{A+1}(\varepsilon,E_n)+\tilde{S}_A(\varepsilon,E_n)+\tilde{S}_{A-1}(\varepsilon,E_n)+\tilde{S}_{A-2}(\varepsilon,E_n)= \\
& \nu^{-1}(E_n)\cdot(\nu_1(E_n)\cdot\beta_1(E_n)\cdot S_{A+1}(\varepsilon,E_n)+\nu_2(E_n)\cdot\beta_2(E_n)\cdot S_A(\varepsilon,E_n)+ \\
& +\beta_2(E_n)\cdot\frac{d\sigma^1_{nnf}}{d\varepsilon}+\nu_3(E_n)\cdot\beta_3(E_n)\cdot S_{A-1}(\varepsilon,E_n)+\beta_3(E_n)\cdot\left[\frac{d\sigma^1_{n2nf}}{d\varepsilon}+\frac{d\sigma^2_{n2nf}}{d\varepsilon}\right]+ \quad 12.17) \\
& +\nu_4(E_n)\cdot\beta_4(E_n)\cdot S_{A-2}(\varepsilon,E_n)+\beta_4(E_n)\cdot\left[\frac{d\sigma^1_{n3nf}}{d\varepsilon}+\frac{d\sigma^2_{n3nf}}{d\varepsilon}+\frac{d\sigma^3_{n3nf}}{d\varepsilon}\right])
\end{aligned}
$$

The pre-fission (n, xnf) neutron emission lowers the excitation energies of the residual Np nuclides. In case of the ^{237}Np(n, F) reaction the spectra of pre-fission (n, xnf) neutrons appear to be rather soft as compared with the spectra of neutrons, emitted by primary fission fragments after scission of the ^{237}Np and ^{236}Np nuclides, fissioning in ^{237}Np(n, nf) and ^{237}Np(n, 2nf) reactions, respectively. Fig. 12.12 shows a comparison of the PFNS at E_n = 7.8 MeV for ^{237}Np (n, F), observed by Trufanov, *et al.* [165]. The sharp increase of the soft neutron yield at $\varepsilon \leq 2$ MeV is exemplified. The shape of the pre-fission neutron contribution much depends on the fissilities and relevant emissive fission contributions, being most pronounced for ^{232}Th(n, F) and much less pronounced in case of the ^{237}Np(n, F) reaction. Fig. 12.13 shows the partial contributions of ^{237}Np(n, f) and ^{237}Np(n, nf) reactions to the observed PFNS, shown on previous Fig. 12.12. The contribution of ^{237}Np(n, nf) reaction is systematically lower than that of ^{237}Np(n, f) reaction. Attempts to fill the soft neutrons excess in the prompt fission neutron spectra for the

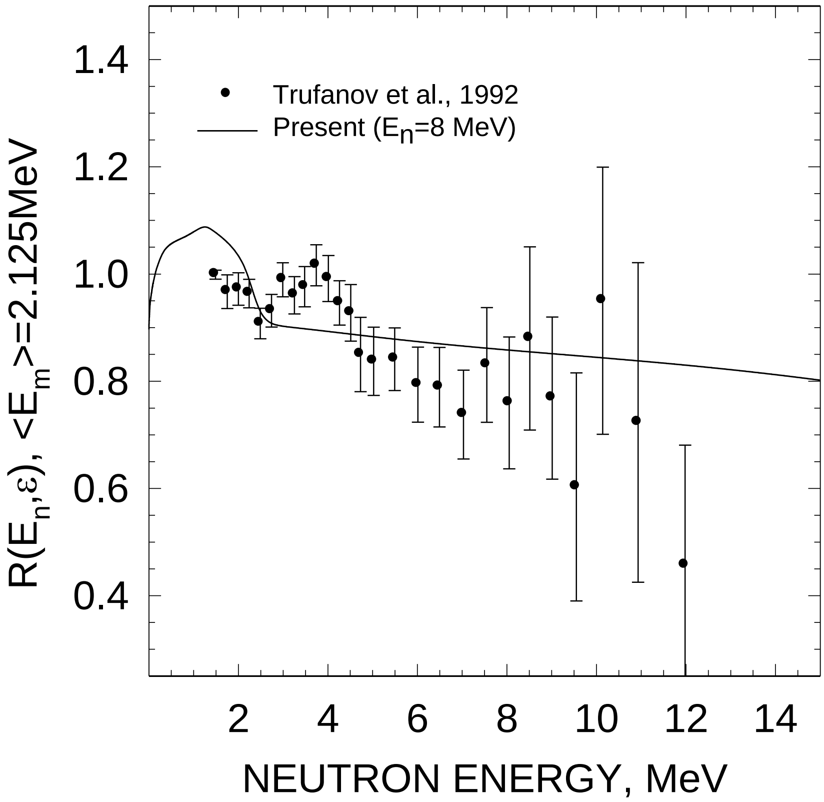

FIG. 12.12. The same as in Fig. 12.9 for E_n= 7.8 MeV. The spectrum is plotted as a ratio to Maxwellian with average energy of $<E_m>$=2.125 MeV.

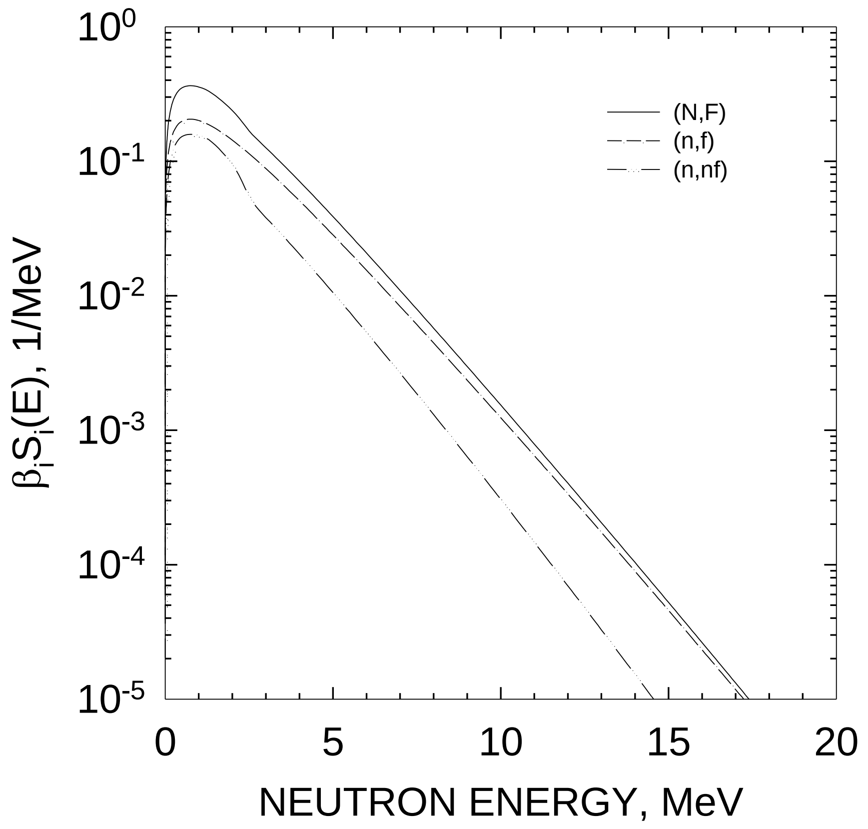

FIG. 12.13. Multiple-chance fission contributions to the prompt fission neutron spectrum for ^{237}Np (n, F) reaction, incident neutron energy 8 MeV.

emissive fission domain either for ^{238}U(n, F) [166] or ^{237}Np(n, F) [166] by arbitrary increase of the second chance fission contribution are not justified. In these approaches one can never reproduce even qualitatively the observed PFNS data.

At incident neutron energy of E_n = 14.7 MeV, the observed PFNS [133] of ^{237}Np(n, F) reaction is composed of ^{237}Np(n, f), ^{237}Np(n, nf) and ^{237}Np(n, 2nf) fission reaction contributions. The (n, nf) reaction contribution produces the broad spikes around ε~7 MeV, and strongly influences the soft part of the PFNS (see Fig. 12.14). Obviously, with previous approaches, based on the model [160], the measured PFNS data in the emissive fission domain are not reproduced even qualitatively. Figure 12.15 shows the partial contributions of ^{237}Np(n, f), ^{237}Np(n, nf) and ^{237}Np(n, 2nf) fission reactions to the observed prompt fission neutron spectrum. The contribution of ^{237}Np(n, nf) reaction is systematically lower than that of ^{237}Np(n, f) reaction, except in the vicinity of the highest energy of the exclusive spectra of the (n, nf) pre-fission neutrons. The contribution of ^{237}Np(n, 2nf) reaction is much lower than both ^{237}Np(n, f) and ^{237}Np(n, nf) reaction contributions. The contribution of pre-fission (n, nf) neutron is evidenced around ε ~ 8 MeV (see Fig. 12.14). The contribution of pre-fission first neutron of (n, 2nf), (n, 2nf)^1, reaction is evidenced in the energy range of ε~0-3 MeV.

Fig. 12.16 shows the partial contributions of ^{237}Np(n, f), ^{237}Np(n, nf), ^{237}Np(n, 2nf) and ^{237}Np(n, 3nf) fission reactions to the prompt fission neutron spectrum at E_n = 20 MeV. The contribution of ^{237}Np(n, nf) reaction is higher than that of ^{237}Np(n, f) reaction, especially for the emitted neutron energies, probing the excitation energies near the fission threshold of ^{237}Np nuclide.

The combined effect of fission chances and exclusive pre-fission neutron spectra leads to the lowering of the average energy of the PFNS of ^{237}Np(n, F) in the vicinity of the ^{237}Np(n, nf) and ^{237}Np (n, 2nf) reaction thresholds. The dips are evidenced in measured PFNS average energy $\langle E \rangle$ of [159]. Fig. 12.17 shows that the present calculated energies of the prompt fission neutron spectra $\langle E \rangle$ closely reproduce the estimate by Trufanov, *et al.* [165] at E_n=7.8 MeV and by Boykov, *et al.* [133] at 2.9 and 14.7 MeV. The normalization point is the energy of $E_n \approx 0.5$ MeV, around which there are data by Kornilov, *et al.* [65] and at E_n = 0.62 by Than Win, *et al.* [167] are also reproduced. The dips, observed by Taieb, *et al.* [159] around ^{237}Np(n, nf) and ^{237}Np(n, 2nf) reaction thresholds are qualitatively consistent with present calculation. In case of ENDF/B-VII.0 [3] or JENDL-3.3 [7] the structure in the average energy of the PFNS $\langle E \rangle$ is ignored. In some previous calculations [166] done with the Madland-Nix model [160h] the variation of $\langle E \rangle$ with the increase of E_n might be reproduced because of an unjustified increase of the second chance fission ^{237}Np(n, nf) contribution to the fission observables. Besides, in previous calculations, done with the Madland-Nix model [166] the pre-fission neutron spectra were never calculated as exclusive ones. In an approach, pursued in [168], scission neutrons, emitted from non-accelerated neutrons are introduced. However, simplified procedure of obtaining pre-fission neutron spectra introduced a number of uncertainties into the estimated in [168] average energy $\langle E \rangle$.

Figs 12.18 - 12.21 compare present PFNS with ENDF/B-VII.0 [3] evaluated PFNS. Drastic shape differences are easily noticed, notwithstanding the reasonable consistency of the average energies of emitted prompt fission neutron spectra both in first-chance and emissive fission domains.

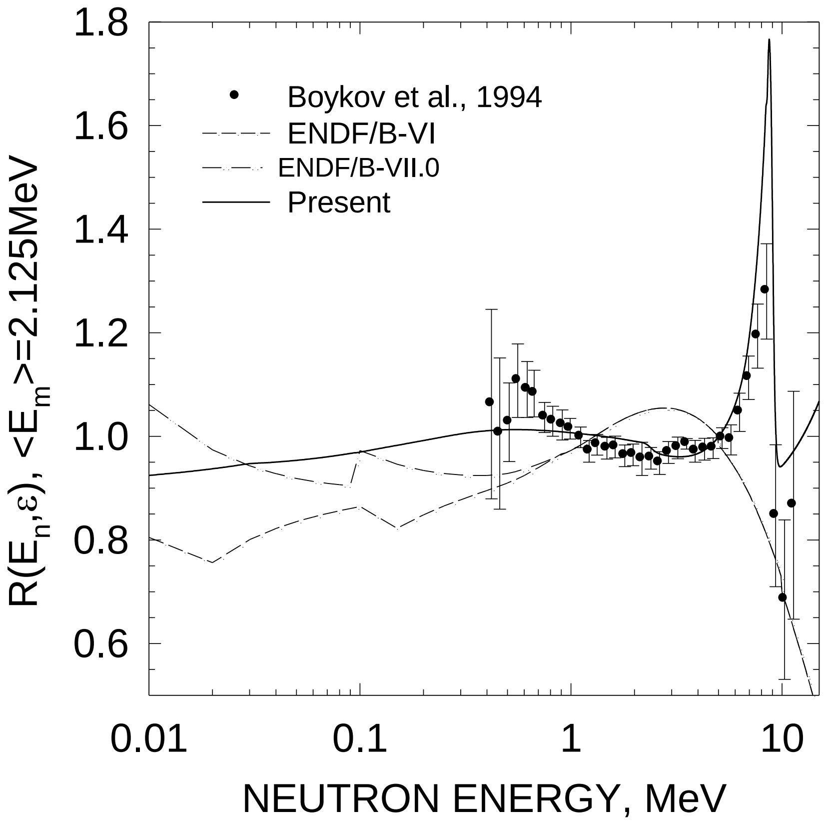

FIG. 12.14. The same as in Fig. 12.9 for E_n= 14.7 MeV. The spectrum is plotted as a ratio to Maxwellian with average energy of $<E_m>$=2.125 MeV.

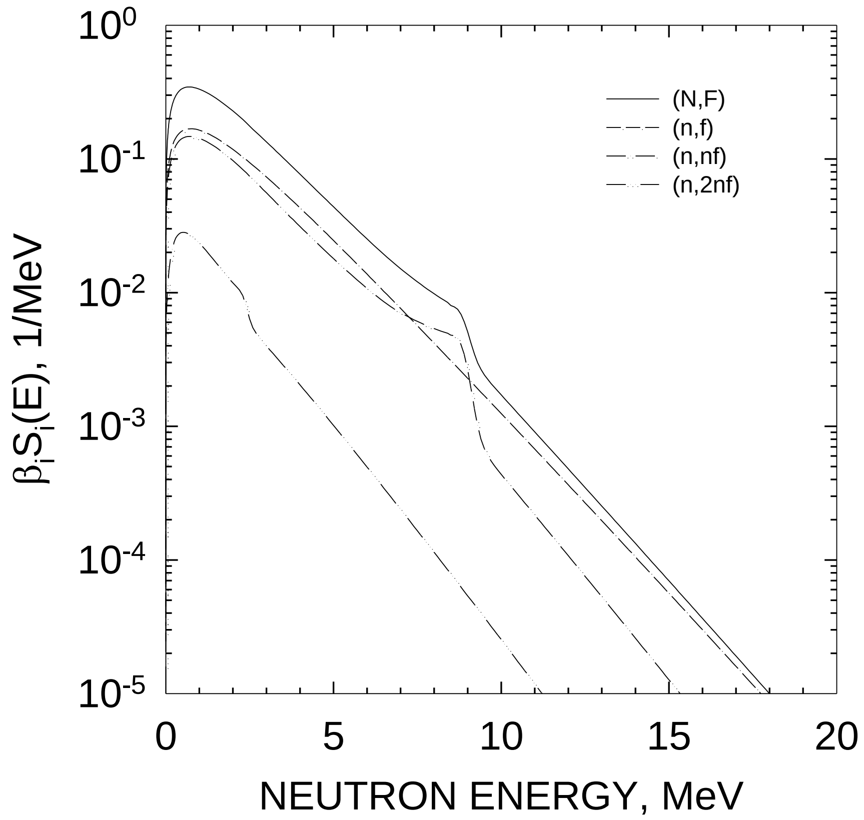

FIG. 12.15. Multiple-chance fission contributions to the prompt fission neutron spectrum for ^{237}Np (n, F) reaction, incident neutron energy 14.7 MeV.

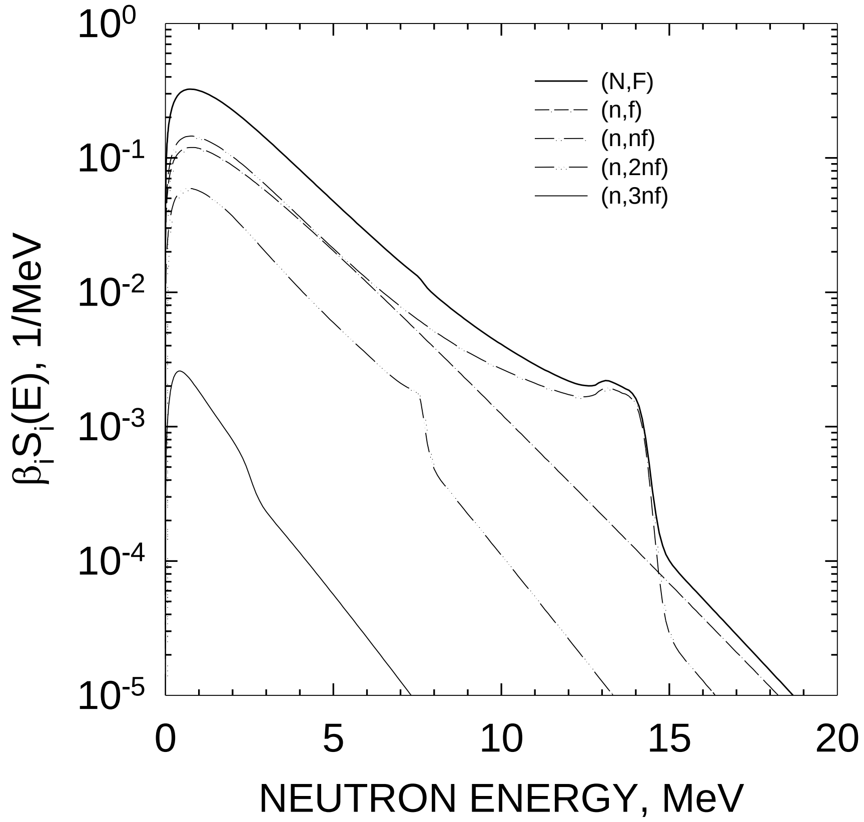

FIG. 12.16. Multiple-chance fission contributions to the prompt fission neutron spectrum for ^{237}Np (n, F) reaction, incident neutron energy 20 MeV.

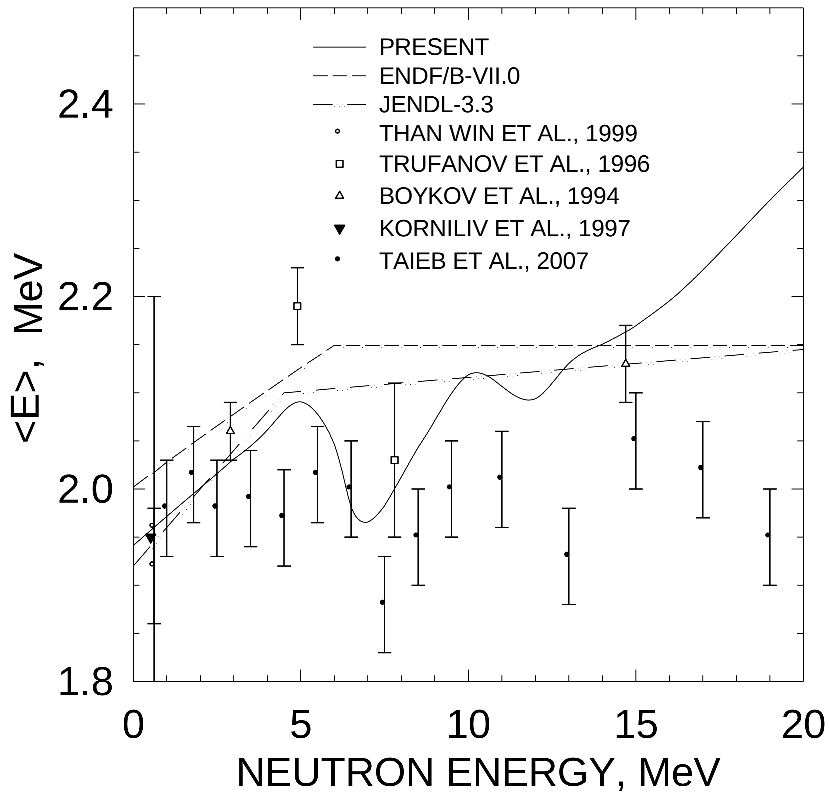

FIG. 12.17. Dependence of average energy of ^{237}Np (n, F) prompt fission neutrons on the incident neutron energy.

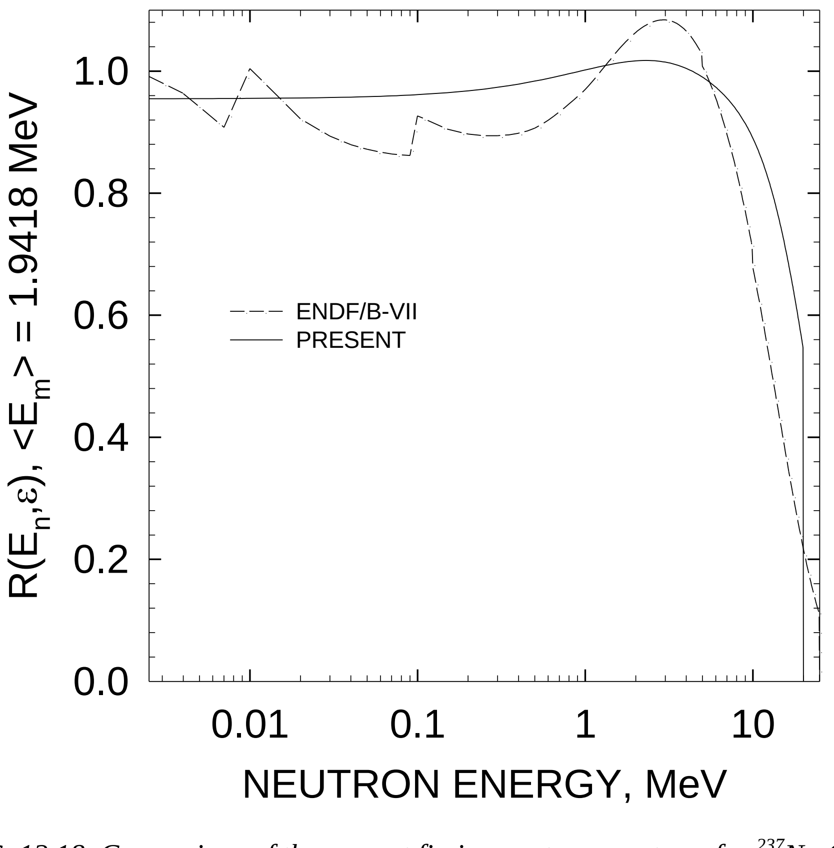

FIG. 12.18. Comparison of the prompt fission neutron spectrum for ^{237}Np (n, F) reaction at incident neutron energy of 10^{-5} MeV.

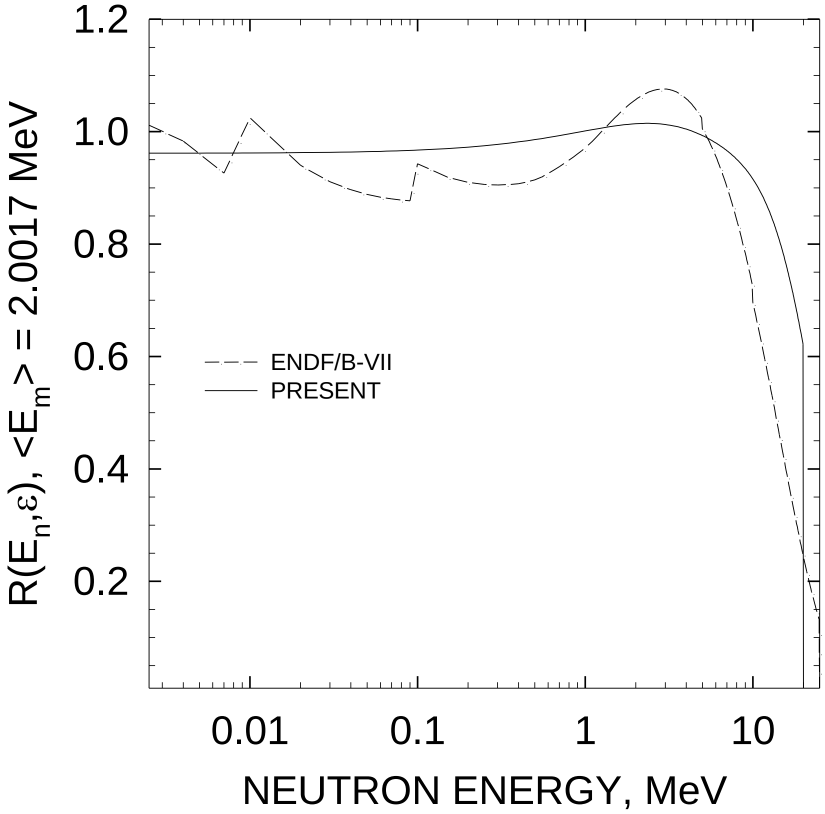

FIG. 12.19. Comparison of the prompt fission neutron spectrum for ^{237}Np (n, F) reaction atincident neutron energy of 2 MeV.

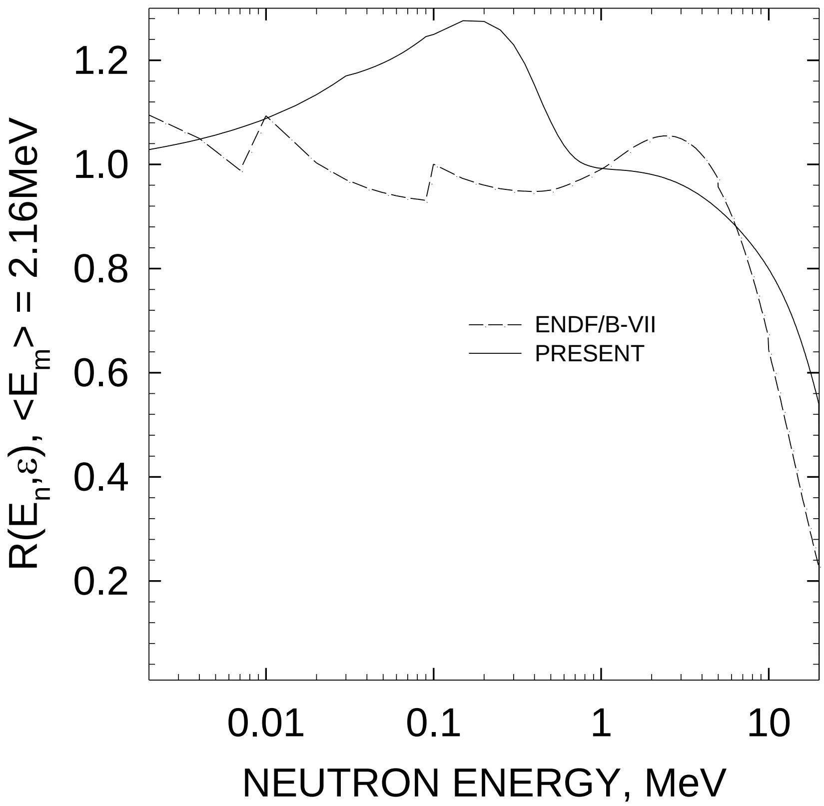

FIG. 12.20. Comparison of the prompt fission neutron spectrum for ^{237}Np (n, F) reaction at incident neutron energy of 6 MeV.

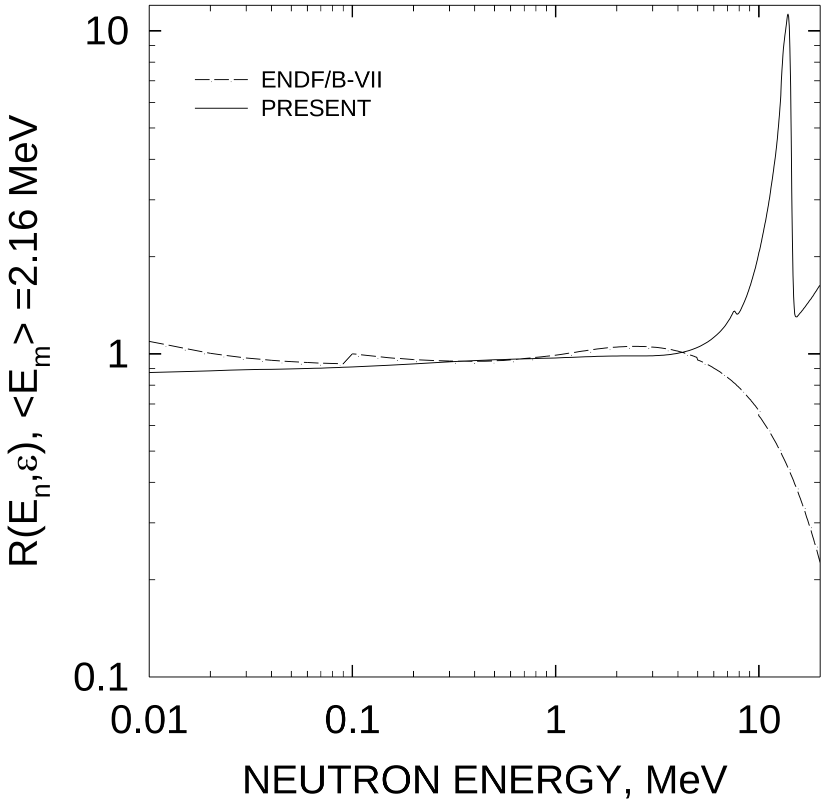

FIG. 12.21. Comparison of the prompt fission neutron spectrum for ^{237}Np (n, F) reaction at incident neutron energy of 20 MeV.

12.3 (n, xn) Reactions Neutron Spectra

There is no measured data on neutron emission spectra for ^{237}Np +n interaction. For incident neutron energy higher than emissive fission threshold, emissive neutron spectra are de-convoluted, components of 1st, 2nd and 3rd neutron spectra are provided, where applicable. We have calculated 1st, 2nd and 3d neutron spectra for the (n, nγ), (n, 2n) and (n, 3n) reactions.

According to the ENDF/B-VI format specifications the secondary neutron spectra were summed up and tabular spectra for the (n, nγ), (n, 2n) and (n, 3n) reactions were obtained.

Spectrum of (n, nγ) reaction actually is just hard energy tail of ‘pre-equilibrium’ component of first neutron spectrum (see Figs 12.1 - 12.3).

Spectrum of the first neutron of (n, 2n) reaction is much softer, although ‘pre-equilibrium’ component still comprise appreciable part of it. Figs 12.22, 12.23 and 12.24 illustrate the variation of the partial contributions of the 1st and 2nd neutrons to the combined spectrum of ^{237}Np(n, 2n) reaction.

First neutron spectrum of (n, 3n) reaction is actually of evaporative nature. First neutron spectrum of (n, nf) reaction has rather long pre-equilibrium high-energy tail. First neutron spectrum of (n, 2nf) reaction, as that of (n, 3n) reaction, is of evaporative nature. Figures 12.25 (E_n = 20 MeV) and 12.26 (E_n = 14 MeV) illustrate the variation of the partial contributions of the 1st, 2nd and 3rd neutrons to the combined spectrum of ^{237}Np(n, 3n) reaction, softening of higher multiplicity neutrons is evident.

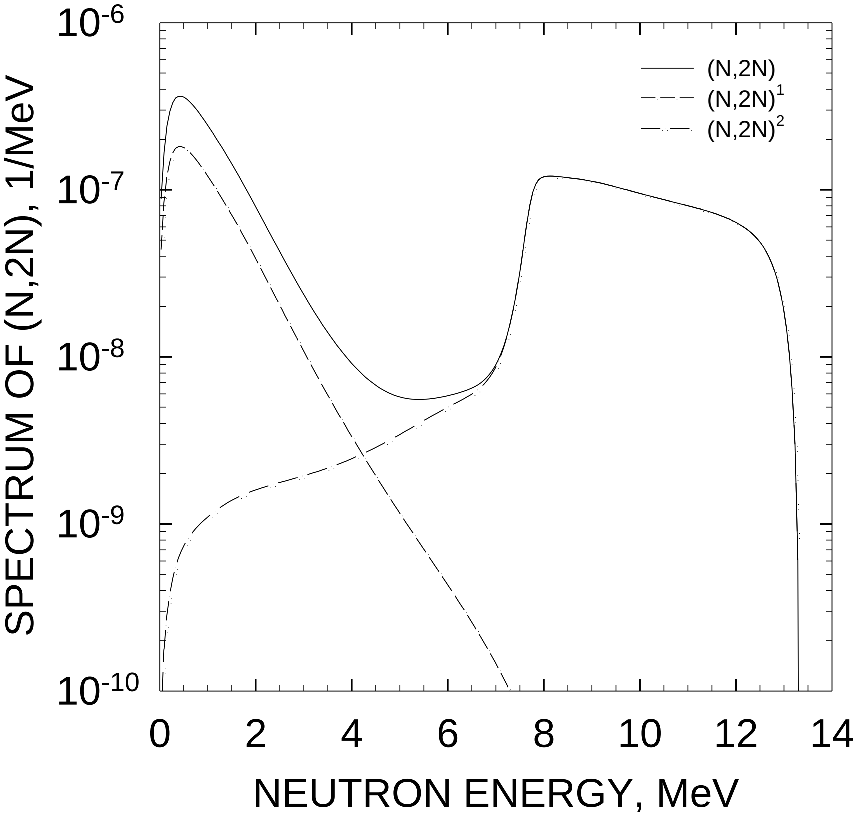

FIG. 12.22. (n, 2n) reaction neutron spectra of $^{237}Np+n$ for incident neutron energy 20 MeV.

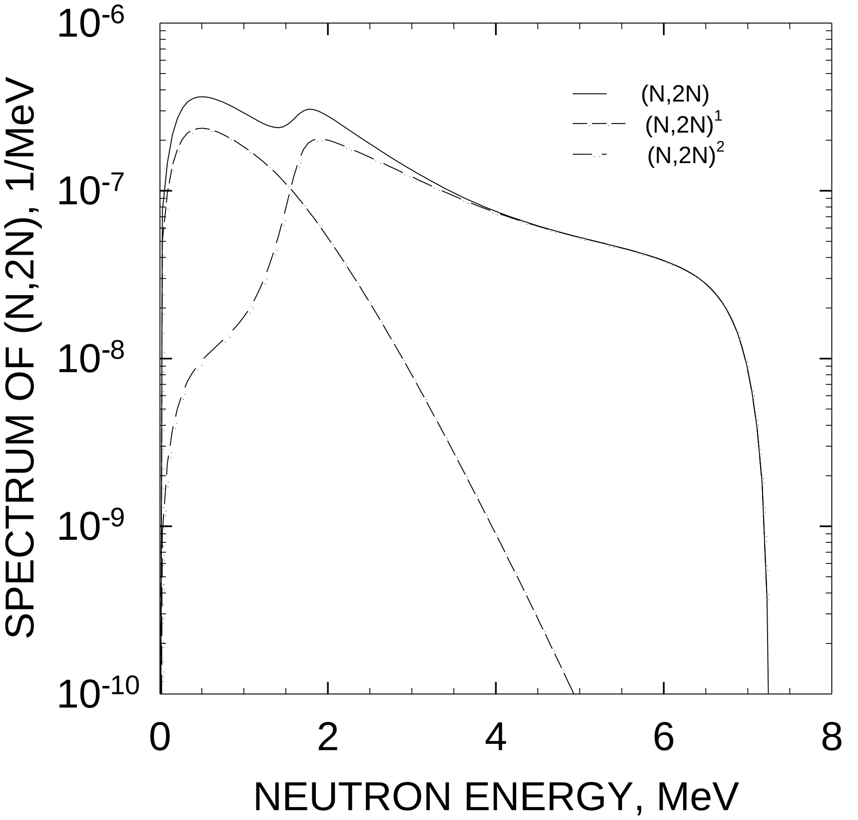

FIG. 12.23. (n, 2n) reaction neutron spectra of $^{237}Np+n$ for incident neutron energy 14.7 MeV.

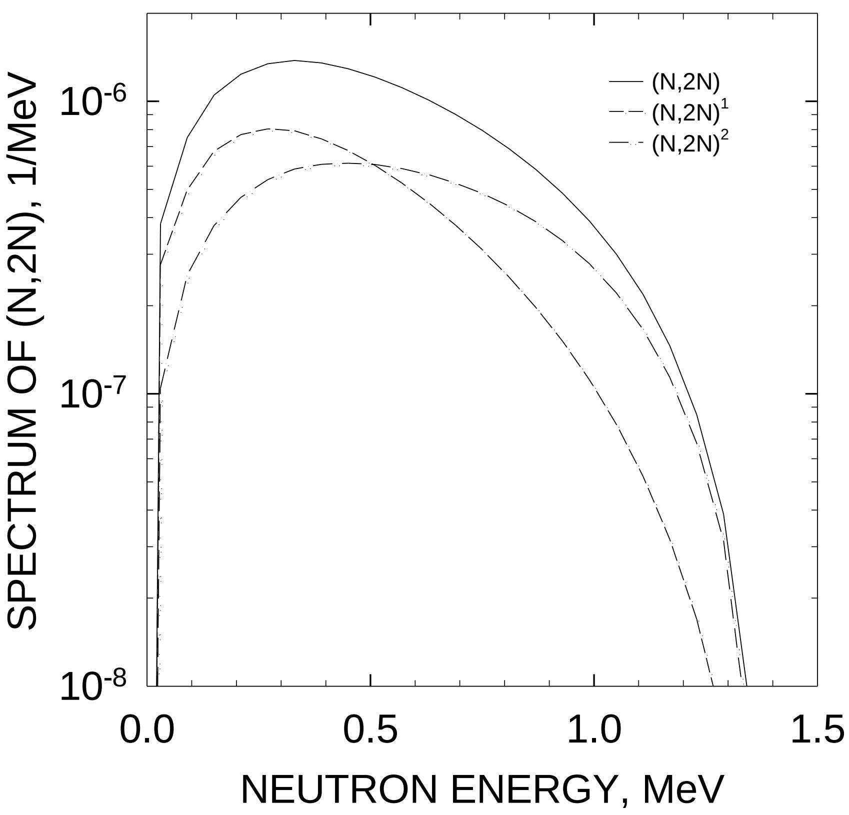

FIG. 12.24. (n, 2n) reaction neutron spectra of ^{237}Np+n for incident neutron energy 8 MeV.

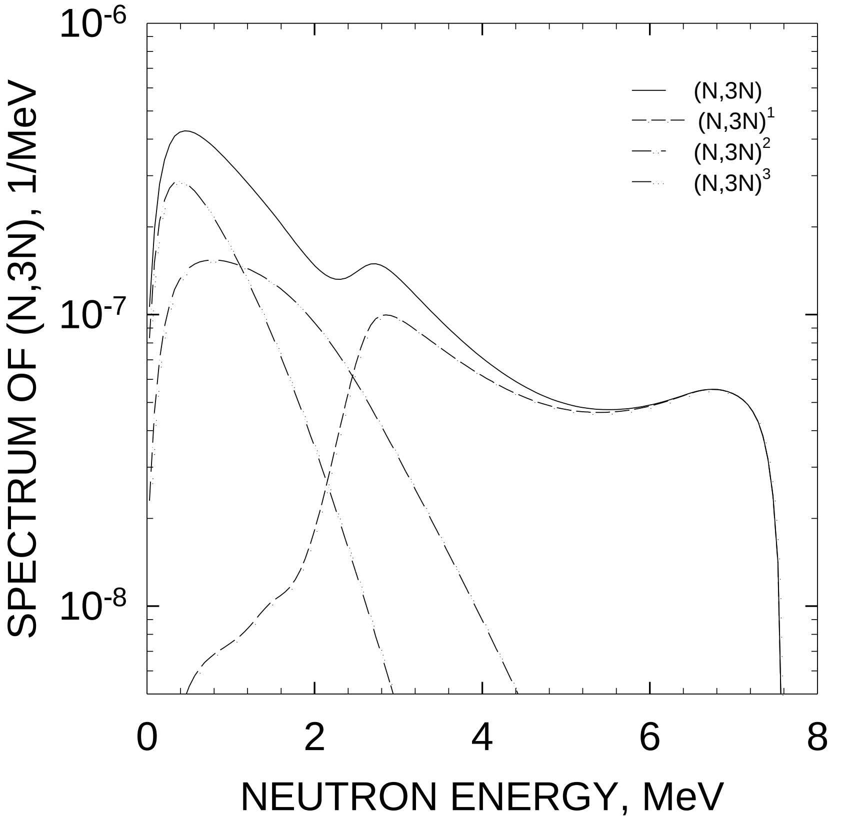

FIG. 12.25. (n, 3n) reaction neutron spectra of ^{237}Np+n for incident neutron energy 20 MeV.

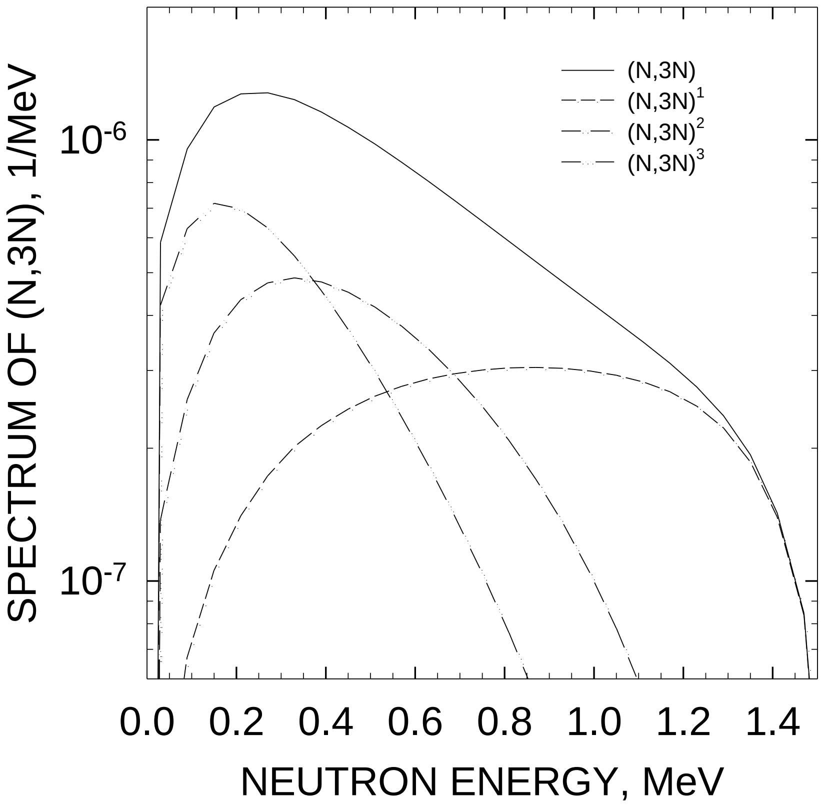

FIG. 12.26. Comparison of (n, 3n) reaction neutron spectra for ^{237}Np+n for incident neutron energy 14 MeV.

13. Conclusion

The diverse measured data base of n+^{237}Np is analyzed using a statistical theory and generalized least squares codes. Consistent description of the total, fission and partial inelastic scattering data in 1-3 MeV energy range provides an important constraint for the absorption cross section, which is quite important for the robust estimate of the capture cross section in the 0.5-500 keV energy range. Important constraints for the measured capture cross section come from the average radiative S_0 and S_1 strength functions. The evaluated inelastic cross section is consistent with measured data on the inelastic scattering of neutrons with excitation of specific groups of levels. A change of the inelastic data shape at E_n ~1.5 MeV is explained by the sharp increase of the level density of the residual odd-even nuclide ^{237}Np due to the onset of three-quasi-particle excitations.

Prompt fission neutron spectra data for the first-chance fission and emissive fission reactions are reproduced, which was not done properly previously. The influence of exclusive (n, xnf) pre-fission neutrons on prompt fission neutron spectra (PFNS) and (n, xn) spectra is modelled. Contributions of emissive/non-emissive fission and exclusive spectra of (n, xnf) reactions are defined by a consistent description of the ^{237}Np(n, F), ^{237}Np (n, 2n) ^{236s}Np reactions and the ratio of the yields of short-lived (1$^-$) and long-lived (6$^-$) ^{236}Np states measured at 14 MeV. Excited levels of ^{236}Np are modelled using predicted Gallher-Moshkowski doublets.

We argue that this evaluation provides neutron data for ^{237}Np just in a just as detailed manner as is rarely done for major actinides. That approach would be strictly persued for ^{237}Am and some other Z-odd, N-even target nuclides.

The job is supported by International Science and Technology Center (Moscow) under B-1604 Project Agreement.

References

1. Sanchez, R., Loaiza, D., Kimpland, R., *et al.*, Criticality of a ^{237}Np sphere, Nucl. Sci. Eng. **158** (2008) 1.
2. Maslov, V.M., Pronyaev, V.G., Tetereva, N.A., *et al.*, ^{235}U prompt fission neutron spectra, in Proc. WONDER 2009 - 2nd International Workshop on Nuclear Data Evaluation for Reactor applications, CEA Cadarache, France, 2009, (in print) (available at http://nea.fr).
3. Chadwick, M.B., Oblozinsky, P., Herman, M., *et al.*, ENDF/B-VII.0: Next generation evaluated data library for nuclear science and technology. Nucl. Data Sheets **107** (2006) 2931-3060.
4. Maslov, V.M., Advanced analysis of ^{237}Np neutron data, in Proc. 5th Workshop on Neutron Measurements, Evaluations and applications. Nuclear Data for sustainable nuclear energy, JRC-IRMM-EU, Geel, Belgium, 2008, Ljubljana, Slovenia.
5. Maslov, V.M., U, Np, Pu, Am Prompt Fission Neutron Spectra, in Proc. Int. 2nd Int. Conf. Frontiers in Nuclear Structure, Astrophysics and Reactions - FINUSTAR 2, Crete, Greece, 2007, AIP, Conf. Proc. 1012 (2008) 398.
6. Maslov, V.M., Average energies of ^{237}Np and ^{241}Am prompt fission neutron spectra, At. Energy 104 (2008) 330-333.
7. Shibata, K., *et al.*, Japanese Evaluated Nuclear Data Library Version 3 Revision-3: JENDL-3.3, J. Nucl. Sci. Technol. **39** (2002) 1125-1200.
8. Gressier, V., *et al.*, Ann. Nucl. Energy **27** (2000) 1115.
9. Auchampaugh, G.F., Moore, M.S., Moses, J.D., *et al.*, Nature of the coupling in subthreshold fission of ^{238}Np. Phys. Rev. **C29** (1984) 174.
10. Borzakov, S.B., Dermendjiev, E., Goverdovskij, A.A., *et al.*, Resonance parameters and fission cross section of ^{237}Np in neutron energy interval below 1000 eV, Phys. At. Nucl. **62** (1999) 872.
11. Dermendjiev, E., Ruskov, I., Zamyatnin, Yu.S., Goverdovskij, A.A., Resonance areas and fission widths of low lying resonsnces of ^{237}Np. Phys. At. Nucl. **57** (1994) 1292.
12. Kozharin, V.V., Kovalenko, S.S., Selicki,j Yu.A., Nemilov, Yu.A., *et al.*, ^{237}Np fission cross section and fission resonance integral for thermal neutrons. At. Ehnergiya **60** (1986) 419.
13. Wagemans, C., Allaert, E., Caitucoli, F., D'Hondt, P., Barreau, G., Perrin, P., Experimental study of some important characteristics of thermal neutron induced fission of ^{237}Np, Nucl. Phys. **A369** (1981) 1.
14. Wagemans, C., D'Hondt, P., Deruytter, A.J., Asghar, M., Emsallem, M., Study of some characteristics of the thermal neutron induced sub-barrier fission of ^{231}Pa, ^{232}Th and ^{237}Np, Nucl. Phys. **A285** (1977) 32.
15. Maslov, V.M., Porodzinskij, Yu.V., Actinide Level Density Parameter Systematic, JAERI-Research, 98-038 (1998).
16. Porodzinskij, Yu.V., Sukhovitskij, E.Sh., Maslov, V.M., Evaluation of Average Neutron Resonance Parameters of Actinides with Account of Experimental Resolution and Discrimination Threshold INDC(BLR)-012 (1998).
17. Capote, R., Herman, M., Oblozinsky, P., *et al.*, RIPL- Reference Input Parameter Library for Calculations of Nuclear Reactions and Nuclear Data Evaluation, Nucl. Data Sheets **110** (2009) 3107.
18. Mughabghab, S. F., Atlas of neutron resonances NNDC, BNL, Upton, USA (2006).
19. Poenitz, W.P., Aumeier, S.E., The simultaneous evaluation of the standards and other cross sections of importance for technology, Rep. ANL/NDM-139, Argonne Natl Lab., (1997).
20. An International Evaluation of Neutron Cross Section Standards, Rep.STI/PUB/1291, IAEA, Vienna, Austria (2007).
21. http://www-nds.iaea.org/exfor/exfor.htm (January 2009).
22. Behrens, J.W., Browne, J.C., Walden, J.C., Measurement of the neutron-induced fission cross section of the ^{237}Np relative to ^{235}U from 0.02 to 30 MeV, Nucl. Sci. Eng. **80** (1982) 239.
23. Tovesson, F. and Hill, T.S., Neutron-induced fission cross section of ^{237}Np from 100 keV to 200 MeV, Phys. Rev. **C75** (2007) 034610.

24. Tovesson, F. and Hill, T.S., Subthreshold fission cross section of ^{237}Np, Nucl. Sci. Eng. **159** (2008) 94.
25. Lisowski, P.W., Gavron, A., Parker, W.E., *et al.*, Fission cross sections in the intermediate energy regions, in Proc. Spec. Meeting on Neutron Cross Section Standards for the Energy Region above 20 MeV, Uppsala, Sweden, 1991, OECD (1991) 177.
26. Meadows, J.W., The fission cross section of ^{237}Np relative to ^{235}U from 0.1 to 10 MeV. Nucl. Sci. Eng. **85** (1983) 271.
27. Varnagy, M., Juhasz, S., Csikai, J., Measurements of fission cross sections around 14 MeV. Nucl. Instr. Meth. **196** (1982) 465.
28. Shcherbakov, O.A., Donets, A., Evdokimov, A., *et al.*, in Proc. Int. Conf. on Nuclear Data for Science and Technology, 2001, Tsukuba, Japan, (2002) 230.
29. Arlt, P., Josch, M., Musiol, G., *et al.*, Absolute measurements fission cross sections at neutron energies of about 8.5 MeV, Isotopenpraxis **21** (1985) 344.
30. Garlea, I., Miron, C., Dobrea, D., *et al.*, Measurement of the integral cross sections in ^{115}In(n,n'), ^{197}Au(n,2n), ^{93}Nb(n,2n), ^{27}Al(n,a), ^{56}Fe(n,p), ^{239}Pu(n,f), ^{238}U(n,f), ^{238}Th(n,f) and ^{237}Np(n,f), Rev. Roum. Phys. **29** (1984) 421.
31. Meadows, J.W., The fission cross sections of ^{230}Th, ^{232}Th, ^{233}U, ^{234}U, ^{236}U, ^{238}U, ^{237}Np, ^{239}Pu and ^{242}Pu relative to ^{235}U at 14.7 MeV neutron energy, Ann. Nucl. Energy **15** (1988) 421.
32. Terayama, H., Karino, Y., Manabe, F., *et al.*, Measurement of fastneutron-induced fission cross section of ^{233}U, ^{237}Np and ^{243}Am relative to ^{235}U from 0.7 to 7 MeV, NEANDC(J)-122 (1986).
33. Grundl, J.A., Study of fission neutron spectra with high-energy activation detectors-Part 1. Detector development and excitation measurement, Nucl. Sci. Eng. **30** (1967) 39.
34. Stein, W.E., Smith, R.L., Smith, H.L., Relative fission cross sections of ^{236}U, ^{238}U and ^{237}Np and ^{236}U, in Proc. Conf. on Neutron Cross Sections and Technology, Washington DC, 1966, AEC, vol. 1, (1968) 627.
35. Kanda, K., Sato, O., Yoshida, K., *et al.*, Measurement of the fast neutron induced fission cross section, JAERI-M-85-035 (1985) 220.
36. White, P.H., Warner, G.P., The fission cross sections of ^{233}U, ^{234}U, ^{236}U, ^{238}U, ^{237}Np, ^{239}Pu and ^{241}Pu relative to that of ^{235}U for neutrons in the energy range 1-14 MeV, J. Nucl. Energy **21** (1967) 671.
37. Cance, M., Grenier, G., Absolute measurements of the ^{240}Pu(n,f), ^{242}Pu(n,f) and ^{237}Np(n,f) cross sections at 2.5 MeV incoming neutron energy, K.H. Bockhoff, (Ed.) in Proc. Int. Conf. Nuclear Data for Science and Technology, Antwerpen, Belgium, 1982, p. 51, Holland (1982).
38. Wu Jingxia, Rong Chaofan, Sun Zhongfa, *et al.*, Measurement of fission cross section for ^{237}Np(n,f) by fast neutrons, Chin. J. Nucl. Phys. **6** (1984) 369.
39. Desdin, L., Szegedi, S., Csikai, J., Measurement of the fission cross section ratio for ^{237}Np/^{235}U around 14 MeV. Acta Phys. Hung. **65** (1989) 271.
40. Kuprijanov, V.M., Fursov, B.I., Ivanov, V.I. Smirenkin, G.N., The measurement of ^{237}Np/^{239}Pu and ^{241}Am/^{239}Pu fission cross section ratios in the 0.13-7.0 MeV neutron energy interval, At. Ehnergiya **45** (1978) 440.
41. Goverdovskij, A.A., Gordyushin, A.K., Kuz'minov, B.D., *et al.*, ^{237}Np to ^{235}U fission cross section ratio measurement for neutrons in the energy range 4-11 MeV, At. Ehnergiya **58** (1985) 137.
42. Goverdovskij, A.A., Gordyushin, A.K., Kuz'minov, B.D., *et al.*, ^{237}Np to ^{235}U fission cross section ratio measurement by the method of isotope impurities, in Proc. 6th All-Union Conf. on Neutron Physics, Kiev, 1983, vol.3 (1983) 115.
43. Alkhazov, I.D., Ganza, E.A., Drapchinskij, L.V., *et al.*, Absolute measurements of the fission ccross sections for some heavy isotopes by the neutrons with energies 2.6, 8.4, 14.7 MeV, in Proc. of the 3rd All-Union Conference on the Neutron Radiation Metrology at Reactors and Accelerators, Moscow, 1983, CNIIAtominform, vol. 2 (1983) 201.
44. Carlson, A.D., Parker, W.E., Lisowski, P.W., *et al.*, Measurement of the fission cross section of ^{237}Np, in Proc. Int. Conf. Nuclear Data for Science and Technology, Gattlinburg, USA, 1994, ANS (1995) 40.

45. Hoffman, M.M., Sanders, W.M., Semon, M.D., Fission, Scattering and Capture cross section for ^{237}Np, Bull. Am. Phys. Soc. **21** (1976) 655.
46. Yamanaka, A., Kimura, I., Kanazawa, S., *et al.*, Measurement of fission cross section of Neptunium-237 in resonance region with electron linac-driven lead spectrometer, J. Nucl. Sci. Technol. **30** (1993) 863.
47. Plattard, S., Pranal, Y., Blons, J., Mazur, C., ^{237}Np fission cross section measurement between 100 keV and 2 MeV, in Proc. 3rd All-Union Conf. on Neutron Physics, Kiev, 1975, vol.2 (1975) 254.
48. Brown, W.K., Dixon, D.R., Drake, D.M., Fission cross section of ^{237}Np from Pommard. Nucl. Phys. **A156** (1970) 609.
49. Zolotarev, K.I., Re-evaluation of microscopic and integral cross sections for important dosimetry reactions, INDC(NDS)-0526 (2008).
50. Weston, L.W., Todd, J.H., Neutron capture cross section of ^{237}Np. Nucl. Sci. Eng. **79** (1981) 184.
51. Esch, E.-I., Reifarth, R., Bond, E.M., *et al.*, Measurement of ^{237}Np(n,g) cross section from 20 meV to 500 keV with a high efficiency, highly segmented 4pi BaF2 detector, Phys. Rev. **C 77** (2008) 034309.
52. Kobayashi, K., Yamanaka, A., Kimura, I. J. Measurement of thermal neutron cross section and resonance integral for ^{237}Np(n,γ) reaction, Nucl. Sci. Techn. **31** (1994) 1239.
53. Buleeva, N.N., Davletshin, A.N., Tipunkov, O.A., *et al.*, Neutron radiation capture cross sections for ^{236}U, ^{238}U and ^{237}Np measured by the activation method. At. Ehnergya **65** (1988) 348.
54. Stupegia, D.C., Schmidt, M., Keedy, C.R., Capture cross section of ^{237}Np, Nucl. Sci. Eng. **29** (1967) 218.
55. Trofimov, Yu. N., Nemilov, Ju.A., ^{237}Np radiation capture cross section for the energy interval 0.3-1.9 MeV, in Proc. 6th All- Union Conf. on Neutron Physics, Kiev, 1983, vol.2 (1983) 142.
56. Lindner, M., Nagle, R.J., Landrum, J.H., Neutron capture cross section from 0.1 to 3 MeV by activation measurements, Nucl. Sci. Eng. **59** (1976) 381.
57. Harada, H., *et al.*, J.Nucl. Sci. Technol. **43** (2006) 1289.
58. Ignatyuk, A.V. Moscow, Energoatomiizdat (1983).
59. Moldauer, P.A., in Proc.Conf. Neutron Cross Sections and Technology, Washington, D.C., USA, 1966, AEC (1966) 613-622.
60. Stavinskij, V.S. and Shaker, M.O., Nucl. Phys. **62** (1965) 667.
61. Basunia, M.S., Nucl. Data Sheets **107** (2006) 2323.
62. Strutinsky, V.M., Shell Effects in Nuclear Masses and Deformation Energies, Nucl. Phys. **A95** (1967) 420.
63. Maslov, V.M., INDC(BLR)-013/L (1998).
64. Maslov, V.M., Pairing effects in ^{232}Th neutron-induced fission cross section. Nucl.Phys. **A743** (2004) 236.
65. Kornilov, N.V., Kagalenko, A.V., Baryba, V.Ya., *et al.*, Inelastic neutron scattering and prompt fission neutron spectra for ^{237}Np, Ann. Nucl. Energy **27** (2000) 1643.
66. Grigoriev, Yu.V., Sinitsa, V.V., Gundorin, N.A., Faikov-Stanczyk, Popov, Yu.P., Measurement of the gamma-ray multiplicity spectra and the alpha value for uranium-235 and plutonium-239, Rep. JINR-E3-98-202 (1998) 194.
67. Maslov, V.M., Porodzinskij, Yu.V., Baba, M., Hasegawa, A., Neutron Capture Cross Section of ^{232}Th, Nucl. Sci. Eng. **143** (2003) 177.
68. Maslov, V.M., ^{232}Th neutron capture cross section, in Proc. 13th International Seminar on Interaction of Neutrons with Nuclei, Dubna, Russia (2005) 321.
69. Maslov, V.M., Porodzinskij, Yu.V., Baba, M. and Hasegawa, A., Evaluation of the unresolved resonance range of ^{238}U, Ann. Nucl. Energy **29** (2002) 1707.
70. Cullen D. PREPRO2000: 2000 ENDF/B Pre-Processing Codes.
71. NJOY 94.10 Code System for Producing Pointwise and Multigroup Neutron and Photon Cross Sections from ENDF/B Data, RSIC Peripheral Shielding Routine Collection, ORNL, PSR-355, LANL, Los Alamos, New Mexico (1995).

72. Maslov, V.M., Porodzinskij, Yu.V., Tetereva, N.A., Baba, M., Hasegawa, A., ^{238}U neutron-nucleus optical potential up to 200 MeV. Nucl. Phys. **A736** (2004) 77-92.
73. Moldauer, P.A., Why the Hauser-Feshbach formula works, Phys. Rev. **C11** (1975) 426.
74. Tepel, J.W., Hoffman, H.M., Weidenmuller, H.A., Hauser Feshbach formulas for medium and strong absorption, Phys. Lett. **49** (1974) 1.
75. Howard, W.M. and Möller, P., Calculated Fission Barriers, Ground-State Masses, and Particle Separation Energies for Nuclei with $76 \leq Z \leq 100$ and $140 \leq N \leq 184$. At. Data Nucl. Data Tables **25** (1980) 219.
76. Fu C., Implementation of an Advanced Pairing Correction for Particle-Hole State Densities in Precompound Nuclear Reaction Theory, Nucl. Sci. Eng. **86** (1984) 344.
77. Maslov, V.M., Yad. Fiz. **63** (2000) 214.
78. Maslov, V.M., Actinide Neutron-Induced Fission up to 20 MeV, Nuclear Reaction Data and Nuclear Reactors, International Center for Theoretical Physics Lecture Notes, Trieste, Italy, No.1 (2001) 231-268.
79. Myers, W.O. and Swiatecky, W.J., Anomalies in Nuclear masses. Ark. Fyzik. **36** (1967) 243.
80. Bjørnholm, S. and Lynn, J.E., The double humped fission barrier. Rev. Mod. Phys. **52** (1980) 725.
81. Maslov, V.M., Porodzinskij, Yu. V., Baba, M., Hasegawa, A., Kornilov, N. V., Kagalenko, A. B., Tetereva, N.A. ,Prompt fission neutron spectra of ^{238}U(n,f) above emissive fission threshold, Europhysics J. **A18** (2003) 93.
82. Britt, H.C., Wilhelmy, J.B., Simulated (n,f) cross sections for exotic Actinide nuclei, Nucl. Sci. Eng. **72** (1979) 222.
83. Valskij, G.V., Gromova, E.A., Danichev, V.V., *et al.*, in Proc. Int. Conf. on Neutron Physics, Kiev, 1987, v.2 (1988) 242.
84. Ignatyuk, A.V., Kornilov, N.V., Maslov, V.M., Isomer ratio and ^{237}Np(n,2n) reaction cross section, At. Ehnergiya **63** (1987) 110.
85. Maslov, V.M., Analysis of the 237-Np fission cross sections and (n,xn) reactions. INDC(CCP)-366 (1994) 27.
86. Belyaev, B.N., Gromova, E.A., Kovalenko, S.S., *et al.*, Fission cross section of the long-lived isomer of ^{236}Np induced by thermal neutrons, At. Energiya **60** (1986) 141.
87. Uhl, M., Strohmaier, B., A Computer Code for Particle Induced Activation Cross Sections and Related Quantities, Rep. IRK-76/01 IRK, Vienna (1976).
88. Maslov, V.M., Porodzinskij, Yu. V., Baba, M., Hasegawa, A., Kornilov, N.V., Kagalenko, A.B., Tetereva, N.A., Prompt fission neutron spectra of ^{238}U(n,f) and ^{232}Th(n,f) above emissive fission threshold, Phys. Rev. **C69** (2004) 034607.
89. Myers, W.A., Lindner, M., Newburry, R.S., The isomer ratio of ^{236l}Np/^{236s}Np in the reaction ^{237}Np(n,2n) ^{236}Np from neutrons, produced in thermonuclear devices, J. Inorg. Nucl. Chem. **37** (1975) 637.
90. Sood, P.C., Low-lying two-particle states in the nucleus ^{236}Np, Z. Phys., A Atoms Nucl. **A348** (1984) 111.
91. Lindner, M., Dupzyk, R.J., Hoff, R.W. and Nagle, R.J., Lifetime of the long-lived isomer of ^{236}Np from α-, β- and electron-capture decay measurements, J. Inorg. Nucl. Chem. **43** (1981) 3071.
92. Gromova, E.A., Kovalenko, S.S., Nemilov, Yu.A., *et al.*, Measurement of ^{237}Np(n,2n) reaction cross section at 14.8 MeV neutron incident energy, At. Ehnergiya **54** (1983) 198.
93. Nishi, T., Fujiwara, I., Imanishi, N., (n,2n) cross sections for the ^{237}Np, NEANDC(J)-42L (1975) 20.
94. Landrum, J.H., Nagel, R.J., Lindner, M., (n,2n) cross sections for ^{238}U and ^{237}Np in the region of 14 MeV, Phys. Rev. **C8** (1973) 1938.
95. Paulson, C.K., Hennelly, E.J., Cross sections measurement of ^{236}Pu formation in ^{238}Pu by ^{237}Np(n,2n) reaction, Nucl. Sci. Eng. **5** (1974) 24.
96. Lindeke, K., Specht, S., Born, H.J., Determination of the ^{237}Np(n,2n) ^{236}Np cross section at 15 MeV neutron energy, Phys. Rev. **C12** (1975) 1507.
97. Perkin, J.L., Coleman, R.F., Cross sections for the (n,2n) reaction of ^{232}Th, ^{238}U and ^{237}Np with 14 MeV neutrons, Ann. Nucl. Energy **14** (1961) 69.

98. Daroczy, S., Raics, P., Csikai, J., Kornilov, N.V. *et al.*, Measurement of ^{237}Np(n,2n) ^{236}Np(22.5hrs) cross section for neutron energy between 7 and 10 MeV, At. Energiya **58** (1985) 117.
99. Fort, E., Derrien, H., Doat, J.P., Evaluation des sections efficaces neutrniques de ^{237}Np entre 5 MeV et 16 MeV, etude particuliere de la reaction (n,2n) pour l'application aux calculs de production de ^{236}Pu., in Proc. Int. Conf. Nuclear Data for Science and Technology, Antwerpen, Belgium, 1982, Reidel Publ. Co., Holland (1983) 673.
100. Huizenga, J.R., Vandenbosh, R., Nucl. Fission **2** (1964) 51.
101. Ahmad, J. Hines, J. and Gindler, J.E., Electron capture decay of ^{237}Pu, ^{237}Np and ^{236}Np., Phys. Rev. **C27** (1983) 2239.
102. Mannhart, W., Status of the Evaluation of the Neutron Spectrum of ^{235}U + n_{th}., IAEA Consultants' Meeting, 13-15 October 2008.
103. International Reactor Dosimetry File 2002 (IRDF-2002), Technical Reports Series No. 452, IAEA, Vienna (2006).
104. Strutinsky, V.M., Groshev, L.V., Akimova, M.K., Gamma-ray spectra of thermal neutron capture of heavy nuclei, At. Ehnergiya **38** (1960) 598.
105. Gray, P.H., Phys. Rev. **101** (1956) 306.
106. Cindler, J. and Sjoblom, R., J. Inorg. Nucl. Chem. **12** (1959) 8.
107. Lederer, C.M., Jaklevic, J.M. and Prussin, S.G., A low lying state in ^{236}U. Nucl. Phys. **A135** (1969) 36.
108. Gorman, D.J., Asaro, F., Alpha decay of ^{240}Am., Phys. Rev. **C2** (1970) 2406.
109. Hoff, R.W., Gardner, D.G. and Gardner, M.A., Reaction cross section calculations using new experimental and theoretical level structure for deformed nuclei, Radiat. Eff. **95** (1986) 119.
110. Firestone, R.B., Table of Isotopes CD-ROM, Eighth Edition, Version 1.0, March 1996, S.Y.Frank Chu, CD-ROM Ed., V.S.Shirley, (Ed.) Wiley-Interscience (1996)
111. Browne, E., Tuli, J.K., Nucl. Data Sheets **107** (2006) 2649.
112. Decay Radiation Data Base, version 12/11/2009, www.nndc.bnl.gov/ nudat2/index dec.jcp.
113. Zolotarev, K.I., Evaluation of cross-section data from threshold to 40-60 MeV for specific neutron reactions important for neutron dosimetry applications. Part 1, Rep. INDC(NDS)-0546, IAEA, Vienna (2009).
114. Zolotarev, K.I., Evaluation of cross-section data for the U-238(n,2n)U-237 reaction from threshold to 30 MeV. Private communication, Obnisk, FEI (2009).
115. Pronjaev, V.G., *et al.*, Status of the International Neutron Cross Section Standards File, in Proc. Int. Conf. on Nuclear Data for Science and Technology, Santa Fe, New Mexico, USA, (2004).
116. Vonach, H., *et al.*, Z. Phys. **237** (1970) 155.
117. Magurno, B., Rep. IAEA-208 (1978) 375.
118. Kornilov, N.V., Vinogradov, *et al.*, Yad. Konst. 1 (45) (1982) 33-41.
119. ENDF/B-V Dosimetry file, MAT=6398, principal evaluators Pennigton, E.M., Smith, A.B., Poenitz, W.P., Rev. 3, Rep. ANL/NDM, Argonne Natl Lab., IL (1979).
120. Weise, H.W., Fischer, U., Coel, B., Analysis of neutron cross sections for the formation of ^{236}Pu and ^{58,60}Co in both thermal and fast reactors, in Proc. Int. Conf. Nuclear Data for Science and Technology, Antwerpen, Belgium, 1982, Reidel Publ. Co., Holland (1983) 202.
121. Cranberg, L., Frye, G., Nereson, N., *et al.*, Fission neutrons spectrum of ^{235}U. Phys. Rev. **103** (1956) 62.
122. Gromova, E.A, *et al.*, At. Ehnergya **60** (1986) 68-70.
123. Mannhart, W., in Proc. Int. Conf. Nuclear Data for Science and Technology, 1982, Antwerp, Holland, D.Reidel Co. (1983) 429-435.
124. Lederer, C., Shirley, V., Table of Isotopes. N.Y. John Wiley and Sons (1978).
125. Mannhart, W., Rep. INDC(NDS)-220/L, IAEA, Vienna (1989) 158.
126. Mannhart, W., Status of the Evaluation of the Neutron Spectrum of 252Cf(sf), Rep. INDC(NDS)-0540, IAEA, Vienna (2008).
127. Khokhlov, Yu. A., Ivanin, I.A., In'kov, V.I., *et al.*, Measurements results of average neutron multiplicity from neutron induced fission of actinides in 0.5-10 MeV energy range, in Proc.

Int. Conf. Nuclear Data for Science and Technology, Gatlinburg, USA, 1994, J.K. Dickens (Ed.), ANS (1994) 272.
128.Veeser, W., Prompt neutrons from neutron-induced fission of ^{237}Np. Phys. Rev. **C17** (1978) 385.
129.Frehaut, J., Bois, R., Bertin, A., in Proc. Int. Conf. Nuclear Data for Science and Technology, Antwerpen, Belgium, 1982, Reidel Publ. Co., Holland (1983) 78.
130.Mueler, R., Naqvi, A.A., Kaeppeler, F., Bao, Z.Y., Numerical results of a (2E, 2V) measurements for fast neutron induced fission of ^{235}U and ^{237}Np, Rep. KFK-3068 (1980) 1.
131.Malinovskyj, V.V., Vorobjova, V.G., Kuzminov, B.D., Piksajkin, V.M., Semjonova, N.N., Valjavkin, V.S., Solovjov, S.M., On the divergence of the results of ν_p measurements for neutron-induced fission of ^{237}Np, At. Energiya **54** (1983) 209.
132.Thierrens, H., Jacobs, E., D'Hondt, P., *et al.*, The thermal neutron sub-barrier fission of ^{237}Np, Nucl. Phys. **A342** (1980) 229.
133.Boykov, G.S., Dmitriev, V.D., Svirin, M.I., Smirenkin, G.N., Neutron spectra in fission of ^{237}Np by the neutrons with energies 2.9 and 14.7 MeV, Phys. At. Nucl. **57** (1994) 2047.
134.Iyer, R.H., Naik, H., Pandey, A.K., *et al.*, Measurements of absolute fission yields in the fast neutron-induced fission of actinides ^{237}U, ^{237}Np, ^{237}Pu, ^{237}Pu, ^{237}Am and ^{237}Cm by track and etch cum Gamma Spectrometry, Nucl. Sci. Eng. **135** (2000) 227.
135.Kornilov, N.V., Kagalenko, A.B., Baryba, V.Ya., *et al.*, Inelastic neutron scattering and prompt fission neutron spectra for ^{237}Np, in Proc. Int. Conf. on Nuclear Data for Science and Technology, Trieste, Italy (1997) 577-579.
136.Malinovskij, V.V., VANT (ser. Yadernie constanty) **2** (1987) 25.
137. Pronyaev, V.G., Piksaikin, V.M., VANT, **1-2** (1997) 32.
138.Piksaikin, V.M., Isaev, S.G., Kazakov, L.E., *et al.*, Phys. At. Nucl. **62** (1999) 1279.
139.Bobkov, E.Yu., Gudkov, A.N., Demin, A.N., Koldobskij, A.B., *et al.*, Yield Measurement for delayed fission neutrons groups arising from fission of the ^{235}U, ^{236}U, ^{238}U, ^{237}Np, ^{242}Pu induced by 14.7 MeV neutrons, At. Ehnergiya **67** (1989) 408.
140.Piksaikin, V.M., Balakshev, Yu.F., Isaev, S.G., Kazakov, L.E., *et al.*, Measurement of energy dependence of relative abundance of delayed neutrons and groups of their precursors from fast neutron-induced fission of ^{237}Np, At. Energiya **85** (1998) 51.
141.Roshchenko, V.A., Piksaykin, V.M., Korolev, G.G., *et al.*, Cumulative yields of delayed neutrons precursors in neutron induced fission of 237-Np and 238-U in the energy range from 0.5 up to 5.0 MeV, Yad. Konst. **1-2** (2006) 43.
142.Loaiza, D., Brunson, G., Sanchez, R., Butterfield, K., Measurement of Absolute Delayed Neutron Yield and Group Constants for the Fast Fission of 235U and 237Np, Nucl. Sci. Eng. **128** (1998) 270.
143.Cesana, A., Sandrelli, G., Sanguist, V., Terrani, M., Absolute total yields of delayed neutrons in the fission of U-233, Np-237, Pu-238,240,241, Am-241, Energ. Nucl. **26** (1979) 542.
144.Gundorin, N.A., Zhdanova, K.V., Zhuchko, V.E., Pikel'ner, L.B., Rebrova, N.V., Salamatin, I.M., Smirnov, V.I., Furman, V.I., Measurements of delayed neutron yields from thermal neutron induced fission of 237-Np. Yad. Fiz. **70** (2007) 1011.
145.Borzakov, S.B., Andreev, A.N., Dermendjiev, E., Filip, A., Furman, W.I., Konovalov, V.Yu., Panteleev, Ts., Ruskov, I., Zamyatnin, Yu.S., Zeinalov, Sh., Measurements of Delayed Neutron Yields from Thermal Neutron Induced Fission of 233-U, 235-U, 239-Pu and 237-Np, Yad. Fiz. **63** (2000) 589.
146.Saleh, H.H., Parish, T.A., Shinohara, N., Measurements of Delayed Neutron Decay Constants and Fission Yields from 235-U, 237-Np, 241-Am, and 243-Am, Nucl. Sci. Eng. **125** (1997) 51.
147. Waldo, R.W., Karam, R.A., Meyer, R.A., Delayed neutron yields: Time dependent measurements and a predictive model, Phys. Rev. **C23** (1981) 1113.
148. Maslov, V.M., Porodzinskij, Yu. V., Baba, M., Hasegawa, A., Kagalenko, A.B., Kornilov, N.V, Tetereva, N.A., Neutron Data Evaluation of ^{238}U, INDC(BLR)-14, IAEA, Vienna, (2003) 239.

149.Maslov, V.M., Porodzinskij, Yu. V., Baba, M., Hasegawa, A., Kagalenko, A.B., Kornilov, N.V, Tetereva, N.A., Neutron Data Evaluation of ^{232}Th. INDC(BLR)-16, IAEA, Vienna, (2003) 241.
150.Kornilov, N.V., Kagalenko, A. B, Hambsch, F.-J., Calculation of the prompt fission neutron spectra on the basis of new systematic of the experimental data, Phys. At. Nucl. **62** (1999) 209.
151.Maslov, V.M., Kornilov, N.V., Kagalenko, A.B., Tetereva, N.A., Prompt fission neutron spectra of ^{235}U up above emissive fission threshold, Nucl. Phys. **A760** (2005) 274.
152.Maslov, V.M., Prompt fission neutron spectra of ^{238}U, Phys. Atom. Nucl. **71** (2008) 9.
153.Maslov, V.M., ^{237}U neutron-induced fission cross section, Phys. Rev. **C72** (2005) 044607.
154.Plettner, C., Ai, H., Beausang, C.W., *et al.*, Estimation of (n,f) cross sections by measuring reaction probability ratios. Phys. Rev. **C71** (2005) 051602.
155.Burke, J. T., Bernstein, L.A., Escher, J., *et al.*, Deducing the ^{237}U(n, f) cross section using the surrogate ratio method, Phys. Rev. **C73** (2006) 054604.
156.Younes, W. and Britt, H.C., Neutron-induced fission cross sections simulated from (t,pf)Results, Phys. Rev. **C67** (2003) 024610.
157.Younes, W. and Britt, H.C., Simulated neutron-induced fission cross sections for various Pu, U, and Th isotopes, Phys. Rev. **C64** (2001) 034610.
158.Goldblum, B.L., Stroberg, S.R., Allmond, J.L., *et al.,* Indirect determination of the ^{230}Th(n,f) and ^{231}Th(n,f) cross sections for thorium-based energy systems, Phys. Rev. **C80** (2000) 044610.
159.Taieb, J., Granier, T., Ethvignot, T., *et al.*, Measurement of the average energy and multiplicity of prompt fission neutrons from ^{238}U(n, f) and ^{237}Np(n, f) from 1 to 200 MeV, in Proc. Int. Conf. on Nuclear Data for Science and Technology (O. Bersillon, F. Gunsing, E. Bauge, R. Jacqmin and S. Leray, Eds) Nice, France, 2007, EDP Sciences (2007) 429.
160.Madland, D., Nix, J., New calculation of prompt fission neutron spectra and average prompt neutron multiplicities, Nucl. Sci. Eng. **81** (1982) 213.
161.Vladuca, G., Tudora, A., Morillon, B., Filipescu, D., Inner barrier shape symmetries in ^{237}Np neutron data evaluation up to 40 MeV incident energy, Nucl. Phys. **A767** (2006) 112.
162. Hambsch, F.-J., Kornilov, N.V. Fabry, I., *et al.*, ^{235}U prompt fission neutron spectrum at thermal input energy, in Proc. IV Int. Workshop on Nuclear Fission and Fiss. Product Spectra, Cadarache, France (2009).
163.Kornilov, N.V., Hambsch F.-J., Fabry I. ^{235}U prompt fission neutron spectrum at thermal input energy. Nucl. Sci. Eng. (2009) (in press).
164.Watt, B.E., Energy spectrum of neutrons from thermal fission of ^{235}U, Phys. Rev. **87** (1952) 1037.
165.Trufanov, A.M., Lovchikova, G.N., Sukhih, S.E., *et al.*, Energy distributions of prompt fission neutrons of ^{237}Np(n,F), Phys. Atom. Nucl. **55** (1992) 289.
166.Vladuca, G., Tudora, A., Morillon, B., Prompt fission neutron multiplicity and spectrum model for 30–80 MeV neutrons incident on ^{238}U, Nucl. Phys. **A740** (2004) 33.
167.Than Win, Baba, M., Ibaraki, M., *et al.*, Measurement of prompt fission neutron spectrum of ^{237}Np for 0.62 incident neutrons, J. Nucl. Sci. Technol. **36** (1999) 486.
168.Svirin, M.I., The shape of spectra and mean energies of prompt fission neutrons in neutron-induced ^{237}Np fission at energy <20 MeV, Yad. Fiz. **71** (2008) 1725.

Nuclear Data Section
International Atomic Energy Agency
Vienna International Centre, P.O. Box 100
A-1400 Vienna
Austria

e-mail: services@iaeand.iaea.org
fax: (43-1) 26007
telephone: (43-1) 2600-21710
Web: http://www-nds.iaea.org